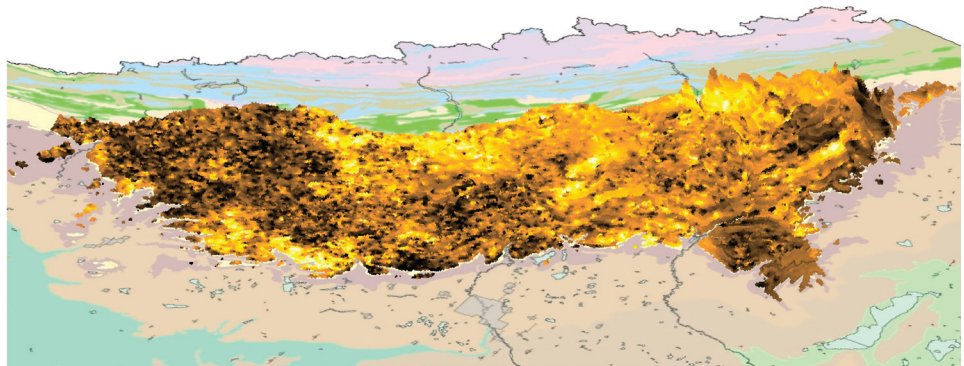


# Geostatistical Rendering of the Architecture of Hydrostratigraphic Units within the Paskapoo Formation, Central Alberta





**Geostatistical Rendering  
of the Architecture of  
Hydrostratigraphic Units  
within the Paskapoo  
Formation, Central Alberta**

*S. Lyster and L.D. Andriashek*

*Energy Resources Conservation Board  
Alberta Geological Survey*

*August 2012*

©Her Majesty the Queen in Right of Alberta, 2012  
ISBN 978-1-4601-0083-7

The Energy Resources Conservation Board/Alberta Geological Survey (ERCB/AGS), its employees and contractors make no warranty, guarantee or representation, express or implied, or assume any legal liability regarding the correctness, accuracy, completeness or reliability of this publication. Any reference to proprietary software and/or any use of proprietary data formats do not constitute endorsement by ERCB/AGS of any manufacturer's product.

If you use information from this publication in other publications or presentations, please acknowledge the ERCB/AGS. We recommend the following reference format:

Lyster, S. and Andriashek, L.D. (2012): Geostatistical rendering of the architecture of hydrostratigraphic units within the Paskapoo Formation, central Alberta; Energy Resources Conservation Board, ERCB/AGS Bulletin 66, 103 p.

**Published August 2012 by:**

Energy Resources Conservation Board  
Alberta Geological Survey  
4th Floor, Twin Atria Building  
4999 – 98th Avenue  
Edmonton, AB T6B 2X3  
Canada

Tel: 780.422.1927  
Fax: 780.422.1918  
E-mail: [AGS-Info@ercb.ca](mailto:AGS-Info@ercb.ca)  
Website: [www.ags.gov.ab.ca](http://www.ags.gov.ab.ca)

# Contents

Acknowledgements.....	ix
Abstract.....	x
1 Introduction.....	1
2 Geological Setting .....	4
2.1 Background.....	4
2.2 Paskapoo Formation Subdivisions .....	4
2.2.1 Internal Stratigraphic Divisions .....	4
2.2.2 Hydrostratigraphic Characterization.....	11
3 Data Sources .....	13
3.1 Data Type and Distribution.....	13
3.2 Data Screening and Culling.....	13
4 Aquifer Mapping Approach.....	17
4.1 Calculating Sandstone Abundance from Depth-Slice Analysis of Log Data .....	17
4.2 Datums.....	18
4.2.1 Datum for Analyzing Sandstone Abundance from Oil and Gas GR Logs.....	18
4.2.2 Datum for Analyzing Sandiness from Water-Well Lithologs .....	18
4.3 Data Extraction .....	19
4.3.1 Extraction of Sandiness Intervals from GR Logs .....	19
4.3.2 Extraction of Sandiness Intervals from Water-Well Lithologs .....	21
4.4 Comparison of Sandiness in GR Log Data and Water-Well Data .....	24
5 Regional-Scale Sandiness.....	27
5.1 Vertical Trend .....	27
5.2 Discussion of Model Dimensions.....	27
5.3 Regional-Scale Modelling.....	28
5.3.1 Normal-Score Transformation .....	29
5.3.2 Variography.....	29
5.3.3 Cross-Validation.....	31
5.3.4 Simple Kriging.....	32
5.3.5 Back Transformation.....	33
5.4 Stochastic Simulation .....	34
6 Geometry of Sandstone Bodies .....	41
6.1 Previous Work .....	41
6.2 Local-Scale Architecture .....	41
6.3 Geostatistical Methods .....	43
6.3.1 Mini-Modelling.....	46
6.3.2 Sandiness-Flow Relationships .....	49
7 Interpretation of Model Results.....	53
7.1 Distributions of Sandstone and Mudstone.....	53
7.2 Hydrostratigraphic Framework .....	55
7.2.1 Sandstone Thresholds and Permeabilities.....	55
7.2.2 Regional Hydrostratigraphic Units in the Paskapoo Formation .....	56
7.2.2.1 Introduction .....	56
7.2.2.2 Haynes Aquifer.....	56
7.2.2.3 Lacombe Aquitard.....	64
7.2.2.4 Sunchild Aquifer .....	67

7.2.3 Hydrogeological Aspects .....	69
7.3 Discussion of Geological Interpretations .....	74
7.3.1 Speculations on Genesis and Sequential Development of the Internal Architecture of the Paskapoo Formation.....	74
7.3.1.1 Introduction – Architectural Models for Continental Strata.....	74
7.3.1.2 Deposition of the Paskapoo Formation .....	76
8 Summary.....	81
9 References.....	82
Appendix 1 – Methodology Flowcharts .....	85
Appendix 1a – Screening Digital Oil and Gas Gamma-Ray Logs to Calculate Net-Sand Thickness Using Slice-Mapping Methods .....	85
Appendix 1b – Constructing Datums for Depth-Slice Analysis of Gamma-Ray Logs .....	86
Appendix 1c – Screening Water-Well Lithologs to Calculate Net-Sand Thickness Using Slice-Mapping Methods .....	87
Appendix 1d – Calculating Per Cent Sand in 25 m Thick Slices Within a Water-Well and Screening Results for 3-D Modelling .....	88
Appendix 1e – Calculating Net-Sand Thickness in Oil and Gas Gamma-Ray Logs .....	89
Appendix 2 – Depth-Slice Maps of Relative Sandstone Abundance in the Paskapoo Formation.....	90
Appendix 3 – Mini-Modelling .....	95

## Tables

Table 1. Regional-scale sandiness model dimensions.....	28
---	----

## Figures

Figure 1. Distribution of the Paskapoo Formation, Scollard Formation, and extent of the Ardley coal zone (modified from Hamilton et al., 1999), central Alberta. Also shown is the Edmonton–Calgary Corridor study area. ....	2
Figure 2. Density of domestic water wells completed in the area underlain by the Paskapoo Formation, central Alberta. ....	3
Figure 3. Regional structural cross-section illustrating the westward-thickening, wedge-like geometry of the Paskapoo Formation and the underlying Scollard Formation, central Alberta (B. Hathway, work in progress, 2011). ....	5
Figure 4. Thickness (isopachs) of the Paskapoo Formation, central Alberta.....	6
Figure 5. Elevation of the top surface of the Paskapoo Formation (bedrock topography), central Alberta. .	7
Figure 6. Structural surface of the base of the Paskapoo Formation (top of Scollard Formation), central Alberta. ....	8
Figure 7. Stratigraphic subdivisions of the Paskapoo Formation in west-central Alberta proposed by Demchuk and Hills (1991). ....	10
Figure 8. Distribution of oil and gas wells used in this study to determine sandstone abundance in the Paskapoo Formation, central Alberta. ....	14
Figure 9. Distribution of water wells used in this study to determine sandstone abundance in the Paskapoo Formation, central Alberta.....	15

Figure 10. Type of well and number of wells with valid data used in this study, relative to height above the base of the Paskapoo Formation. ....	16
Figure 11. Structural cross-section illustrating both 25 m thick slices constructed parallel to the base of the Paskapoo Formation for analysis of sandiness from oil and gas gamma-ray logs, and 25 m thick slices (thin purple lines) constructed parallel to the bedrock topography for analysis of sandiness from water-well lithologs. ....	19
Figure 12. Estimation of sandstone abundance in the Paskapoo Formation using a) gamma-ray logs and b) water-well lithologs. Logs are from wells at different locations. ....	20
Figure 13. Three-dimensional distribution of approximately 14 570 sandstone-abundance values derived from depth-slice analysis of oil and gas gamma-ray logs, Paskapoo Formation, central Alberta. Values were derived from net sand estimates using a 75 API cutoff over a 25 m thick slice interval. ....	21
Figure 14. Comparison of water-well lithologs to nearby outcrops of Paskapoo Formation strata: a) view across North Saskatchewan River at Willey West Park, near Drayton Valley (Zone 11, 638046E, 5897802N, NAD83), outcrop approximately 500 m from borehole (Zone 11, 6377543E, 5897856N); and b) outcrop along North Saskatchewan River (Zone 11, 621180E, 5862369N), approximately 800 m from borehole (Zone 11, 621006E, 5861608N). ....	22
Figure 15. a) Sandiness of the upper 25 m of Paskapoo Formation using water-well litholog analyses and b) the resistivity of the upper 20 m below ground surface recorded by airborne electromagnetic surveys (Barker et al., 2011). ....	23
Figure 16. Three dimensional distributions of about 48 160 sandstone-abundance values derived from depth-slice analysis of water-well lithologs, Paskapoo Formation, central Alberta. ....	24
Figure 17. Jackknife validation results between the water-well litholog and gamma-ray (GR) log datasets. Water-well (WW) sandiness estimated from GR log data on the left. Gamma-ray log sandiness estimated from water-well data on the right. a) crossplots of true values and jackknife estimates of sandiness in normal-score units; b) crossplots of true values and jackknife estimates of sand proportion; c) accuracy plots; d) histograms of estimation variances, in normal-score units. Abbreviations: coef. of var., coefficient of variation; std. dev., standard deviation. ....	25
Figure 18. Three-dimensional distribution of approximately 62 700 sandstone-abundance values from the combined analyses of water-well lithologs and gamma-ray logs, Paskapoo Formation, central Alberta. ....	26
Figure 19. Vertical trend of the per cent sandiness within 25 m slices of the Paskapoo Formation with 95% confidence limits. ....	27
Figure 20. Cartoon of the Paskapoo Formation showing the 25 m slices parallel to the base and a conceptual boundary (dark line) between the Haynes and Lacombe members. ....	29
Figure 21. Omnidirectional horizontal variogram calculated from gamma-ray log data. ....	30
Figure 22. Omnidirectional horizontal variogram calculated from water-well litholog data. ....	30
Figure 23. Cross-validation results for the sandiness modelling. Abbreviation: std. dev., standard deviation. ....	31
Figure 24. Accuracy of the sandiness cross-validation. ....	32
Figure 25. Kriging estimates in the bottom slice of the sandiness model, Paskapoo Formation, central Alberta. ....	33
Figure 26. Kriging variances in the bottom slice of the sandiness model, Paskapoo Formation, central Alberta. ....	34

Figure 27. Back-transformed kriging estimates of sandiness values in the bottom slice of the model, Paskapoo Formation, central Alberta. ....	35
Figure 28. Back-transformed P10 (tenth percentile, low case) sandiness values in the bottom slice of the model, Paskapoo Formation, central Alberta. ....	36
Figure 29. Back-transformed P90 (ninetieth percentile, high case) sandiness values in the bottom slice of the model, Paskapoo Formation, central Alberta. ....	37
Figure 30. Unconditional simulated realization in the bottom slice of the model, Paskapoo Formation, central Alberta. ....	38
Figure 31. Conditional simulated realization in the bottom slice of the model, Paskapoo Formation, central Alberta. ....	39
Figure 32. Back-transformed simulated realization of sandiness in the bottom slice of the model, Paskapoo Formation, central Alberta. ....	40
Figure 33. Outcrops of sandstone-body types within the Paskapoo Formation, central Alberta: a) Whitecourt area (Zone 11, 579594E, 5984239N); b) North Saskatchewan River (Zone 11, 635404E, 5824455N); c) North Saskatchewan River (Zone 11, 623068E, 5853349N); d) North Saskatchewan River (Zone 11, 622862E, 5852491N); e) North Saskatchewan River (Zone 11, 629811E, 5841462N); f) North Saskatchewan River (Zone 11, 629118E, 5844863N). ....	42
Figure 34. Data histograms for the gamma-ray log data at a) 1 m increments and b) 25 m increments. ....	43
Figure 35. Examples of logs intersecting sandstone geobodies: a) logs intersecting splays and a single channel sandstone body (both shaded yellow) where only a single log intersects the full vertical extent of the largest sandstone body; b) logs intersecting a stacked channel sequence with small and large sandstone intervals encountered. ....	44
Figure 36. Vertical variogram of the gamma-ray log sandiness data at 1 m intervals. ....	45
Figure 37. Distribution of sandstone body thicknesses encountered in the gamma-ray log data showing the interpreted sandstone-body type corresponding to the different thicknesses. ....	45
Figure 38. Distribution of sandstone body thickness encountered in the gamma-ray log data showing the interpreted proportion of sandstone corresponding to each type of sandstone body. ....	46
Figure 39. Fence diagram of a mini-model created using the SISIM program. Blue is sandstone, grey is mudstone. ....	47
Figure 40. Fence diagram of a mini-model created using the ELLIPSIM program. Blue is sandstone, grey is mudstone. ....	48
Figure 41. Fence diagram of a mini-model created using the FLUVSIM program. Blue is sandstone, grey is mudstone. ....	49
Figure 42. Per cent sandiness versus horizontal permeability relationship derived from the FLUVSIM mini-modelling results. ....	50
Figure 43. Per cent sandiness versus vertical permeability relationship derived from the FLUVSIM mini-modelling results. ....	50
Figure 44. Simulated realization of horizontal permeability ( $k_h$ ) in the bottom slice of the model. ....	51
Figure 45. Simulated realization of vertical permeability ( $k_v$ ) in the bottom slice of the model. ....	52
Figure 46. Modelled 3-D distribution of sandiness within the Paskapoo Formation flattened to base of formation: a) oblique aerial view to west of modelled Paskapoo Formation and b) view to east of vertical slice along the undeformed western edge of the Paskapoo Formation. ....	54
Figure 47. Modelled 3-D distribution of sandiness within the Paskapoo Formation referenced to sea level. View to east of vertical slice along western edge of the undeformed edge of the Paskapoo Formation. ....	54

Figure 48. Probability of connected hydraulic paths with increase in sandstone abundance from three mini-model simulations (P50 curves) of the Paskapoo Formation. At about 55%–60% sandstone abundance in the FLUVSIM model, the probability that local sandstone bodies become vertically connected to form a regional system increases significantly. ....	55
Figure 49. a) West and b) east views showing the combined distribution of >55% sandstone isovalues and >65% mudstone isovalues in the Paskapoo Formation. c) West and d) east views showing only those parts of the Paskapoo Formation where sandstone isovalues are >55%. ....	57
Figure 50. Distribution of the Haynes aquifer. The figure is a composite of the >55% sandstone distribution of the first five 25 m thick slices above the base of the Paskapoo Formation. ....	58
Figure 51. a) Edge-on, section view of the Sunchild aquifer, Lacombe aquitard, and Haynes aquifer and b) structural surfaces of the tops of the Sunchild and Haynes aquifers. Remnants of the Sunchild aquifer almost onlap the Haynes aquifer as the wedge of muddy sediments of the Lacombe aquitard thins to the east. ....	59
Figure 52. Outcrop of stacked channel sandstone (interpreted as part of the Haynes aquifer within the Paskapoo Formation), Hard Luck Canyon, Whitecourt area (Zone 11, 579594E, 5984239N, elevation top ~815 m asl). ....	60
Figure 53. Elevation of the upper surface of the Haynes aquifer. ....	61
Figure 54. Thickness (isopachs) of the Haynes aquifer. ....	62
Figure 55. Stratigraphic relationship between the Haynes aquifer and the overlying Lacombe aquitard. ..	63
Figure 56. Distribution of Haynes aquifer at >55% and >70% sandstone isovalue thresholds. ....	63
Figure 57. Outcrop of mudstone, minor sandstone and ironstone (interpreted as part of the Lacombe aquitard within the Paskapoo Formation), Dickson Dam location (Zone 11, 690340E, 5765105N, NAD83, elevation top ~935 m asl). ....	64
Figure 58. Elevation of the upper surface of the Lacombe aquitard. ....	65
Figure 59. Distribution of the Lacombe aquitard. The figure is a composite distribution of >65% clayey sedimentary rock from 25 m thick slices, encompassing a thickness of as much as 350 m of muddy sedimentary rock. ....	66
Figure 60. Thickness (isopachs) of the Lacombe aquitard. ....	68
Figure 61. Outcrop of sandstone along the Obed mine road (interpreted as part of the Sunchild aquifer, Zone 11, 470934E, 5936971N, elevation ~1300 m asl). ....	69
Figure 62. Distribution of the Sunchild aquifer. The figure is a composite of the >55% sandstone distribution from 25 m thick slices, encompassing an elevation range of as much as 600 m within the Paskapoo Formation. ....	70
Figure 63. Comparison of the modelled distribution of the Sunchild aquifer with the sandiest areas of the upper 20 m of ground, as interpreted from airborne resistivity surveys. The regional pattern of sandiness in the airborne resistivity survey northeast of Rocky Mountain House is similar to that of the modelled Sunchild aquifer, and highlights the near-surface expression of sandstone-dominated bodies that comprise the Sunchild aquifer. ....	71
Figure 64. Elevation of the upper surface of the Sunchild aquifer. ....	72
Figure 65. Thickness (isopachs) of the Sunchild aquifer. ....	73
Figure 66. Location of high-producing licensed water wells within aquifers of the Paskapoo Formation. ....	74
Figure 67. Interplay between accommodation space and sediment supply resulting in stratigraphic stacking (modified from Shanley and McCabe, 1994, Figure 2, reprinted by permission of the American Association of Petroleum Geologists, whose permission is required for further use)... ..	75

Figure 68. Influence of avulsion styles on the architecture of channel sandstone bodies (modified from Mackey and Bridge, 1995, Figures 13–15, copyright permission granted by Society for Sedimentary Geology).....	77
Figure 69. Structural and depositional history of hydrostratigraphic units as interpreted from the model of sandiness within the Paskapoo Formation.....	79
Figure 70. Stacked channel sandstone complex within the Haynes aquifer, west of Drayton Valley, illustrating possible loci of stream emergence into foreland basin.....	80
Figure 71. Screening digital oil and gas gamma-ray logs to calculate net-sand thickness using slice-mapping methods.....	85
Figure 72. Constructing datums for depth-slice analysis of gamma-ray logs.....	86
Figure 73. Screening water-well lithologs to calculate net-sand thickness using slice-mapping methods.....	87
Figure 74. Calculating per cent sand in 25 m thick slices within a water-well and screening 3-D modelling.....	88
Figure 75. Calculating net-sand thickness in oil and gas gamma-ray logs.....	89
Figure 76. Distribution of sandstone in 25 m thick slices from 0 to 150 m above the base of Paskapoo Formation.....	90
Figure 77. Distribution of sandstone in 25 m thick slices from 150 to 300 m above the base of Paskapoo Formation.....	91
Figure 78. Distribution of sandstone in 25 m thick slices from 300 to 450 m above the base of Paskapoo Formation.....	92
Figure 79. Distribution of sandstone in 25 m thick slices from 450 to 600 m above the base of Paskapoo Formation.....	93
Figure 80. Distribution of sandstone in 25 m thick slices from 600 to 750 m above the base of Paskapoo Formation.....	94
Figure 81. Slices of the mini-model created using the SISIM program. Vertical exaggeration is 40 times. Dark areas are sandy, light areas are muddy.....	95
Figure 82. Mini-modelling variogram reproduction for SISIM.....	96
Figure 83. Sandiness–permeability relationships from the SISIM mini-models. Abbreviation: std. dev., standard deviation.....	97
Figure 84. Slices of the mini-model created using the ELLIPSIM program. Vertical exaggeration is 40 times. Dark areas are sandy, light areas are muddy.....	98
Figure 85. Mini-modelling variogram reproduction for ELLIPSIM.....	99
Figure 86. Sandiness–permeability relationships from the ELLIPSIM mini-models. Abbreviation: std. dev., standard deviation.....	100
Figure 87. Slices of the mini-model created using the FLUVSIM program. Vertical exaggeration is 40 times. Dark areas are sandy, light areas are muddy.....	101
Figure 88. Mini-modelling variogram reproduction for FLUVSIM.....	102
Figure 89. Sandiness–permeability relationships from the FLUVSIM mini-models. Abbreviation: std. dev., standard deviation.....	103

## Acknowledgements

The authors acknowledge the following individuals at the Alberta Geological Survey for their contribution to this report:

- B. Hathway's work to define the base of the Paskapoo Formation from petroleum geophysical well logs was an important element in our analysis of aquifer systems within the Paskapoo Formation. We are also appreciative of B. Hathway's critical review of our report.
- P. Glombick, N. Atkinson, and D. Bechtel provided many critical and useful comments on the report.
- S. Slattery's classification of geological units from water-well drillers' lithologs provided the link to integrate descriptive information with downhole geophysical well logs.
- G. Jean's management of large and diverse datasets and databases was critical to the success of the geostatistical analysis of hydrostratigraphic units in the Paskapoo Formation.

The authors also wish to acknowledge the contributions and improvements to this report made by the following reviewers:

- L. Bentley, University of Calgary
- J. Boisvert, University of Alberta
- K. Parks, ERCB

## Abstract

The Paskapoo Formation is one of the largest and most intensely used bedrock aquifer systems in Alberta, yet little is known about the internal architecture of the major hydrostratigraphic units contained within. This study summarizes the results of a computer-based geostatistical analysis of more than 35 000 borehole logs from the petroleum and water-well industries in an effort to define the internal three-dimensional geometry of sandstone bodies that can be considered regional aquifers. Sandstone abundance was estimated using cutoffs on gamma-ray logs and from an expert-based, subjective classification of sandiness from drillers' lithologs, and averaged in a series of 25 m thick slices extending through 750 m of sedimentary rock within the Paskapoo Formation. Analysis of the sandiness estimates reveals information on the relative abundance and three-dimensional distribution of sandstone found in splay and channel depositional settings.

A three-dimensional variogram analysis of sandiness data derived from depth-slice mapping methods enabled the construction of a regional, three-dimensional model of the subsurface distribution of sandstone- and mudstone-dominated units in the Paskapoo Formation. An analysis of the thickness of sandstone intervals in boreholes and a workflow using mini-models were used to determine the geometry of channel and splay sandstone bodies at a local scale within the Paskapoo Formation. To delineate those parts of the sandstone distribution model that would constitute an aquifer, we first derived horizontal and vertical permeabilities from the mini-models and determined that sandstone bodies in the Paskapoo Formation likely become hydraulically connected in horizontal and vertical directions when sandstone abundance exceeds 55% of the volume. Applying the >55% sandstone abundance cutoff as the criterion that defines an aquifer, we tested our model to see what shape and volume of rock was represented by this value. We similarly determined that if sandstone abundance is below 35%, there is a significant reduction in vertical permeability. We used this criterion to define our mudstone-dominated (or aquitard) units.

The delineation of an internal architecture of the Paskapoo Formation, including two regional aquifers and one aquitard, emerged from the application of this aquifer/aquitard cutoff criterion. The lowermost unit is correlative with sandstone of the Haynes Member and we refer to it as the Haynes aquifer. Overlying the Haynes aquifer is a regionally extensive mudstone- and siltstone-dominated unit correlative with the Lacombe Member, which we refer to as the Lacombe aquitard. The uppermost unit is a sandstone-dominated unit, which we herein name the Sunchild aquifer. Planimetric maps have been constructed showing approximate distribution and structural and erosional surfaces within each unit. Recently collected airborne resistivity data helped to both define and confirm the subcrop geometry of each of these units.

The combination of isopach and structural surface maps for each of the hydrostratigraphic units provides insight into the tectonic history of the Alberta Basin during deposition of the Paskapoo Formation. The deformed surface, consisting of the amalgamation of sandstone bodies that define the Haynes aquifer, indicates deposition prior to a phase of mountain building to the west. The Lacombe aquitard, which forms the bulk of the Paskapoo Formation, occupies the foreland accommodation space, possibly created by enhanced subsidence. An apparent vertical propagation of sandstone bodies from the Haynes aquifer upward into the Lacombe aquitard along the eastern edge of the foothills possibly marks the locus of sediment shed eastward from the rising Cordillera. The (undeformed) upper Sunchild aquifer lies atop the Lacombe aquitard and extends eastward into the Alberta Plains as an eastward-thinning wedge. Subsequent erosion during the middle to late Paleogene resulted in all three units subcropping beneath a Quaternary sedimentary cover.

# 1 Introduction

A significant increase in economic activity and population growth has placed demands on Alberta's potable water supplies over the past decade. This, combined with climatic fluctuations, has led to restrictions on the allocation of surface-water use in parts of the province, and, at the same time, has heightened awareness of groundwater resources as an alternative. In response to the concern that Alberta's groundwater resources are poorly understood, the Alberta Geological Survey (AGS) partnered with Alberta Environment and Sustainable Resource Development (ESRD) to conduct a multi-year study of groundwater resources in the most populated and industrialized part of the province: the corridor between Calgary and Edmonton, so called the Edmonton–Calgary Corridor (ECC; Figure 1). More than half of the ECC study area is underlain by the Paskapoo Formation, which supplies groundwater to more than 120 000 domestic users (Figure 2) and more than 30 000 licensed users, and is considered to be one of the largest and most prolific aquifers in Alberta.

Numerous studies have recognized the importance of the Paskapoo Formation as a groundwater source and have attempted to assess the regional distribution and sustainable yield of its associated aquifer systems (Hamblin, 2004; Grasby et al., 2008; Burns et al., 2010a, b). The AGS recently evaluated the risk to groundwater from coalbed methane development by characterizing the internal architecture of the Paskapoo Formation from the perspective of natural hydraulic pathways both within the formation, as well as between the Paskapoo Formation and underlying coal beds of the Scollard Formation (Parks and Andriashek, 2009).

The Paskapoo Formation is a heterogeneous assemblage of nonmarine mudstone and siltstone together with single- and multi-storey sandstone units that defy easy classification within a hydrostratigraphic framework. However, the spatial distribution of heterogeneous porous sedimentary rocks is one of the most important elements in the construction of a regional groundwater-flow model, perhaps even more important than hydraulic parameter inputs (Fogg, 1986). Attempts to

subdivide the Paskapoo Formation have been based on the occurrence and distribution of sandstone, mudstone/siltstone, and coal (Demchuk and Hills, 1991); the presence of a disconformable sandstone/conglomerate unit within the formation (Jerzykiewicz, 1997); and on palynology, biostratigraphy, and magnetostratigraphy (Lerbekmo and Sweet, 2000, 2008; Lerbekmo et al., 2008). Although these subdivisions may be evident at the borehole, outcrop, or local scale, regional correlations have largely been conceptual in nature and difficult to apply to defining discrete, mappable aquifer units.

Recognizing past challenges in defining hydrostratigraphic units within the Paskapoo Formation from conventional well-to-well correlation methods, our study was designed to characterize the formation from the perspective of mapping regional differences and trends in sandiness as a means to define aquifer systems. We applied a probabilistic approach to demonstrate the application of computer-assisted analysis and geostatistical mapping methods to integrated datasets from the water-well and petroleum industries to construct a three-dimensional (3-D) model of sandstone (aquifer) and mudstone (aquitard) distributions within the Paskapoo Formation. The model enables us to vary criteria, such as defining values for sandiness, to reveal differences in the distribution and geometry of the resulting aquifer body. The model also permits the simulation of possible distributions of sandstone- and mudstone-dominated units within the formation and how aquifer geometry varies accordingly. By applying smaller-scale flow simulations, predictions can be made about the nature and degree of both horizontal and vertical hydraulic connections between sandstone units, thereby providing input for numerical modelling and simulations of groundwater flow.

This report describes the geostatistical approach used to construct a 3-D model of sandstone and mudstone distribution within the Paskapoo Formation and discusses the geological and hydrogeological implications of our model. We conclude that two regional Paskapoo aquifer systems can be defined using our approach.

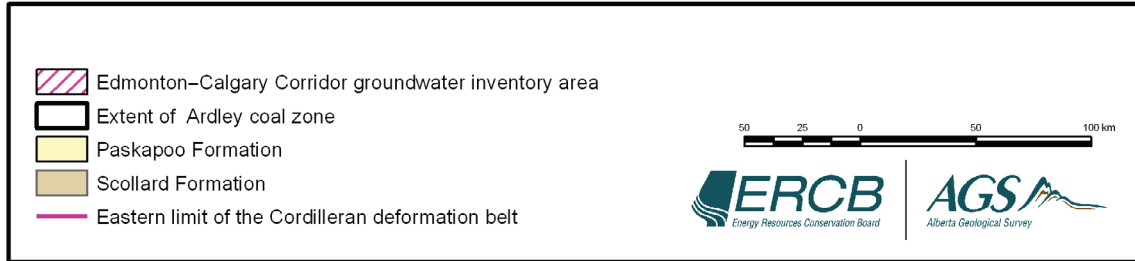
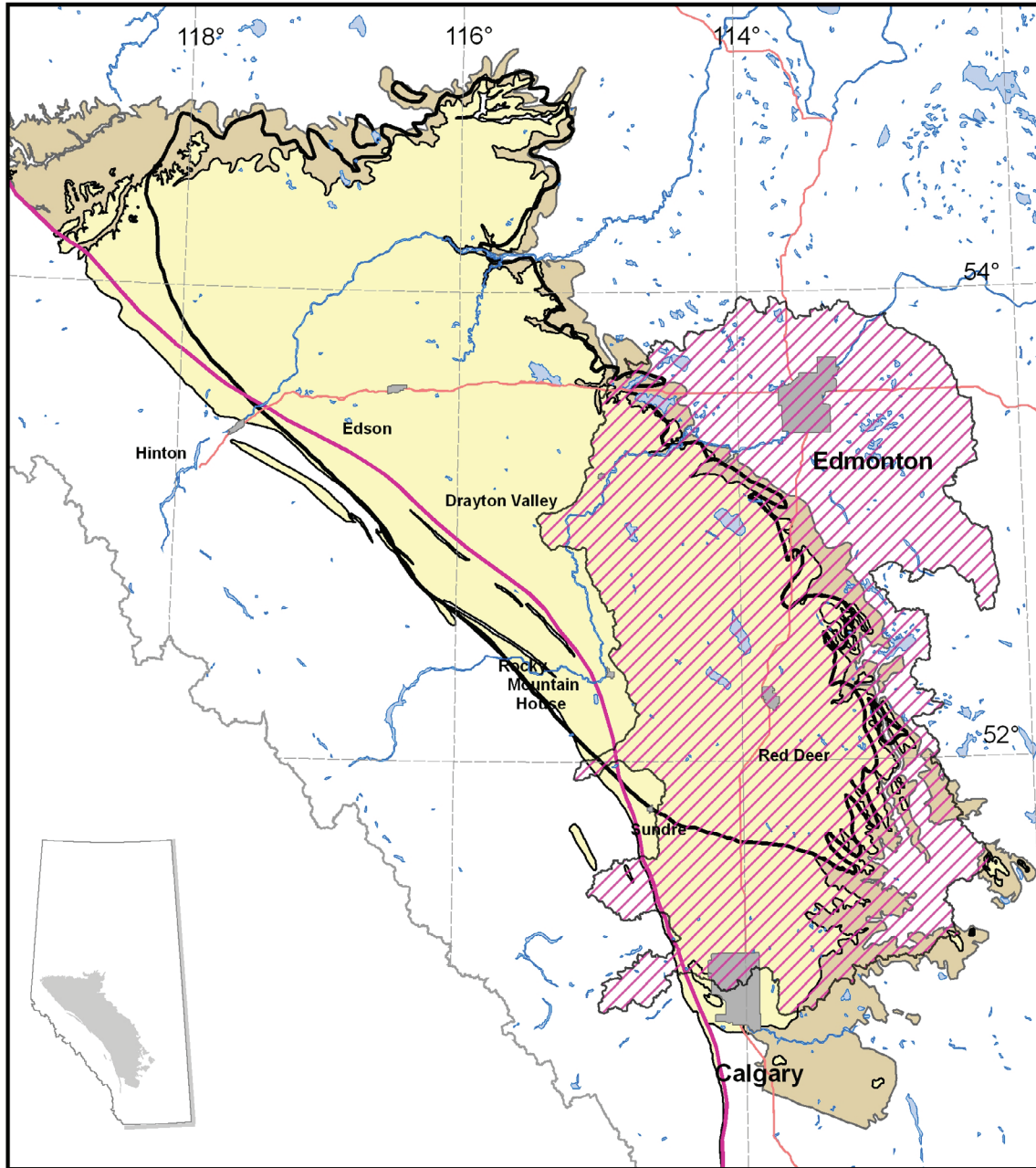


Figure 1. Distribution of the Paskapoo Formation, Scollard Formation, and extent of the Ardley coal zone (modified from Hamilton et al., 1999), central Alberta. Also shown is the Edmonton-Calgary Corridor study area.

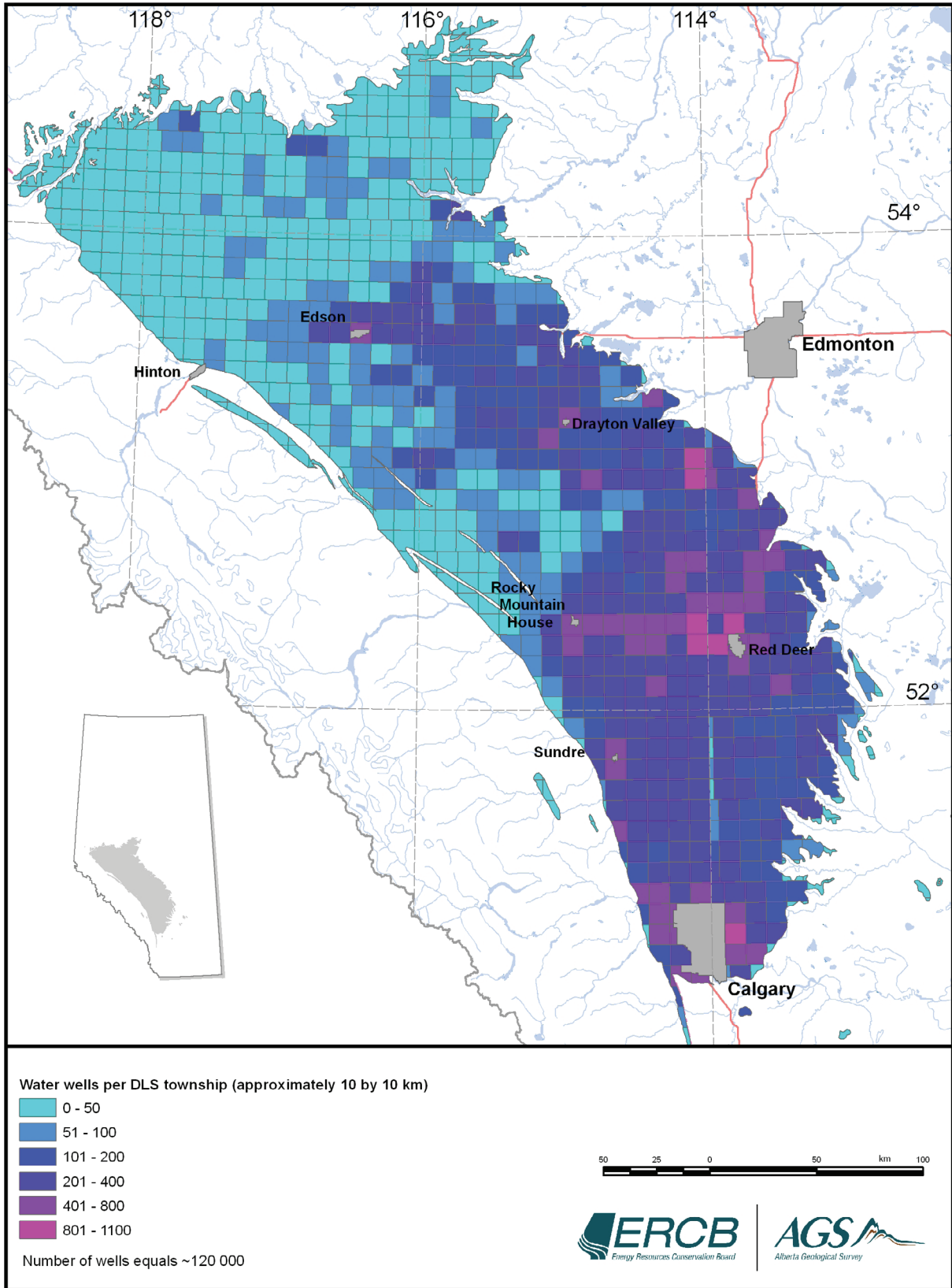


Figure 2. Density of domestic water wells completed in the area underlain by the Paskapoo Formation, central Alberta.

## 2 Geological Setting

### 2.1 Background

The Paleogene Paskapoo Formation constitutes the uppermost preserved clastic unit of a series of eastward-thinning, continentally derived wedges deposited in a foreland setting within the Alberta Basin (Jerzykiewicz, 1997; Hamblin, 2004). Strata in the lower part of the Paskapoo Formation lie in a shallow homocline that dips westward, forming the eastern limb of the Alberta Syncline. In contrast, upper strata of the Paskapoo Formation are nearly horizontal due to the eastward-tapering wedge geometry of the formation (Hamblin, 2004; Figure 3).

The Paskapoo Formation comprises dominantly alluvial fan and fluvial floodplain facies resulting from deposition associated with orogeny (Hamblin, 2004). Dominant lithologies consist of light grey, buff-weathering sandstone and grey siltstone and mudstone with minor coal. From its eastern subcrop and outcrop margin, the Paskapoo Formation increases in thickness westward to as much as 800 m at the margin of the Cordilleran deformation belt (Figure 4). The upper boundary of the Paskapoo Formation is an erosion surface, which marks the bedrock top across its extent (Parks and Andriashek, 2009; Figure 5). An evaluation of the quality and rank of coal beds in the near-surface of the Alberta Plains indicates that these coal beds had previously been buried by sedimentary cover at depths of at least 900 m, implying that the thickness of the Paskapoo Formation may have been significantly greater prior to erosion (Nurkowski, 1985). Discontinuous deposits of Neogene gravel or Quaternary sediment unconformably overlie the Paskapoo Formation.

Although there has been considerable debate regarding the placement of the lower boundary of the Paskapoo Formation (Demchuk and Hills, 1991; Jerzykiewicz, 1997; Hamblin, 2004), it is generally accepted that the first thick sandstone that overlies the uppermost coal seam of the Ardley coal zone of the Scollard Formation defines the base (Gibson, 1977; Demchuk and Hills, 1991). Parks and Andriashek (2009) argued that

this definition of the lower boundary is dependent on the distribution of sandstone channels, and that time-equivalent, fine-grained sedimentary rocks of the Paskapoo Formation would therefore be included in the upper Scollard Formation. In the south, the base of the Paskapoo Formation is more difficult to define because distinctive log responses are lacking (Lerbekmo and Sweet, 2000; Chen et al., 2007). Lerbekmo et al. (1990, 1992) and Lerbekmo and Sweet (2000, 2008) show that the basal Paskapoo Formation rests disconformably on the Scollard Formation, with a hiatus of about 1.2 million years, based on magnetostratigraphy along the Red Deer valley, southeast of Red Deer.

In the absence of other criteria, the AGS has adopted Gibson's (1977) approach to differentiate the Paskapoo Formation from the underlying Scollard Formation (i.e., the first thick sandstone above the uppermost coal seam of the Ardley coal zone) but additionally defines 'thick sandstone' to be 5 m thick or more. Figure 6 shows a structural surface of the base of the Paskapoo Formation modelled from B. Hathway's stratigraphic picks. These picks were from oil and gas gamma-ray (GR) logs, and the base of the formation was placed at the base of the lowermost sandstone unit with a thickness of >5 m and situated above the Ardley coal zone. The figure illustrates an elongated, concave surface with a westward-dipping central region flanked by higher elevations to the northwest and southeast. Section 4 gives details of the construction of this surface and its importance as a datum for geostatistical analysis of sandiness within the Paskapoo Formation.

### 2.2 Paskapoo Formation Subdivisions

#### 2.2.1 Internal Stratigraphic Divisions

Demchuk and Hills (1991) were the first to propose an informal stratigraphic subdivision of the Paskapoo Formation. Incorporating outcrop observations, core descriptions from boreholes, and palynology, they recognized a three-member division exhibiting a generally fining-upward succession, from coarse-grained sandstone to siltstone and mudstone. Thick,

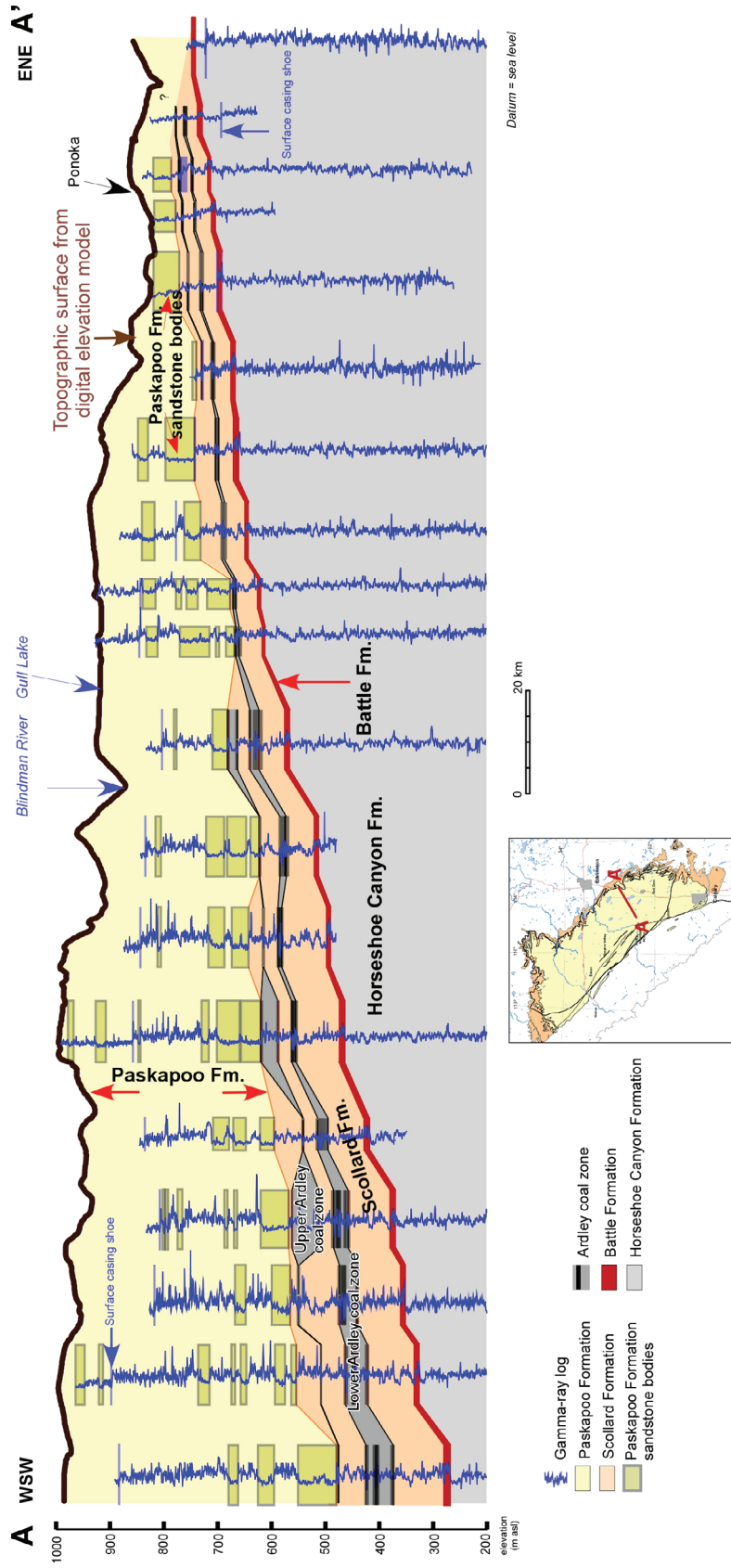


Figure 3. Regional structural cross-section illustrating the westward-thickening, wedge-like geometry of the Paskapoo Formation and the underlying Scollard Formation, central Alberta (B. Hathway, work in progress, 2011).

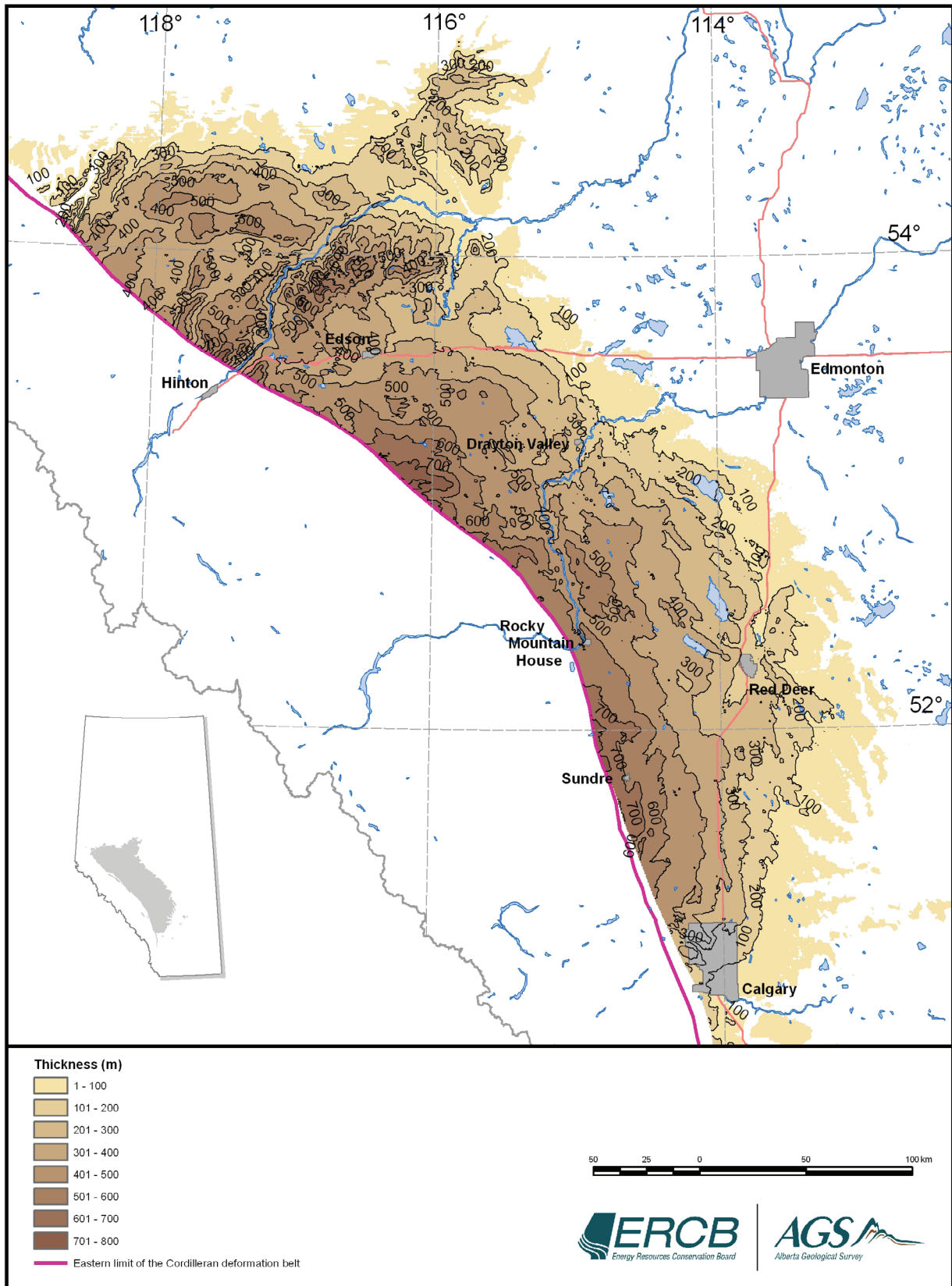


Figure 4. Thickness (isopachs) of the Paskapoo Formation, central Alberta.

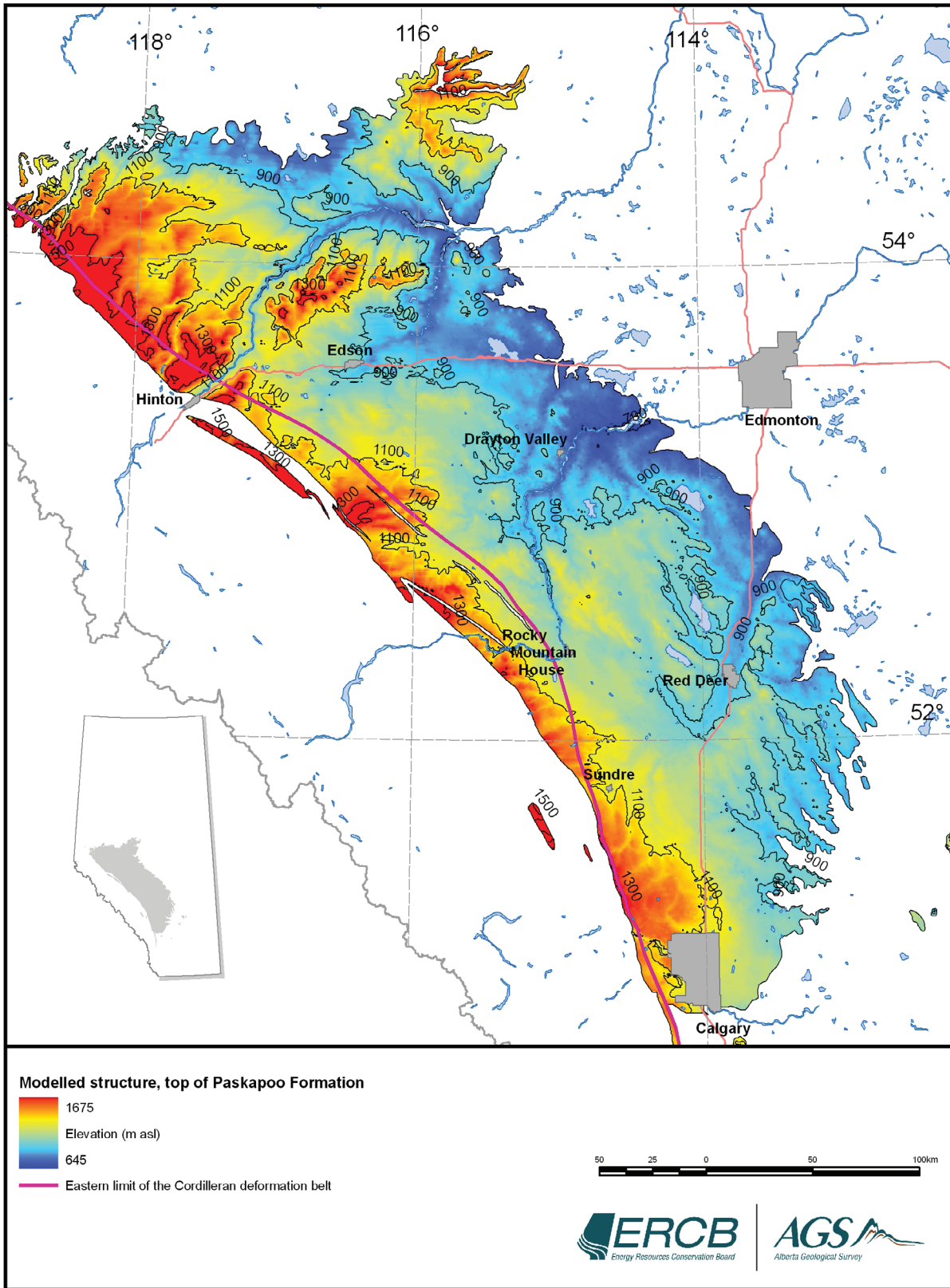


Figure 5. Elevation of the top surface of the Paskapoo Formation (bedrock topography), central Alberta.

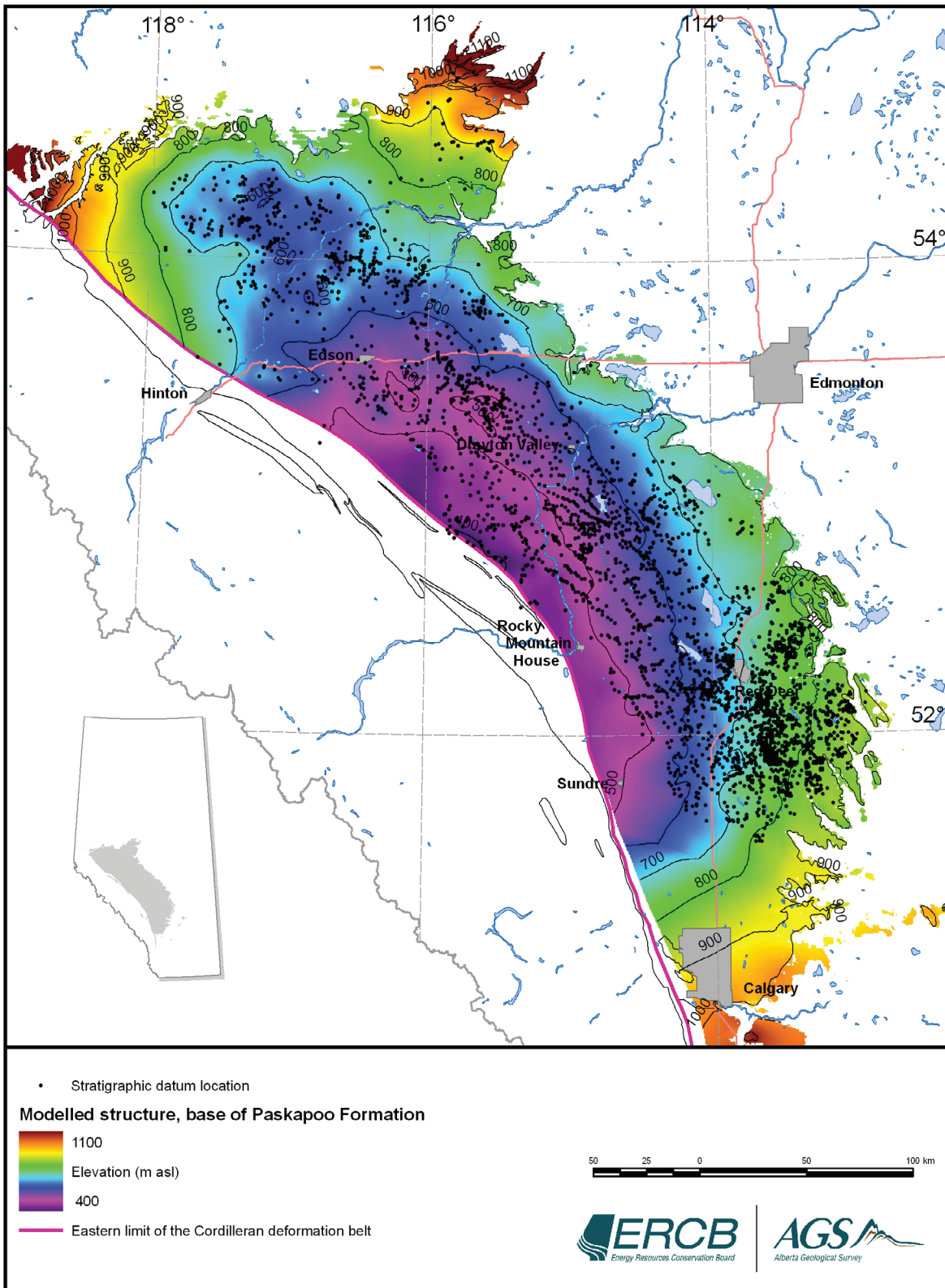


Figure 6. Structural surface of the base of the Paskapoo Formation (top of Scollard Formation), central Alberta.

massive, conglomeratic sandstone characterizes the lowermost Haynes Member (Figure 7). Multi-storey channel bodies collectively form a regionally extensive and apparently continuous unit up to 100 m thick (Demchuk and Hills, 1991; Hamblin, 2004; Grasby et al., 2008). In outcrop, this channel sandstone unit weathers to a buff colour and forms resistant cliffs along valleys. This characteristic may have biased early interpretations of the Paskapoo Formation as being dominantly composed of sandstone. In GR and resistivity logs, sandstone of the Haynes Member is easily recognized by its uniform, blocky signature and its abrupt lower contact with siltstone and mudstone of the underlying Scollard Formation. The Haynes Member has an erosional, unconformable contact with the underlying Scollard Formation, which exhibits variable relief and evidence of incision and deposition of conglomeratic beds directly above coal of the upper Ardley coal zone (Parks and Andriashek, 2009).

Whereas channel sandstone bodies of the Haynes Member are prominent in outcrop, siltstone and mudstone of the overlying Lacombe Member constitute the bulk of the middle Paskapoo Formation (Demchuk and Hills, 1991; Figure 7). Light grey to olive-green, interbedded siltstone and mudstone, with thin coal or carbonaceous beds and minor sandstone and conglomerate, characterizes the Lacombe Member. Because of its recessive nature, outcrops of the Lacombe Member are relatively uncommon. The member is inferred to form the present-day bedrock surface over much of the central subcrop area of the Paskapoo Formation.

The Dalehurst Member, the uppermost member of the Paskapoo Formation defined by Demchuk and Hills (1991), is composed of interbedded sandstone, siltstone, mudstone, shale, and coal, with the type section (type log) dominated by sandstone and siltstone. The Dalehurst Member is differentiated primarily by the occurrence of thick coal beds of the Obed-Marsh coal zone, which is close to the Cordilleran deformation front in the Hinton area. Demchuk and Hills (1991) debated whether these thick coal beds were lateral facies equivalents of thinner coal seams in the upper part of the Lacombe Member to the southeast in

the Red Deer area. Demchuk and Hills (1991) also struggled with defining the lower contact of the Dalehurst Member in the Obed-Marsh area, as indicated by their description of the contact in core from the type section. The Dalehurst Member is confined to a small erosional remnant located northeast of Hinton and cannot be easily correlated eastward into the plains.

Jerzykiewicz (1997) discussed the depositional facies and environments of Paskapoo Formation strata in the context of five geographically defined regions. In his view, the Paskapoo Formation records the progressive eastward transition from coarse alluvial fan facies, deposited close to the deformation belt, to fluvial channel deposits in central Alberta and fine-grained sediments deposited in distal fluviolacustrine and swamp settings farther to the east. Jerzykiewicz (1997) highlighted three factors that make it difficult to define regional stratigraphic relationships within the Paskapoo Formation:

- an absence of index fossils throughout
- an absence of a continuous surface section to correlate Foothills outcrop with those in the Plains
- an incomplete subsurface record, owing in large part to limited hydrocarbon potential and lack of exploratory drilling and logging

Nevertheless, Jerzykiewicz (1997) divided the Paskapoo Formation into informal upper and lower members. A thick, continuous, basinwide sandstone unit, attributed to flash-flood deposition, defines the base of the lower member.

The basal sandstone unit that defines Demchuk and Hills' (1991) Haynes Member correlates to this lower sandy member. A regional southeast trend in distribution of the basal sandstone unit of the lower member coincides with deposition within a depocentre trending southeast along the axis of the Alberta Basin (Jerzykiewicz, 1997). Similarly, sandstone or conglomerate, which characteristically forms cliffs, cuestas, or steep escarpments, defines the base of the upper member. Jerzykiewicz (1997) attributed these coarse-grained intervals to deposition by flash floods that carried sediment in a dominantly northeastward direction, transverse to the foothills.

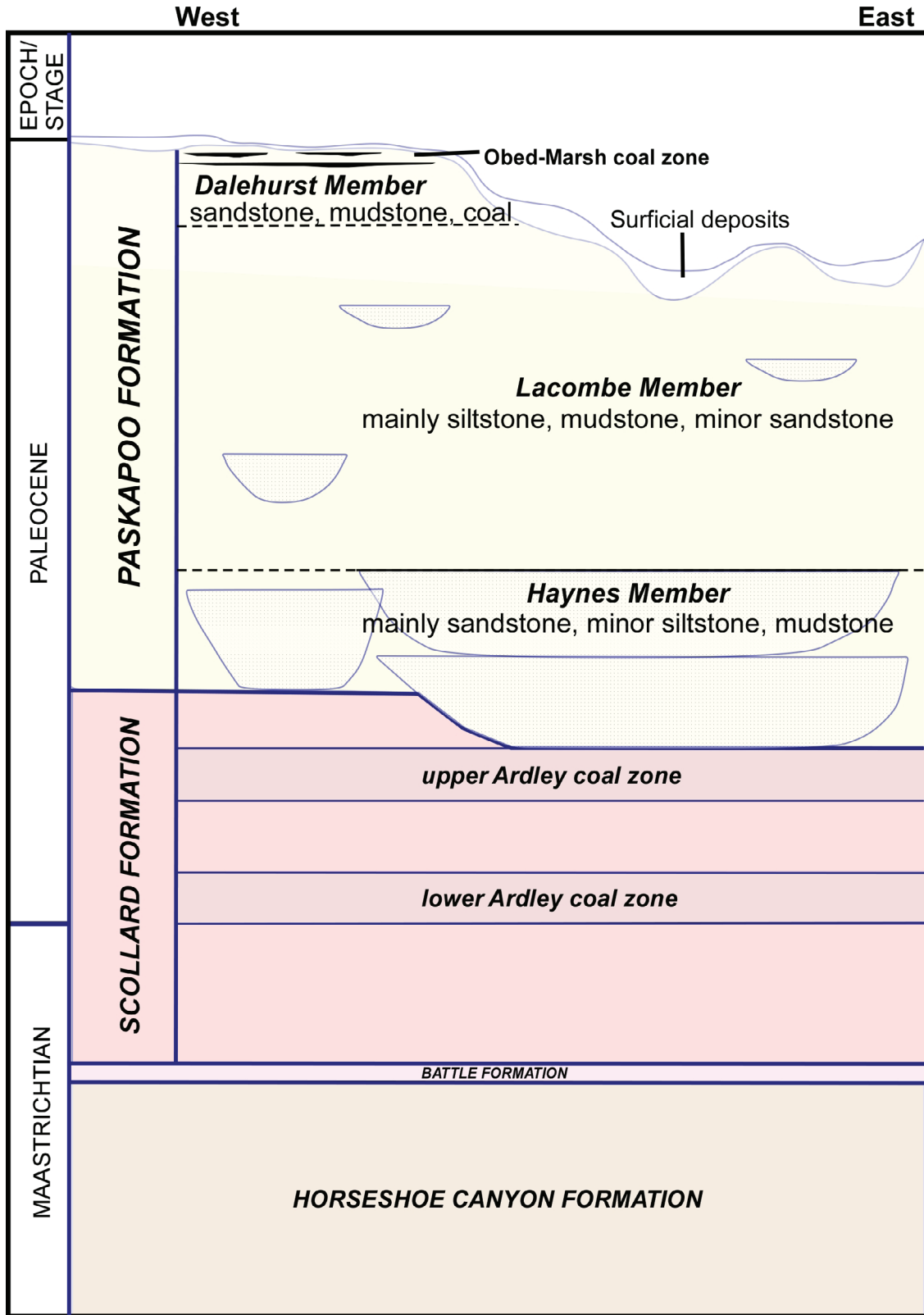


Figure 7. Stratigraphic subdivisions of the Paskapoo Formation in west-central Alberta proposed by Demchuk and Hills (1991).

Demchuk and Hills (1991) and Jerzykiewicz's (1997) stratigraphic subdivisions of the Paskapoo Formation were both based more on observations at point locations than on regional correlation and mapping of lithological rock properties from large datasets. Neither study generated interpretations of the subsurface distribution of the members nor delineated boundaries and distributions of rock properties in the three dimensions required to define major aquifer systems.

### **2.2.2 Hydrostratigraphic Characterization**

The basis of groundwater modelling is defining a hydrostratigraphic framework grounded in geology. For purposes of modelling groundwater flow, intrinsic rock properties (such as porosity and permeability) and the 3-D distribution of those properties must define the hydrostratigraphic units. In other words, they must be mappable. The difficulty of characterizing aquifers in heterogeneous rock units and the challenges of understanding groundwater flow in interconnected sandstone bodies within multiple aquifer systems was addressed by Fogg (1986), who concluded that sandstone-body interconnectedness could not be reliably predicted using qualitative geological methods but could be achieved using geostatistics or other stochastic approaches.

Most of the Paskapoo Formation consists of fine-grained sedimentary rocks with thin sandstone layers (Hamblin, 2004). Intervals of these fine-grained facies range up to tens of metres in thickness and are interpreted to have been deposited in regionally extensive floodplains. These fine-grained rocks are considered to function as local aquitards. Coarse-grained rocks within the Paskapoo Formation occur as single and stacked channel sandstone bodies, or thin, individual sandstone beds interpreted as crevasse splays (Jerzykiewicz, 1997; Hamblin, 2004; Grasby et al., 2008). Individual channel sandstone bodies may be up to 15 m thick (typically between 5 and 10 m) and pinch out laterally over several hundred metres. Stacked channel sandstone intervals may be up to 50 m thick and extend laterally for hundreds to thousands of metres. From the perspective of defining aquifer units, these stacked channel sandstone complexes can be considered thick, but laterally confined, aquifers.

Splay sandstone beds are generally <3 m thick (typically <1 m), with lateral extents of <100 m.

Regional correlation of single and stacked fluvial channel bodies nested within fine-grained floodplain deposits in the Paskapoo Formation has proven to be difficult using conventional geological mapping methods. Recent studies have attempted to map the spatial variation of rock properties within the Paskapoo Formation by applying automated analytical mapping methods to digital datasets. Chen et al. (2007) calculated net sandstone thickness and porosity from quantitative analysis of GR logs in wells completed within the lower part of the Paskapoo Formation (Jerzykiewicz's [1997] lower member). Their analysis revealed a regional aquifer at the base of the Paskapoo Formation that appears to be continuous along a northwest trend. They concluded that other aquifers in the Paskapoo Formation do not comprise regionally continuous sheets, but instead comprise isolated-to-coalesced channel systems with limited spatial extent.

Following the work of Chen et al. (2007), Grasby et al. (2008) incorporated water-well litholog data to address the gap in GR coverage caused by cased portions of oil and gas wells in the uppermost part of the Paskapoo Formation. Grasby et al. (2008) demonstrated that maps of sandstone ratios derived from water-well data have a similar pattern to those of Chen et al. (2007) with high sandstone ratios in a northwest trend, parallel to the deformation belt and the axis of the Alberta Basin. Although Grasby et al. (2008) concluded that sandstone-body trends have a southeast orientation near the Foothills, they believed dominant paleoflow was to the northeast, suggesting that sandstone channel aquifer systems may have greater continuity in that direction (cf. Jerzykiewicz, 1997).

To assess the effects of coalbed methane development within the Ardley coal zone on water wells, Parks and Andriashek (2009) investigated two key hydrogeological components of the Paskapoo Formation: the degree of hydraulic connection between the Ardley coal zone and the overlying Paskapoo Formation, and the degree of hydraulic connection and continuity within the Paskapoo Formation itself. Critical to this assessment of potential hydraulic behaviour was

the development of a method to assess variability in permeability using existing data sources. Parks and Andriashek (2009) characterized the spatial variability of permeability by determining sandstone abundance from the analysis of GR logs in 50 m thick slices through the Scollard and Paskapoo formations. Based on observed lithofacies and gas-derived permeability values from core, GR values of <75 API (American Petroleum Institute standard unit of measure for GR response) were considered to be representative of sandstone. The results of the depth-slice analysis demonstrated that the lowermost 150 to 200 m of the Paskapoo Formation includes regionally extensive zones of >40% sandstone abundance, and in many zones >60% sandstone abundance, which collectively form an elongated trend subparallel to the Cordilleran deformation front. This lower, sandy interval is capped by >300 m of sedimentary rock with generally <40% vertically averaged sandstone abundance, which Parks and Andriashek (2009) considered correlative to the Lacombe Member (Demchuk and Hills, 1991). The presence of commercially significant quantities of gas at the base of this member suggests that this finer grained unit acts as a hydrocarbon seal. Although oil- and gas-well data are sparse for the upper parts of the Paskapoo Formation, Parks and Andriashek (2009) mapped a narrow belt of high sandstone abundance adjacent to the Cordilleran deformation front, which they speculated might be equivalent to the Dalehurst Member (Demchuk and Hills, 1991).

Parks and Andriashek (2009) applied percolation theory (Stauffer and Aharony, 1994) to demonstrate that with an increasing abundance of sandstone, there is a threshold at which discrete sandstone bodies encased in mud become connected to other sandstone bodies, and vertical hydraulic pathways are established. They used sandstone abundance, determined from depth-slice maps, to help assess hydraulic continuity within the Paskapoo Formation and concluded that where regional sandstone abundances are above a regional percolation threshold (>60% sandstone), sandstone hydraulic conductivity values should be used to characterize regional formation transmissivity. Conversely, where regional sandstone abundances are below the regional percolation threshold (<40% sandstone),

mudstone hydraulic conductivity values should be used to characterize formation transmissivity. A later section of this report will introduce the principle of critical permeability thresholds and show its application as a criterion to help define aquifer systems and aquifer geometry in the Paskapoo Formation when using depth-slice mapping methods.

Recently developed object-based, stochastic-numerical groundwater-flow models can evaluate the influence of various geological parameters on groundwater flow within the upper 100 m of the Paskapoo Formation (Burns et al., 2010a, b; Matthews, 2011). From the analysis of water-well lithologies and outcrop observations, Burns et al. (2010a) tested such parameters as fraction of facies (channel, splay, or floodplain deposits) and channel geometry (channel width, width-to-thickness ratio, sinuosity as determined from modern-day analogs, and meander amplitude) and assigned hydraulic conductivity values to the facies based on air-permeametry tests. Burns et al. (2010b) developed a rule-based, upscaling algorithm to generate an irregular, coarse modelling grid that matches channel geometry, minimizes boundary effects, and facilitates ease of computation. The grid was populated with relevant hydraulic parameters, and flow simulations were conducted using HydroGeoSphere modelling software. Matthews (2011) similarly applied a 3-D, object-based facies model to arrive at realistic geometries of geological shapes and the distributions of hydrofacies within the Paskapoo Formation. Both studies demonstrated that flow in channel sandstone bodies within the Paskapoo Formation is anisotropic, with effective conductivities being highest along the channel axis and lowest in the vertical direction. Burns et al. (2010a) found that the longitudinal hydraulic conductivity of paleochannels is a function of the fraction of channel sandstone facies (thickness of channel sandstone as a per cent of the upper 100 m of formation), the conductivity of the channel facies, and the channel sinuosity. Conductivity was most sensitive to those factors that most influenced the frequency of channel intersection (i.e., channel fraction and channel sinuosity), with along-channel flow being about two orders of magnitude greater than in the vertical direction.

## 3 Data Sources

### 3.1 Data Type and Distribution

In this bulletin, the hydrostratigraphic interpretations of the Paskapoo Formation were assessed by calculating sandstone abundance using downhole well-log data. The analysis incorporated two sources of log data:

- digital data consisting of about 2400 oil- and gas-well geophysical logs (Figure 8), specifically GR logs in ASCII (log ASCII standard [LAS]) format
- descriptive data consisting of about 33 500 water-well drillers' lithologs (Figure 9)

Gamma-ray logs are numerous in the central parts of the study area but decrease in abundance to the south and east (Figure 8). In contrast, water-well litholog coverage is more densely distributed in the central populated areas and to the southeast, but is sparse in unpopulated areas to the north and west (Figure 9). Because the middle to lower parts of the Paskapoo Formation subcrop or outcrop in central and southeastern parts of the study area, there is correspondingly a greater amount of water-well litholog data available for that interval (Figure 10). Nevertheless, water-well litholog data span almost the entire range of the Paskapoo Formation, from less dense data for the uppermost part of the formation in the west, to an abundance of data near the base of the formation in the east.

Water-well litholog and GR log data also differ in their 3-D distribution within the Paskapoo Formation. As discussed previously, the Paskapoo Formation is the uppermost bedrock unit across its subcrop extent, and therefore steel casings generally protect the upper parts of the formation from drill fluids. GR logs for most oil and gas wells do not extend to surface but terminate at the base of the cased portion of the hole. In many locations, this casing depth extends as much as 150 m below surface. For this reason, GR logs provide more information about the lower part of the Paskapoo Formation than the upper part (Figure 10). This is why the eastern part of the study area is under-represented by GR log data, since the base of the Paskapoo Formation is

within 150 m of surface and is therefore obscured by the casing (Figure 8). Conversely, downhole information from the water-well industry describes the lithology from surface down to the first source of potable water (generally to depths of <150 m). Thus, water-well litholog data better represents the geology of the upper parts of the Paskapoo Formation.

Although Figure 10 provides no information regarding the spatial distribution of data, it illustrates that, collectively, there is a greater amount of information from both water-well and GR logs for the lower parts of the Paskapoo Formation than the upper parts. To a large degree, this abundance reflects a greater number of water wells progressively intersecting the lower part of the formation as it rises to the northeast, and the prevalence of surface casing in the oil and gas wells drilled through the upper parts of the formation.

In summary, the combination of water-well litholog and GR log datasets ensures that one or both sets of data represent most of the rock record of the Paskapoo Formation and that analysis of sandiness can extend from the surface to the base of the formation. However, because of the differences in data density and 3-D distribution, subjective litholog data play a bigger role in determining sandstone abundance in the eastern and southern parts of the study area than do GR log data.

### 3.2 Data Screening and Culling

Figures 71–75 in Appendix 1 detail the data screening procedures undertaken to ensure appropriateness of LAS data for sandstone determinations. To facilitate ease of computation, proprietary software (VIEWLOG) was used to convert LAS data into binary format. Next, depth information was standardized to metric units. To ensure consistency and quality of the GR log data, only those logs recorded after 1985 were selected, since the well-logging industry introduced standardized calibration of tools

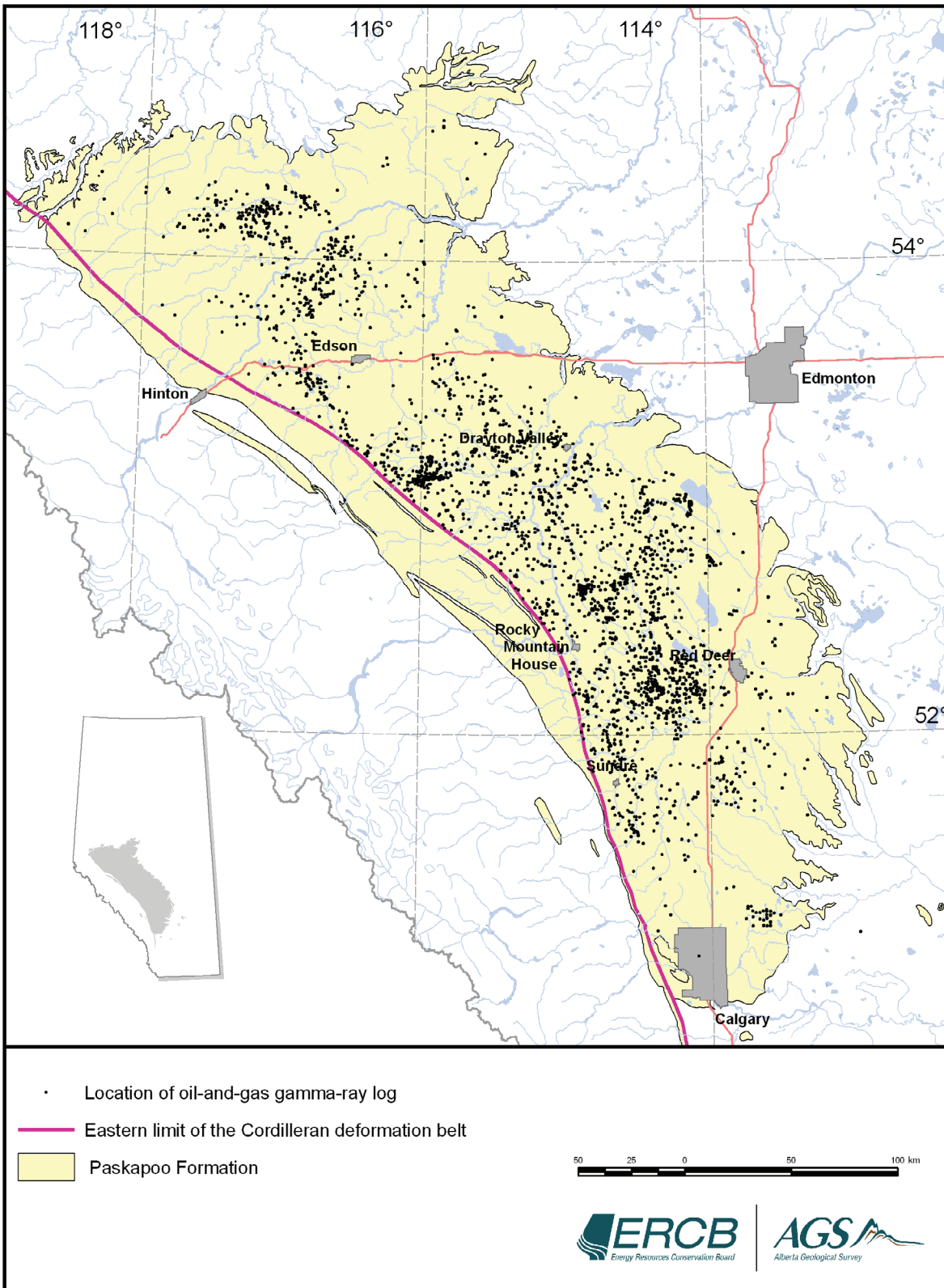


Figure 8. Distribution of oil and gas wells used in this study to determine sandstone abundance in the Paskapoo Formation, central Alberta.

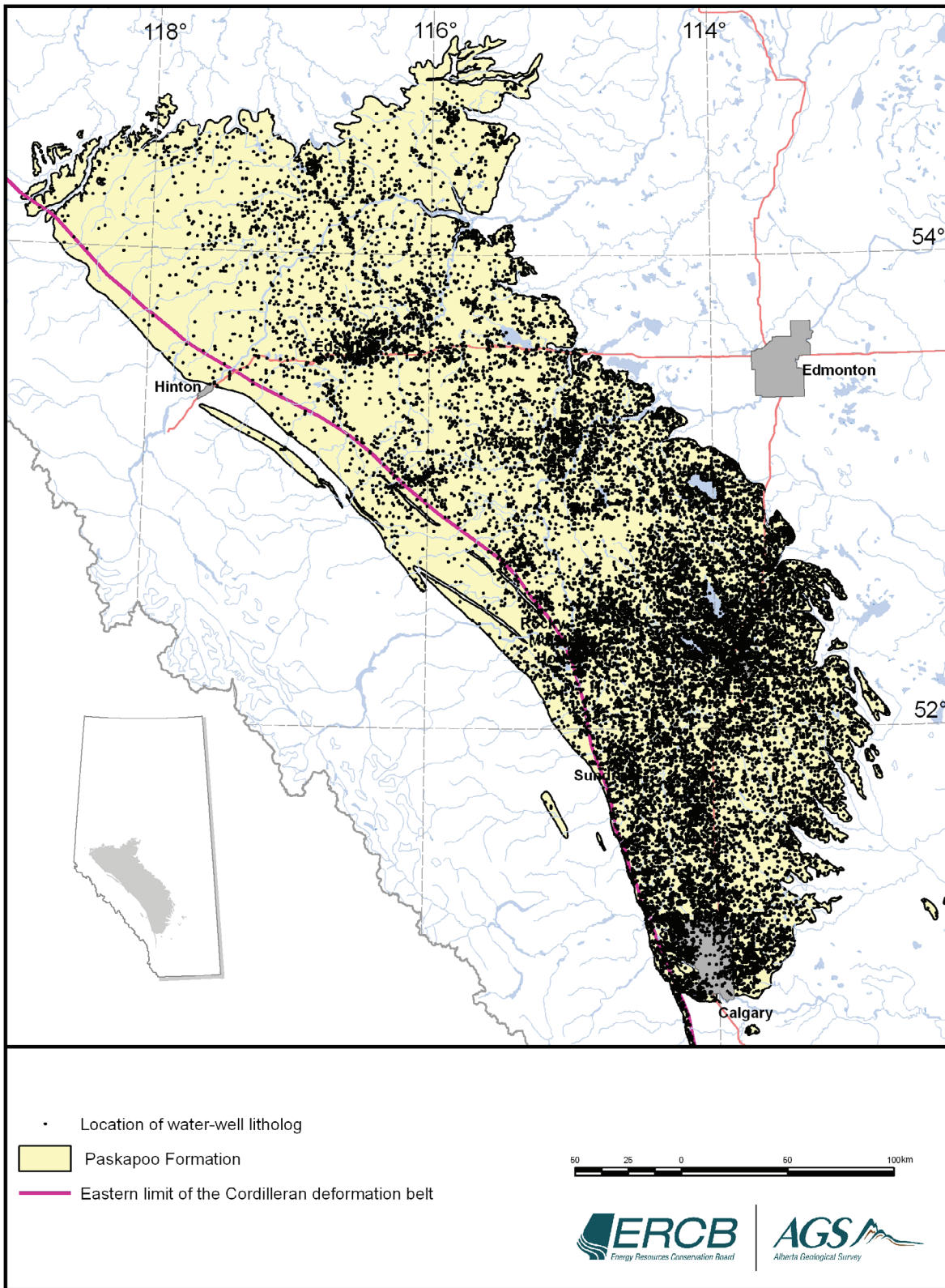
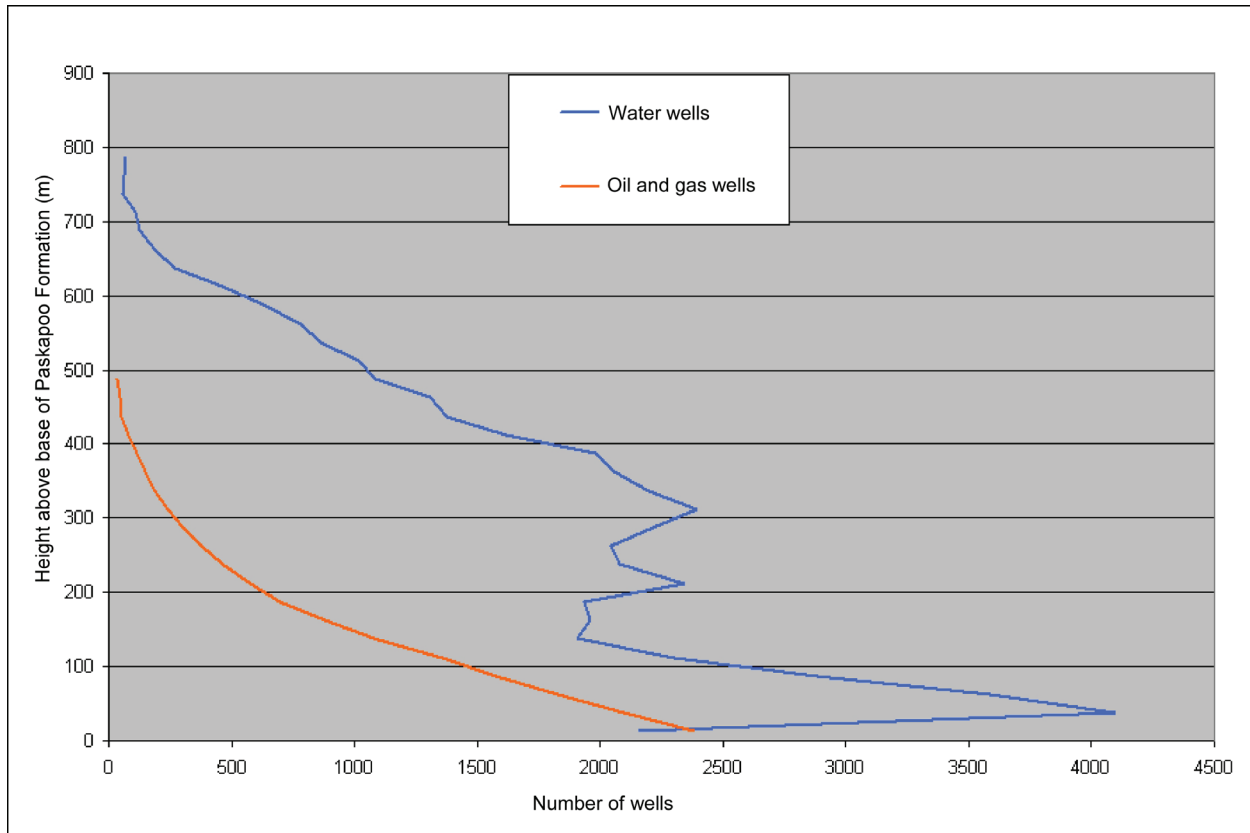


Figure 9. Distribution of water wells used in this study to determine sandstone abundance in the Paskapoo Formation, central Alberta.



**Figure 10. Type of well and number of wells with valid data used in this study, relative to height above the base of the Paskapoo Formation.**

in 1986. A well datum was assigned to either a reference point on the drill rig (kelly bushing [KB]) or ground level if KB information was absent. In the case where an interval of interest had more than one GR log, the log that terminated nearest to ground surface and with the most data was selected. Log data were tested for completeness of records. Null, incomplete, or unsuitable data were excluded from the analysis.

Water-well lithologs were extracted from ESRD's digital water-well records. These records lack rigorous geospatial attributes, other than approximations of x, y coordinates based on the Dominion Land Survey system that were converted to a geographic coordinate system. A computer digital extraction method was applied to assign borehole top elevations from a Shuttle Radar Topography Mission (SRTM) digital elevation model (United States Geological Survey, 2000).

## 4 Aquifer Mapping Approach

The objective of this study is to define permeable units within the Paskapoo Formation that can be considered regional aquifers. Previous studies of the 3-D distribution of discrete and interconnected sandstone bodies within the Paskapoo Formation illustrate the difficulty of defining aquifer systems based on traditional geological methods such as stratigraphic position. For example, Grasby et al. (2008) recognized a localized upper aquifer and a regional, well-connected lower aquifer, but only provided maps of net sandstone thickness as a function of total formation thickness. Parks and Andriashek (2009) attempted to quantify sandstone abundance in three dimensions by evaluating sandstone distribution using a series of stacked slice maps, but fundamentally based their interpolations of the 3-D distribution of sandiness on 2-D modelling methods.

This study builds on the work of Parks and Andriashek (2009) in that we similarly adopt a depth-slice analysis method to derive sandstone values for intervals within the Paskapoo Formation. However, rather than delineating individual sandstone bodies from depth-slice maps, we apply a probabilistic approach that uses geostatistical methods to model the proportion of sandstone within specified volumes within the subsurface. In this regard, our model is designed to identify the geometry of both horizontal and vertical sandstone connections, which would define the boundaries of regional aquifer systems. The following sections of this bulletin describe our approach and assumptions, as well as the limitations of using a probabilistic modelling method.

### 4.1 *Calculating Sandstone Abundance from Depth-Slice Analysis of Log Data*

Depth-slice mapping has been commonly applied to characterize rock properties where the stratigraphic framework is either complex or difficult to define (e.g., Domenico and Stephenson, 1964; Jones, 1977; Fogg, 1986). The method generally establishes a datum from which uniform

slices (either equal thickness or proportionally thick) are generated. Rock-property values are averaged over the thickness of a slice at a particular x, y location and assigned to respective slices. The method is an effective tool for creating a subset of averaged data that lends itself to modelling 3-D trends. Emerging methodologies in computer geosciences (e.g., Bonomi, 2009) demonstrate the ability to model multiple variables using this type of analysis. However, as the purpose of this study is to define major aquifer units, we calculated the relative abundance of the more permeable material (sandstone) and poorly permeable material (siltstone and mudstone) within discrete depth intervals. We then applied a 3-D modelling algorithm to construct a 3-D distribution of sandiness within the Paskapoo Formation.

The selection of an appropriate slice interval was somewhat subjective. Choosing too thick of an interval skews the analysis toward uniform values of sandstone and mudstone abundance, whereas too thin of a slice thickness results in numerous, discrete lithological bodies that might lack regional continuity. The decision to capture sandstone bodies that are likely to have regional extent within a single slice, such as discrete, single-storey channel sandstone bodies, influenced our selection of a slice thickness. Previous studies have established the maximum thickness of individual channel sandstone bodies in the Paskapoo Formation to be about 15 m, with most ranging between 5 and 10 m (Hamblin, 2004; Chen et al., 2007), so our selection of a 25 m thick slice interval satisfied that objective.

The selection of an appropriate datum is important in depth-slice analysis, as the geometry of the datum will bias the analysis and assignment of data into slices. Ideally, the datum should reflect the surface of a geological process or event so that genetically related sediments are averaged in the analysis. The selection of an appropriate datum for slice analysis in the Paskapoo Formation was challenging because its geometry comprises a clastic wedge with its base dipping westward and its top rising toward the foothills. Jerzykiewicz

(1997) attributed this wedge-shaped geometry to a change in depositional style, from the infill and subsequent flexure of the foreland basin along the deformation belt, to enhanced infill of a continental trough resulting from reactivated mountain building. Although consideration was given to selecting two (or more) separate datums that reflected the change in depositional style, there were no criteria or data that permitted the mapping of a dividing surface within the Paskapoo Formation.

## **4.2 Datums**

Because of fundamental differences in the nature of the data between water-well lithologs and GR logs, different datums were chosen to assess sandstone abundance from each of these datasets, discussed as follows.

### **4.2.1 Datum for Analyzing Sandstone Abundance from Oil and Gas GR Logs**

Parks and Andriashek (2009) used oil and gas GR logs to determine the distribution of sandstone within slices of the Paskapoo Formation. They constructed slices parallel to the top of the Battle Formation (base of Scollard Formation), resulting in the lowermost few slices representing sandstone abundance within the Scollard Formation and the next few slices above that representing a mix of sandiness within the Scollard and Paskapoo formations. Our study benefited from a new dataset of regional stratigraphic picks (B. Hathway, pers. comm., 2010), which enabled us to use the structural surface of the base of the Paskapoo Formation as the datum for slice analysis. The picks were made using the first thick (>5 m) sandstone unit located above the uppermost coal unit in the Ardley coal zone of the Scollard Formation. As discussed previously, the base of the Paskapoo Formation is unconformable with the underlying Scollard Formation. Because of uncertainty in defining the Paskapoo Formation–Scollard Formation contact, we have selected the P20 (twentieth percentile, or low estimate) modelled surface of those data (Figure 6) as the datum for our sandstone analysis, which

is about 5 m deeper than the P50, or median, estimated surface. Selecting this lower surface ensured that <5 m thick sandstone bodies at the Paskapoo Formation–Scollard Formation contact were captured as part of the analysis of sandstone abundance in the Paskapoo Formation. Subsequent boundaries of slices were constructed parallel to this surface (Figure 11), recognizing that, locally, the base of the Paskapoo Formation has an undulating and incised erosional contact with the underlying Scollard Formation.

In total, 30 slice surfaces were constructed, which accounted for the 750 m thickness of sediment within the study area. As discussed, GR log data are most abundant in the lowermost slices and decrease in abundance within the higher slices. All have been truncated at the upper surface of the Paskapoo Formation (bedrock topography), resulting in each progressively having a reduced areal extent, as elevation rises to the west.

### **4.2.2 Datum for Analyzing Sandiness from Water-Well Lithologs**

Unlike the datum used for the oil- and gas-well GR log analysis, sandstone abundances from water-well lithologs were calculated in 25 m thick slices constructed parallel to the eroded upper surface of the Paskapoo Formation (Figure 11). This datum ensured that the maximum number of water-well lithologs met the screening criteria for completeness of data in the sandstone calculations. As will be detailed later, calculations of sandstone abundance for the same stratigraphic horizon were not appreciably affected by the differing geometries of the oil- and gas-well GR log and water-well litholog datums.

Water wells generally do not penetrate to depths >150 m; consequently, only six slices were constructed, each truncating at the contact of the Paskapoo and Scollard formations. Data are most abundant in the uppermost slice (>30 000 wells), but because the slices are constructed parallel to the bedrock topography, which truncates the Paskapoo Formation, the uppermost slice includes wells that span the highest to lowest parts of the formation.

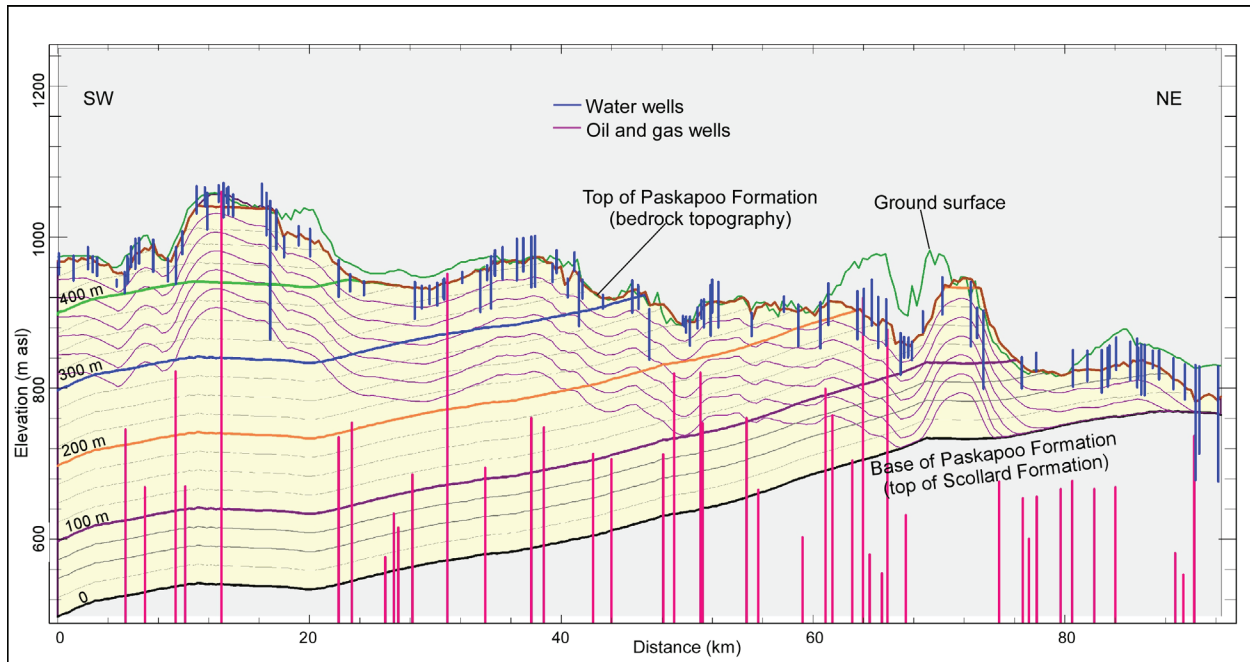


Figure 11. Structural cross-section illustrating both 25 m thick slices (thin grey, and thicker 100 m interval coloured lines) constructed parallel to the base of the Paskapoo Formation for analysis of sandiness from oil and gas gamma-ray logs, and 25 m thick slices (thin purple lines) constructed parallel to the bedrock topography for analysis of sandiness from water-well lithologs.

### 4.3 Data Extraction

#### 4.3.1 Extraction of Sandiness Intervals from GR Logs

Following the same procedures described by Parks and Andriashek (2009), for each GR log we summed the thickness of every interval with a GR value  $\leq 75$  API and expressed that total as a percentage of sandstone for the 25 m thick slice (Figure 12). Beds of coal or limestone can also have GR values of  $\leq 75$  API. Based in part on observations of core of the Paskapoo Formation (Riddell et al., 2009), we assumed these beds did not contribute substantially to the overall sums, and thus we did not distinguish them from the sandstone. GR data are recorded at uniform intervals within a borehole, but the spacing of those intervals may differ from hole to hole. Generally, most GR data were recorded at 0.1 to 0.2 m spacing. Those sections of a log that did not span the entire 25 m slice interval were not included in the calculations. No differentiation was made regarding the thickness of individual sandstone beds within the 25 m thick slice, other

than a minimum cutoff of 0.1 to 0.2 m thickness, corresponding to the logging tool sample interval. The cumulative thickness of sandstone calculated for a 25 m thick slice could therefore represent a single thick bed or numerous thin discrete beds.

A 75 API cutoff best matched sandstone accumulations as interpreted by AGS geologists on geophysical well-logs. Parks and Andriashek (2009) demonstrated, using a distribution plot of air-permeability values measured in core samples of Paskapoo Formation sandstone with a GR response of  $\leq 75$  API, that core-scale hydraulic conductivities at this magnitude of GR response fall in the typical range of permeability of sandstones to groundwater flow. Parks and Andriashek (2009) also investigated the need for rescaling the available GR logs to reflect baseline shifts between well-logging companies (e.g., Shier, 2004) and deemed rescaling unimportant for logs that postdated 1985. Quality-control steps included screening for factors such as GR readings through casing (only uncased portions of GR logs were analyzed), intervals where no GR measurements were collected, log curves mislabelled in source

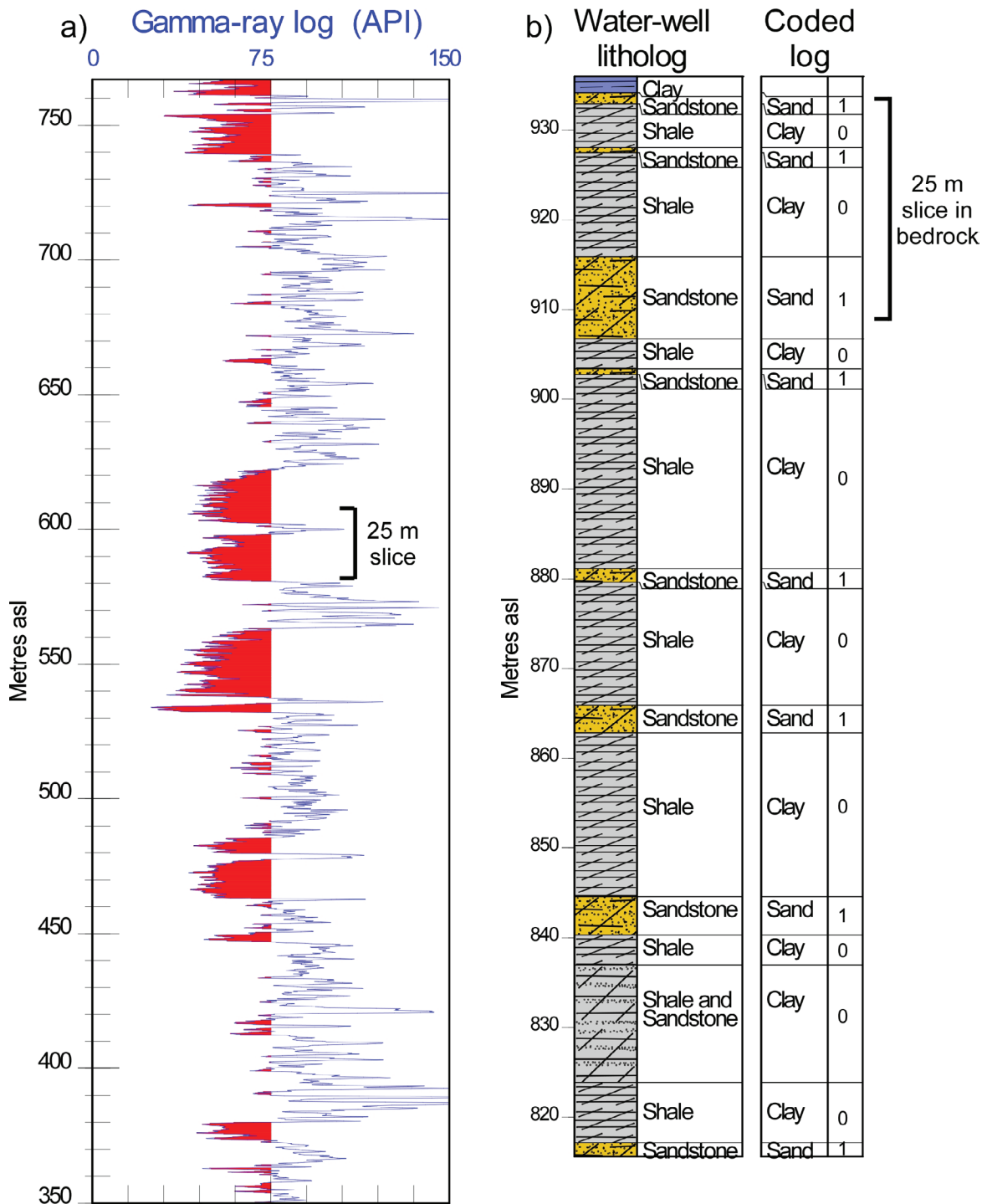


Figure 12. Estimation of sandstone abundance in the Paskapoo Formation using a) gamma-ray logs and b) water-well lithologs. Logs are from wells at different locations.

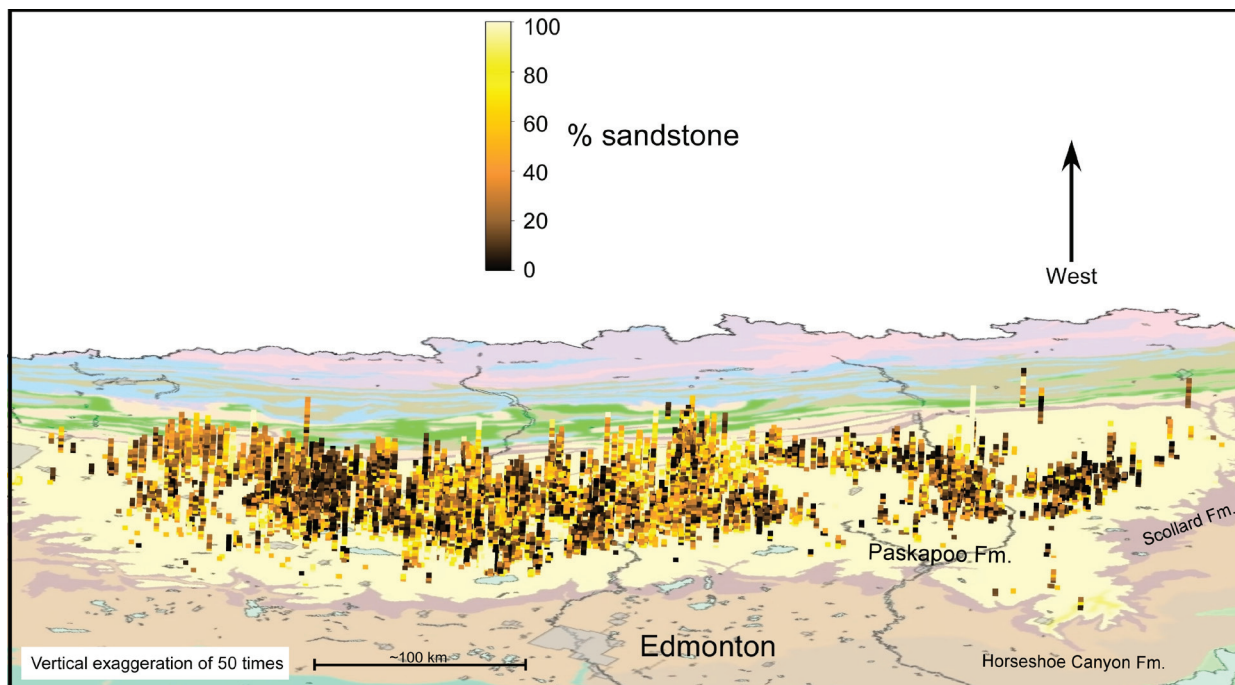


Figure 13. Three-dimensional distribution of approximately 14 570 sandstone-abundance values derived from depth-slice analysis of oil and gas gamma-ray logs, Paskapoo Formation, central Alberta. Values were derived from net sand estimates using a 75 API cutoff over a 25 m thick slice interval.

files, and the presence of placeholder numerical values in third-party data files, indicating absence of data.

The analysis of sandstone abundance in 25 m thick slice intervals from approximately 2400 GR logs yielded 14 566 point values, each of which was assigned a depth value corresponding to the midpoint of its respective slice above the base of the Paskapoo Formation. Figure 13 shows the 3-D distribution of those midpoint sandstone values.

#### 4.3.2 Extraction of Sandiness Intervals from Water-Well Lithologies

A criticism commonly voiced by geologists is that water-well lithologies are not of sufficient quality to be used in any meaningful interpretation of geology. Although this may be true for defining sedimentary facies for a detailed lithostratigraphic model, we believe water-well lithologies provide information suitable for characterizing sandiness of a regional study area. In fact, lithologies for some water wells located near outcrops quite reasonably

represent the major lithological properties of the bedrock in that area (Figure 14). Unlike GR log data, drillers do not capture water-well data at regular intervals but only record major changes in lithology. The quality and rigour of these descriptions is dependent on the driller's ability to recognize lithological changes from drill cuttings, interpret the behaviour of the drilling rig in response to different rock types, and being knowledgeable about the local geological setting. Because the purpose of drilling water wells is to develop a supply of useable groundwater, drillers generally key in on the presence of coarse deposits such as sand or sandstone, which would indicate relative production values. Conceivably, they might describe finer grained deposits, even muddy sand, as 'clay' in the case of unconsolidated sediment or 'shale' in the case of bedrock units.

A subjective decision-making approach was applied to translate more than 2700 unique water-well drillers' descriptions of geological material into 25 lithology terms (Slattery et al., 2011). The nine terms for bedrock materials

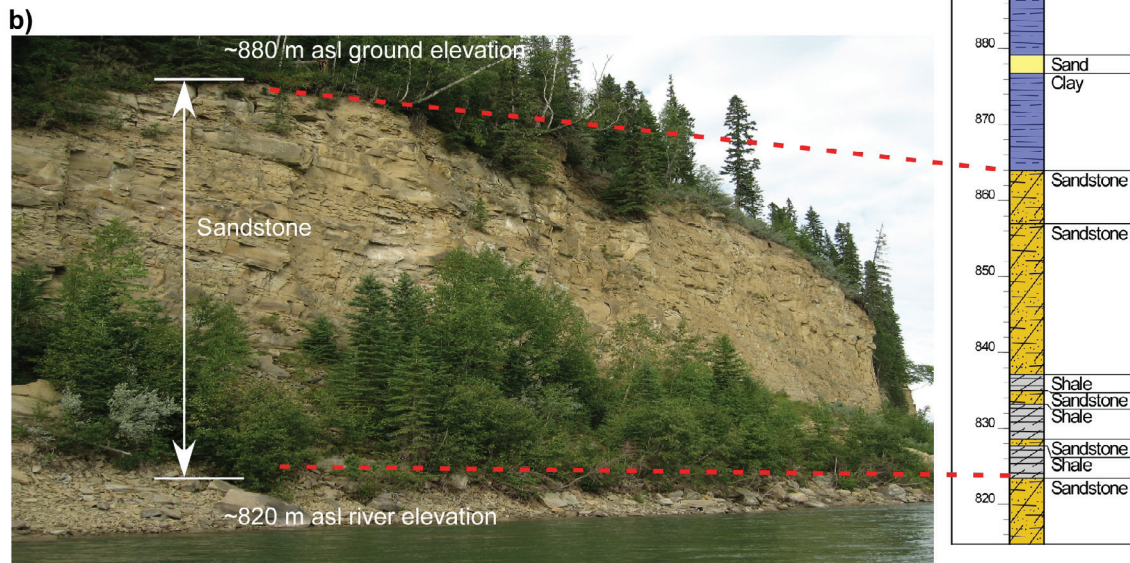
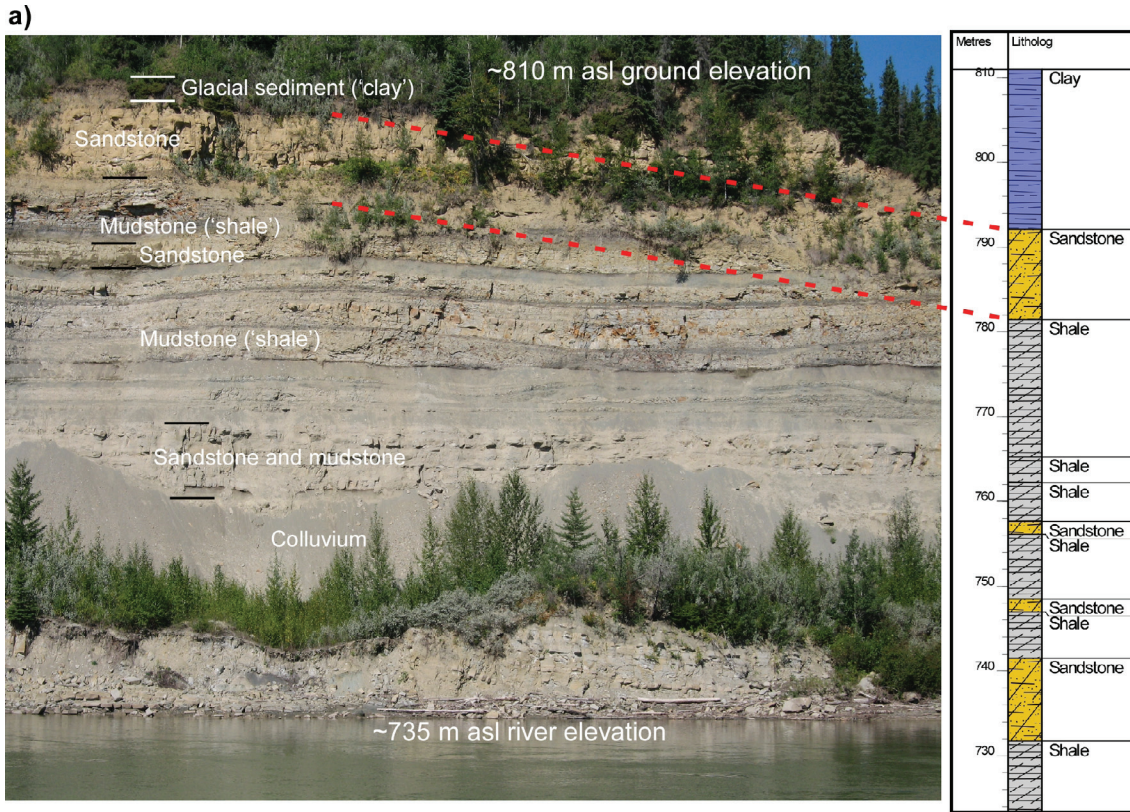


Figure 14. Comparison of water-well lithologs to nearby outcrops of Paskapoo Formation strata: a) view across North Saskatchewan River at Willey West Park, near Drayton Valley (Zone 11, 638046E, 5897802N, NAD83), outcrop approximately 500 m from borehole (Zone 11, 6377543E, 5897856N); and b) outcrop along North Saskatchewan River (Zone 11, 621180E, 5862369N), approximately 800 m from borehole (Zone 11, 621006E, 5861608N).

classified by Slattery et al. (2011) were further collapsed in this study into a bimodal classification: sandy or nonsandy sediment (Appendix 1). An indicator value (Dreiss and Johnson, 1989) of 1 (100% sandstone) was assigned for every described interval in a litholog if the sediment was deemed to be sandy, and a value of 0 was assigned if the sediment was silty or clayey (Figure 12). The top of bedrock, in this case the Paskapoo Formation, was determined and the thicknesses of all sandy intervals were summed in each 25 m thick slice from the bedrock surface downward and expressed as a percent of the slice thickness.

To test the validity of our subjective classification method, we compared the results of sandstone abundance from water-well data in the uppermost 25 m thick slice (parallel to the bedrock surface of the Paskapoo Formation) with the resistivity values from an airborne electromagnetic survey flown over the east-central part of the study

area (Barker et al., 2011). Figure 15a shows the modelled results of the analysis of more than 30 000 water-well lithologs, illustrating the sandiness of the upper 25 m of the Paskapoo Formation. Encircled areas highlight two prominent regions where sandstone abundance is estimated to be >60% and bedrock is close to surface. Figure 15b shows a modelled resistivity depth slice of the electromagnetic properties of the ground to a depth of approximately 20 m below surface for parts of the study area. This shows an average of both the unconsolidated sediments above bedrock and the underlying Paskapoo Formation. Higher resistivity areas ( $\geq 20 \text{ ohm}\cdot\text{m}$ ) are interpreted as sandy sedimentary rock, based on downhole resistivity values collected from geophysical logs run in coreholes (Riddell et al., 2009). Encircled regions highlight areas where the sediment cover above bedrock is thin to absent (Slattery and Barker, 2010), and the resistivity shown therefore characterizes a 20 m thick

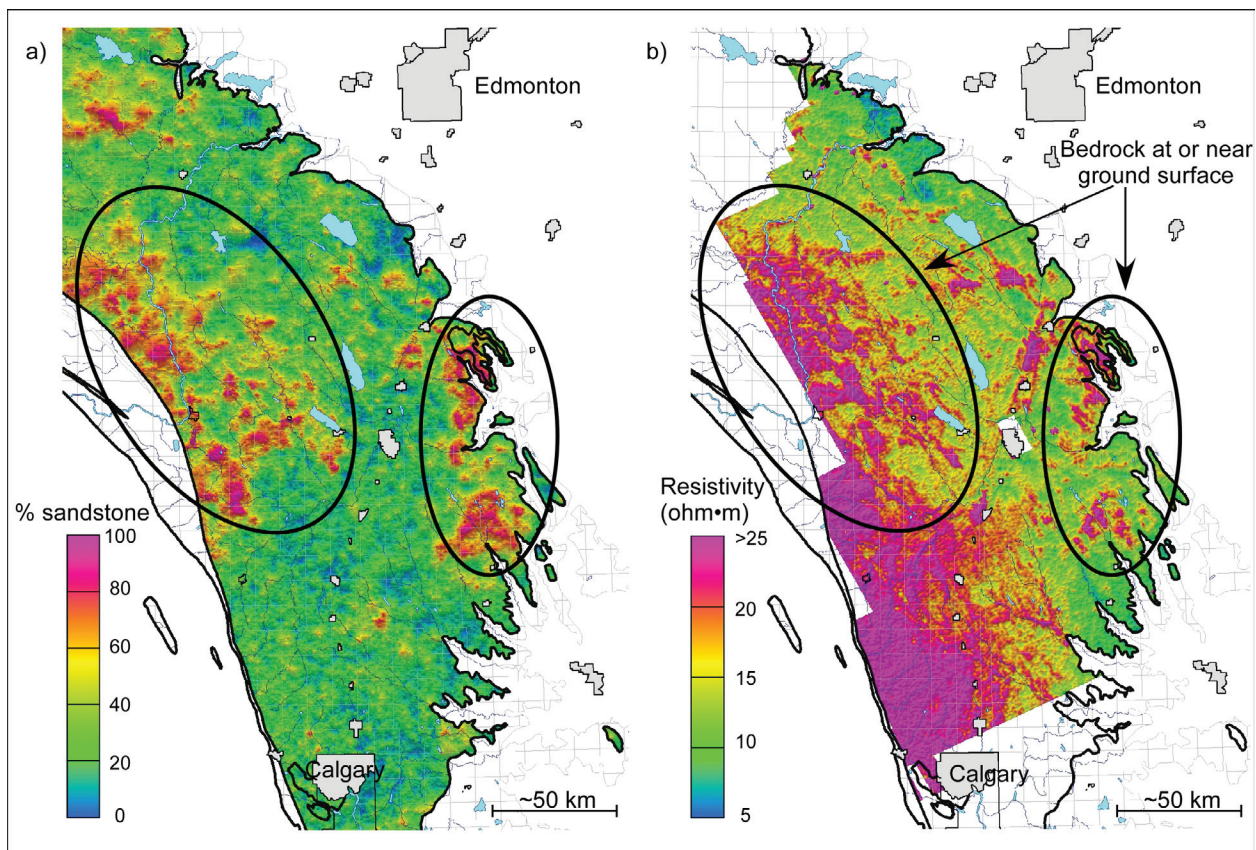


Figure 15. a) Sandiness of the upper 25 m of Paskapoo Formation using water-well litholog analyses and b) the resistivity of the upper 20 m below ground surface recorded by airborne electromagnetic surveys (Barker et al., 2011).

interval at the top of the Paskapoo Formation. The correlation between the circled areas of the two images shows that the sandiness interpretations from the resistivity images are consistent with the sandiness interpretations from the subjective classification method. Differences in pattern can be explained by differences in data density and size of measurement support (e.g., discrete value derived at a point [wellbore] versus composite value derived from a broader airborne electromagnetic footprint), the airborne data being significantly greater. The strong correlation is indirect validation that the water-well drilling industry is doing a reasonable job of recording the major lithological changes in the sedimentary record and that these logs can contribute to the mapping of regional geological units.

As in the case of GR log analysis, the per cent sandstone value (n) was assigned to the midpoint (z) of the height of the slice above the base of the Paskapoo Formation. This process was repeated for approximately 33 500 water-well lithologs, creating a dataset consisting of approximately 48 160 x, y, z, n data (3-D distribution; Figure 16).

Finally, although no attempt was made to differentiate between discrete beds of thick and continuous channel-dominated sandstone and numerous, but discrete, thin, splay-dominated

sandstone intervals within a given depth slice, our GR log analyses methods could have been modified to generate a three-parameter classification (mud, crevasse splay sand, and channel sand), similar to that of Burns et al. (2010a).

#### 4.4 Comparison of Sandiness in GR Log Data and Water-Well Data

Concluding that the water-well data meaningfully captured regional trends in sandiness with depth, sandstone-abundance estimates from water-well lithologs were compared to those derived from the analysis of GR logs to determine how similar, or dissimilar, the values from the different sources are. Figure 17 shows the results of jackknife validation (Deutsch and Journel, 1998) between the two datasets. Jackknife validation is a process that uses one dataset to estimate the values of another dataset with uncertainty. The results can be used to test a model, such as kriging, or to perform quality control on new data. In this case, the GR log data were used to estimate the sandiness values at the water-well locations and vice versa to see if they are representative of the same distribution.

Figure 17 shows that there is little predictive power between the two datasets, as demonstrated by the poor correlation in the crossplots and the high estimation variances. However, the results are

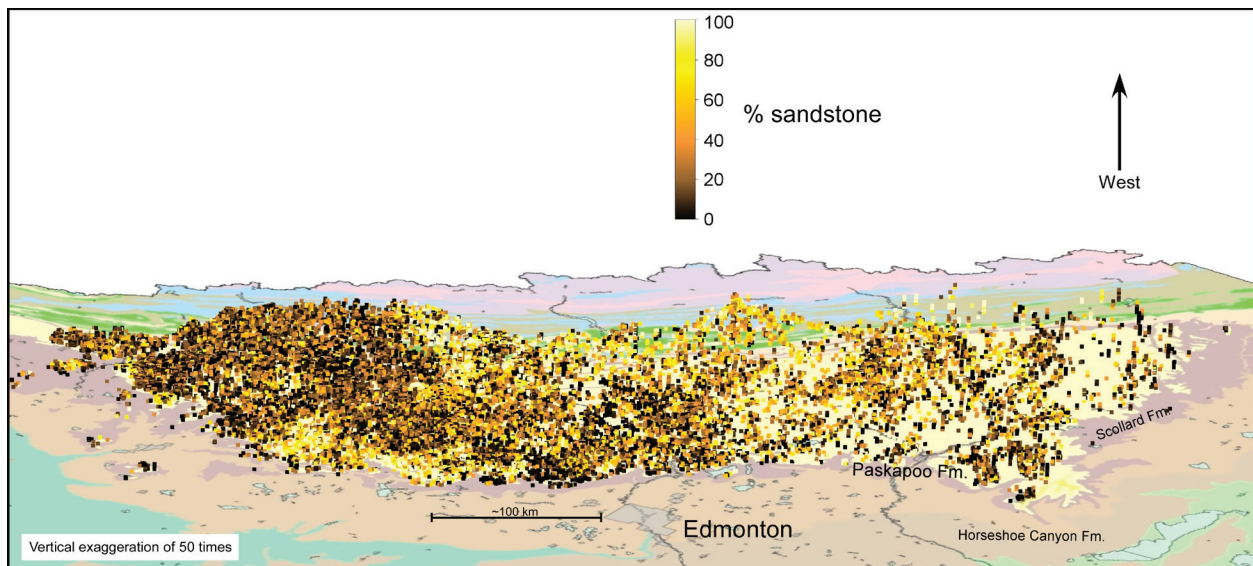


Figure 16. Three dimensional distributions of about 48 160 sandstone-abundance values derived from depth-slice analysis of water-well lithologs, Paskapoo Formation, central Alberta.

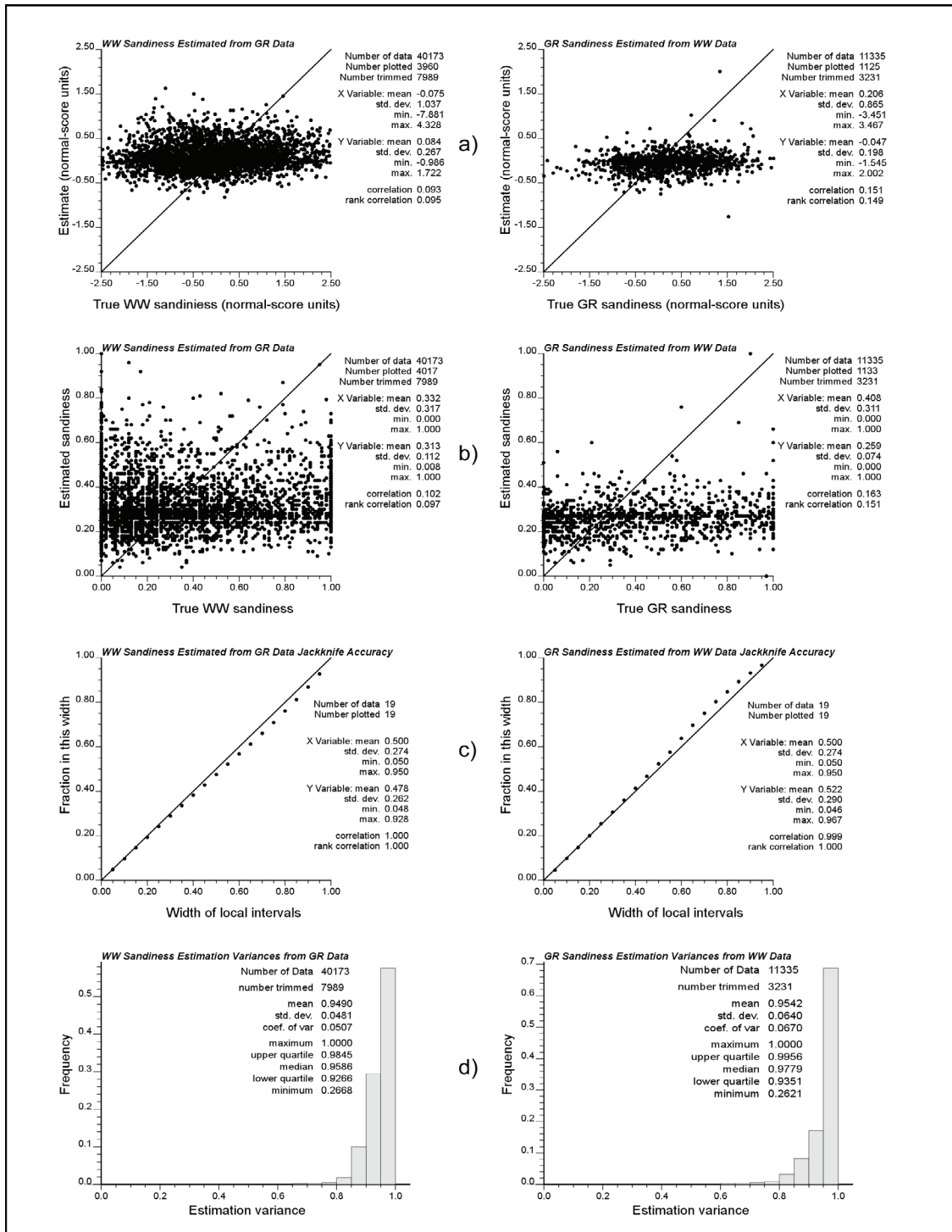
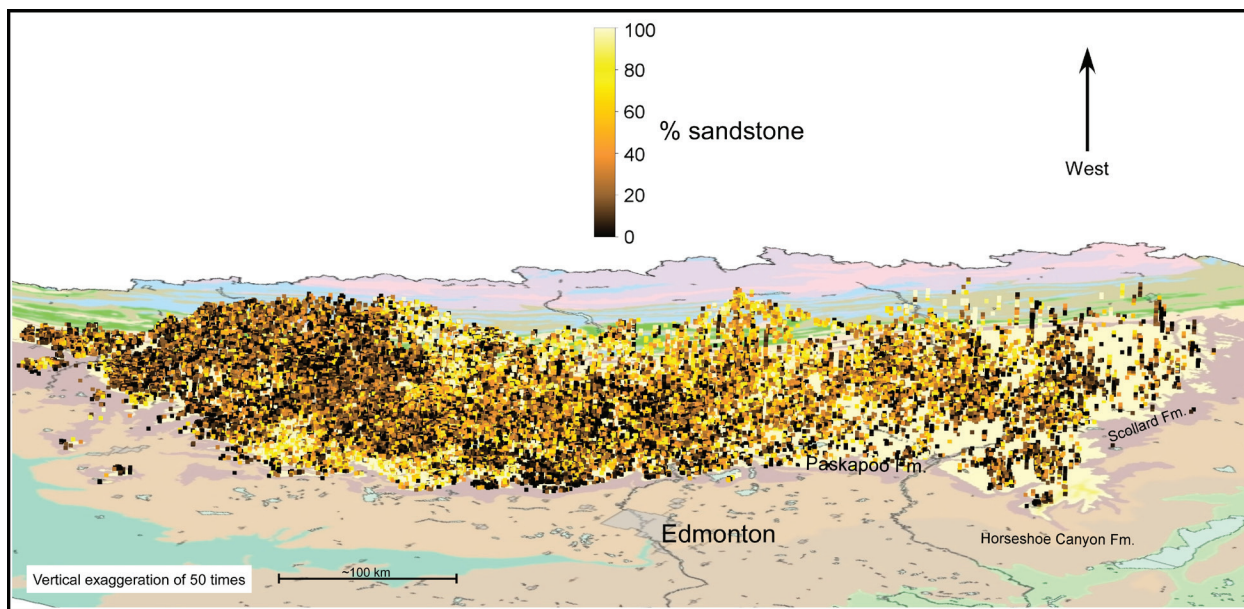


Figure 17. Jackknife validation results between the water-well litholog and gamma-ray (GR) log datasets. Water-well (WW) sandiness estimated from GR log data on the left. Gamma-ray log sandiness estimated from water-well data on the right. a) crossplots of true values and jackknife estimates of sandiness in normal-score units; b) crossplots of true values and jackknife estimates of sand proportion; c) accuracy plots; d) histograms of estimation variances, in normal-score units. Abbreviations: coef. of var., coefficient of variation; std. dev., standard deviation.



**Figure 18. Three-dimensional distribution of approximately 62 700 sandstone-abundance values from the combined analyses of water-well lithologs and gamma-ray logs, Paskapoo Formation, central Alberta.**

accurate as shown by the accuracy plots (Figure 17c). The high estimation variances and lack of predictive power are due to there being little spatial overlap between the two distributions. This lack of overlap led to the combining of the two datasets in the first place, so the lack of a bias and the accuracy of the quantification of uncertainty (even if the uncertainty is quite high) led us to believe the two datasets are congruent with one another and can be treated as one. The spatial gap between the datasets also means there is little redundancy between the data, and this improves the estimation of sandiness at unsampled locations.

In summary, even though the data sources differ between the oil and gas GR log and water-well litholog datasets, both analyses independently characterize the same trends in sandstone distributions with depth in the Paskapoo Formation. For this reason, the two datasets were combined and averaged into a single set for 3-D modelling (Figure 18).

## 5 Regional-Scale Sandiness

The sandstone-abundance data was modelled at several scales to investigate the overall internal distribution of sandiness within the Paskapoo Formation. The coarsest resolution of sandstone abundance is revealed within a vertical trend, which can be used to identify the approximate thicknesses and stratigraphic positions of possible hydrostratigraphic units. A more detailed model, but at a relatively coarse scale, was created using kriging to populate a grid in 3-D, which is representative of the expected sandiness at various locations throughout the Paskapoo Formation. Each of these models uses the base of the Paskapoo Formation as the datum, and all vertical heights and distances are relative to that datum.

### 5.1 Vertical Trend

Averaging all of the sandiness data in each 25 m thick slice and plotting these values against height above the base of the Paskapoo Formation produces a vertical trend (Deutsch, 2002; McLennan, 2007), which gives a stratified view of the Paskapoo Formation. Figure 19 shows the vertical proportion curve for the combined GR

log and water-well litholog datasets. In this view, a number of discrete units can be distinguished: a lowermost sandy unit to approximately 50 m; a muddy middle unit from 50 m to approximately 300 m; and an upper sandy unit above 300 m.

Figure 19 also shows 95% confidence limits for the mean (average) sandiness within each slice over the entire Paskapoo Formation. The uncertainty was determined by using a spatial bootstrap method (Journel, 1994). This statistical resampling method accounts for the spatial redundancy between clustered data points. Taking into account the erosion of the upper slices of the Paskapoo Formation, the mean sandiness of the entire formation was calculated to be about 40%.

### 5.2 Discussion of Model Dimensions

The regional-scale model of sandiness is cell based, with the lowermost slice flattened to the base of the Paskapoo Formation and the higher slices parallel to the base. The x and y model axes are aligned with the easting and

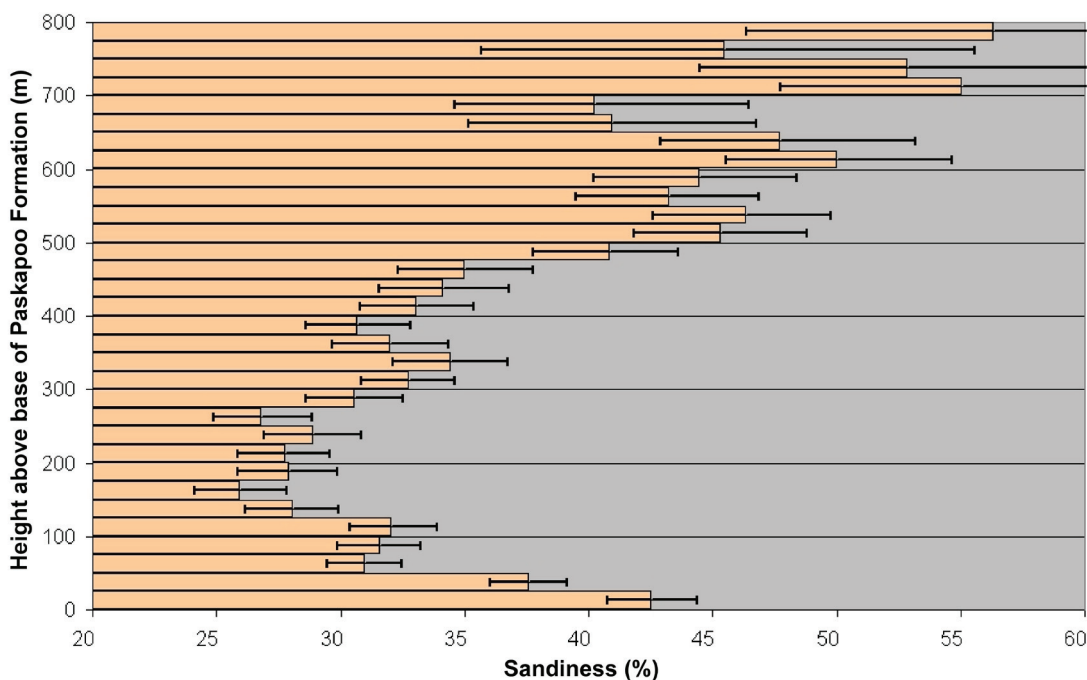


Figure 19. Vertical trend of the per cent sandiness within 25 m slices of the Paskapoo Formation with 95% confidence limits.

northing directions, respectively, of the 10-Degree Transverse Mercator (10TM) provincial UTM coordinate system, and the z axis is vertical. Each cell is 1 by 1 km in the x and y directions and 25 m in the z direction. There are 440 by 490 by 30 cells in the x, y, and z directions respectively, yielding a total of 6 468 000 cells. Of these, there are 686 382 ‘active’ cells, which were populated during modelling; the remainder contain null values representing those parts of the model where the Paskapoo Formation is absent. Table 1 shows a summary of the model dimensions.

The vertical cell size of 25 m was chosen to coincide roughly with the maximum thickness of a single channel sandstone body in the Paskapoo Formation (see Section 6 for details). The horizontal cell dimensions were chosen to balance resolution with computational efficiency.

model parameters. Simple kriging is a standard geostatistical algorithm that is used to determine the value of a variable (in this case, sandiness) at unsampled locations. The back transformation is a quantile-to-quantile transformation that allows the estimated normal-score values and range of uncertainty to be restored to the original units of proportion of sand. See Deutsch (2002) or Deutsch and Journel (1998) for a more technical explanation of these steps.

This standard geostatistical modelling workflow is used to estimate values of a variable, in this case sandiness, at unsampled locations and to assess the uncertainty in the estimates. A trend model was not considered for this work because initially it was not known if the Haynes and Lacombe members were regionally developed. Later, as the distinctions between sand-dominant and mud-dominant units emerged, it became clear

**Table 1. Regional-scale sandiness model dimensions.**

Axis	Cell Size (m)	Number of Cells	Coordinate Range	Coordinate System
x (easting)	1000	1000	220 000–660 000	10TM <sup>1</sup> NAD83
y (northing)	1000	490	5 600 000–6 090 000	10TM NAD83
z (vertical)	25	30	0–750	Height above base of Paskapoo Formation

<sup>1</sup>10-Degree Transverse Mercator

### 5.3 Regional-Scale Modelling

To identify areas of laterally extensive sandstone or mudstone units within the Paskapoo Formation, a kriged model of the sandiness was created. The following steps were taken to accomplish this:

- 1) normal-score transformation of the data
- 2) variogram calculation and modelling
- 3) cross-validation to check the kriging model
- 4) simple kriging of the data
- 5) back transformation to original units

The normal-score transformation is used because of its advantageous mathematical properties. The cross-validation is a ‘leave-one-out’ procedure, which assesses the accuracy and precision of the

that further work would be required to refine the hydrostratigraphic subdivisions in a quantitative manner.

The vertical trend visible in the lowermost slices of Figure 19 (25 to ~100 m) may be a combination of sandstone-abundance values from within both the Haynes and Lacombe members. Figure 20 shows a cartoon of the Paskapoo Formation with a conceptual boundary between the Haynes and Lacombe members. Since the member boundary crosses the model slices, assigning a local mean value to the slices would overstate the sandiness in the eastern part of the Lacombe Member and understate the sandiness in the western part of the Haynes Member.

### 5.3.1 Normal-Score Transformation

The normal-score transformation is a quantile-to-quantile transformation that forces the data distribution to be Gaussian (normal). This has mathematical advantages and allows an assessment of local (i.e., location-by-location) uncertainty after the workflow is complete without violating the constraint that sandiness must be between 0.0 and 1.0. The variogram calculation and modelling is performed on the normal-score data.

### 5.3.2 Variography

Experimental variograms in the horizontal and vertical directions were calculated from the normal-score data, and models were fitted to match the spatial structure. For this analysis, the structure of the sandiness is assumed to be isotropic in the horizontal direction. There is insignificant dip or plunge in the major directions of continuity because of the vertical coordinate system used. The experimental variograms were calculated from the GR log, water-well litholog, and combined datasets; the shape of the structure was found to be the same, but the water wells have more randomness than the GR logs. The GR-log

variogram therefore was considered to provide a better indication of the true spatial structure of the sandiness within the Paskapoo Formation. The following is the fit variogram model:

$$\gamma(h) = 0.1 + 0.628 \cdot \text{Exp}_{\substack{ah=4005 \\ av=50}}(h) + 0.272 \cdot \text{Sph}_{\substack{ah=54279 \\ av=50}}(h)$$

Figure 21 shows the GR log data horizontal experimental variogram (points) and the fit variogram model (line). Figure 22 shows the water-well litholog data experimental variogram and the fit model. The higher variogram values in Figure 22 at short ranges demonstrate the increased randomness in the water-well data that is probably due to misclassification of thin sandstone/mudstone intervals in the water-well lithologs. The GR logs detect thin ( $\geq 0.1$  m) sand/mud intervals, whereas a water-well driller is not likely to record data at this level of detail. When the proportion of sandstone is calculated at a 25 m scale, this misclassification is seen as increased random error and higher variogram values. Beyond 10 km, the experimental variograms show similar structure.

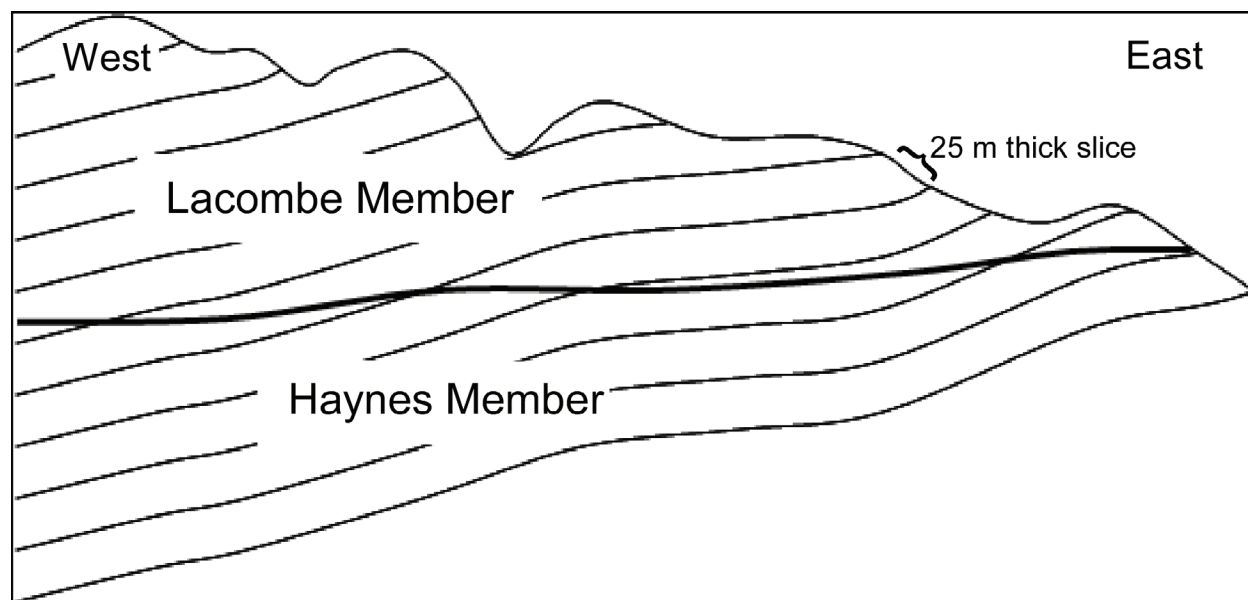


Figure 20. Cartoon of the Paskapoo Formation showing the 25 m slices parallel to the base and a conceptual boundary (dark line) between the Haynes and Lacombe members.

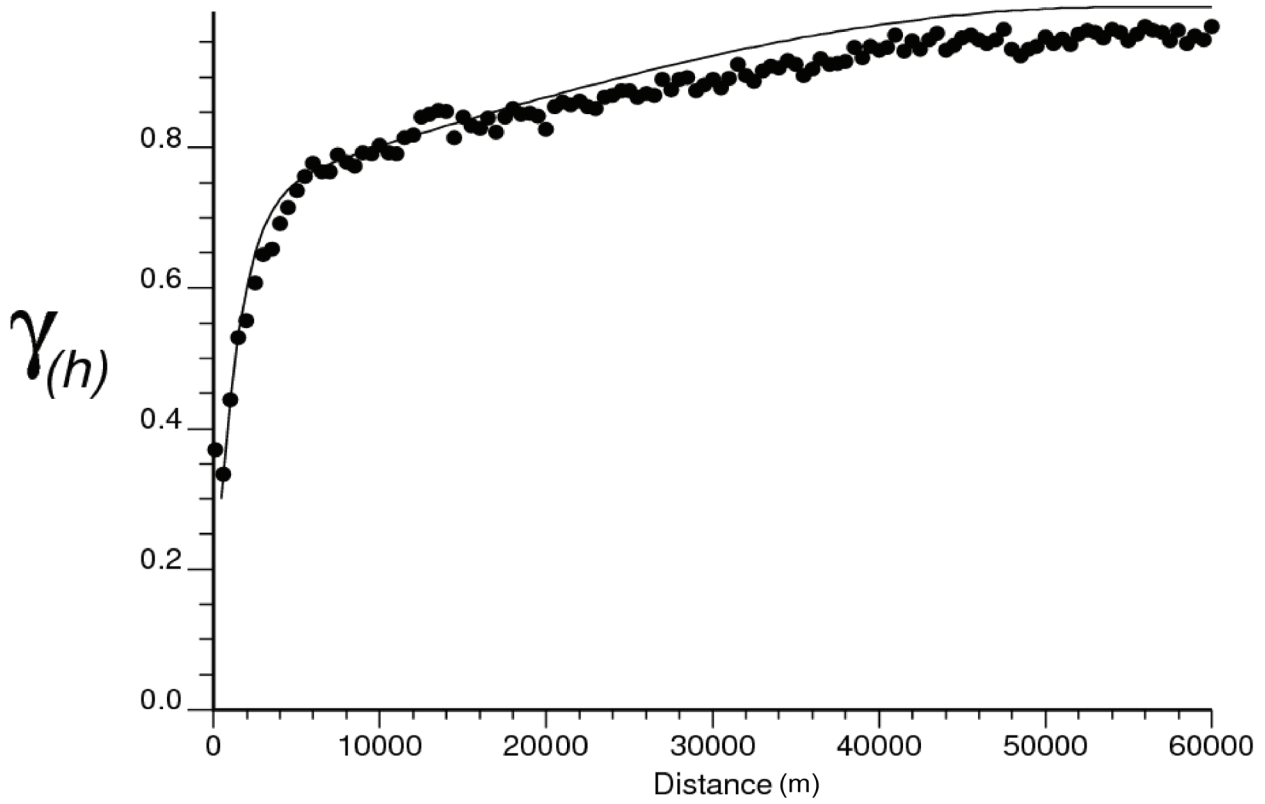


Figure 21. Omnidirectional horizontal variogram calculated from gamma-ray log data.

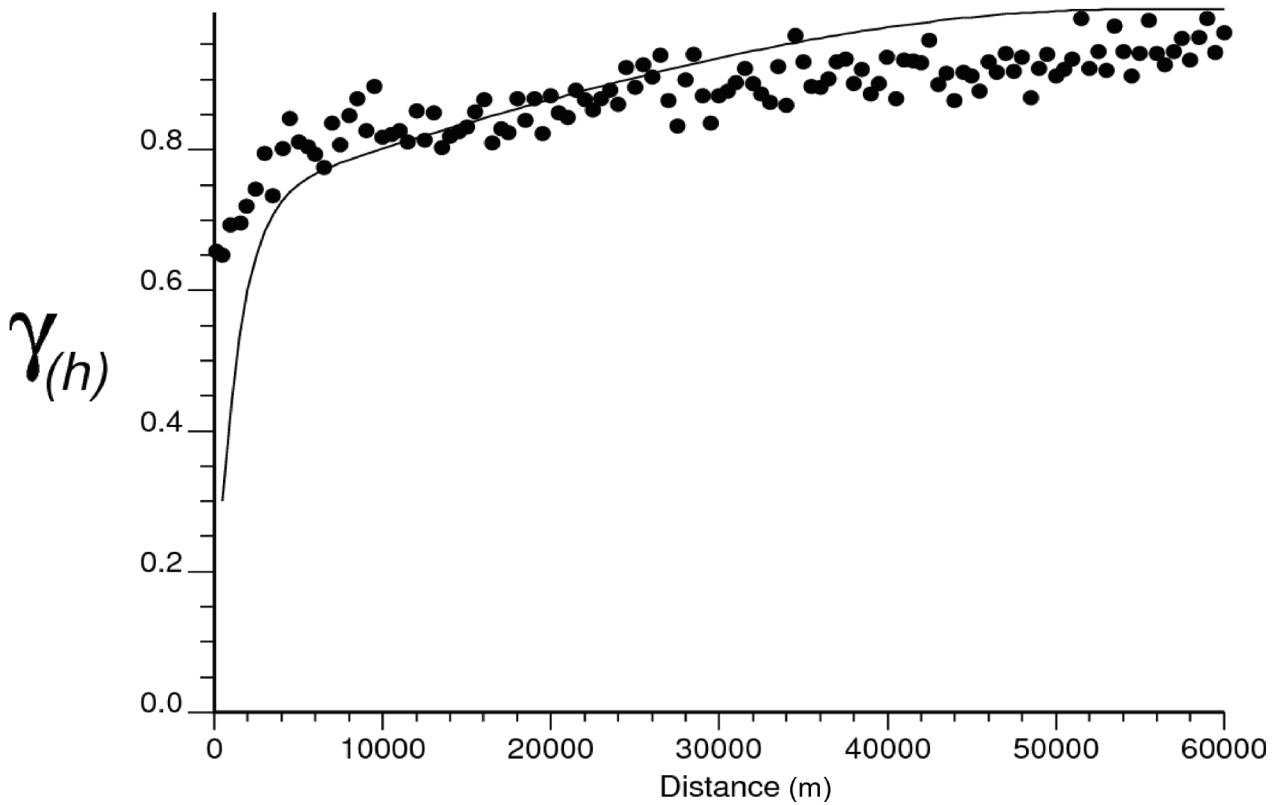


Figure 22. Omnidirectional horizontal variogram calculated from water-well litholog data.

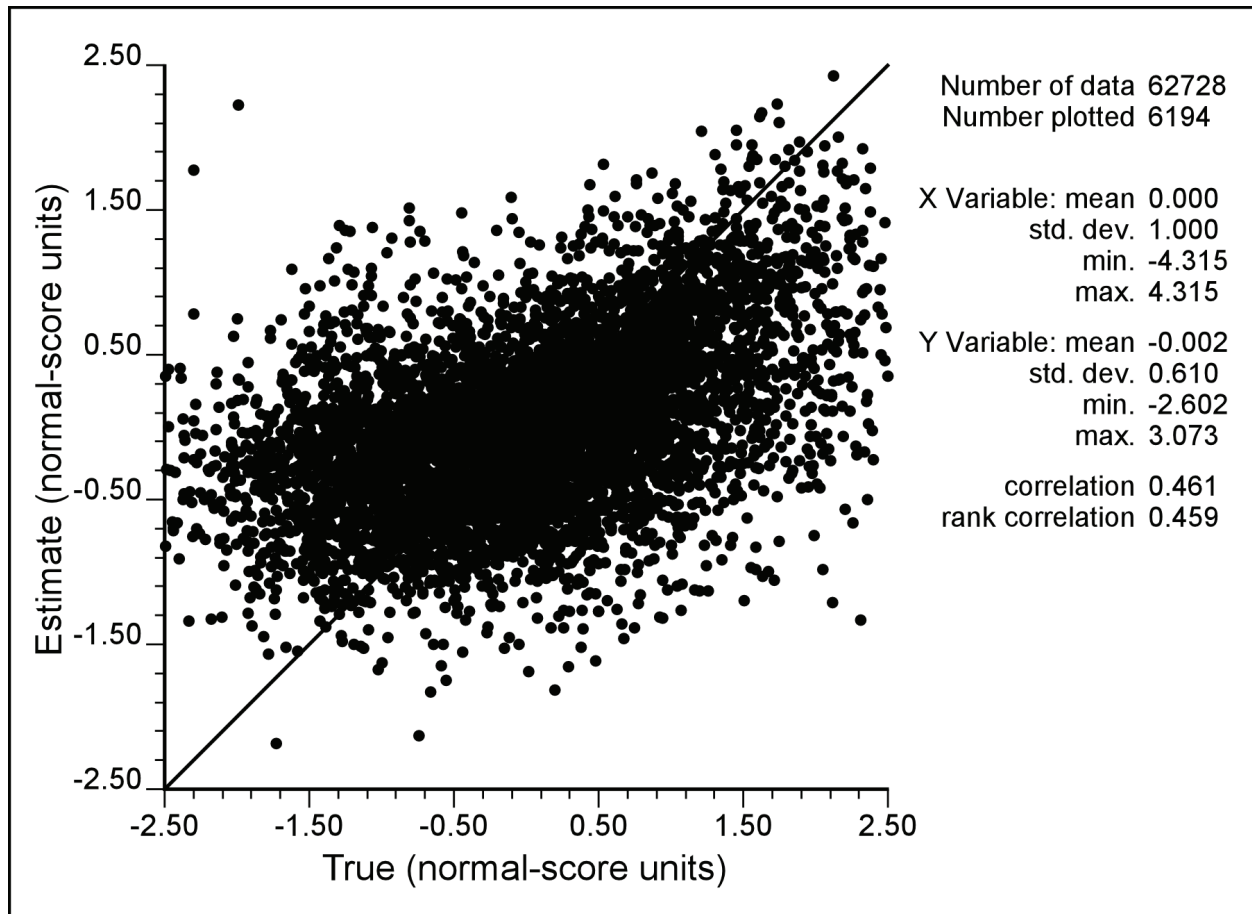


Figure 23. Cross-validation results for the sandiness modelling. Abbreviation: std. dev., standard deviation.

### 5.3.3 Cross-Validation

Using the fitted variogram, ‘leave-one-out’ cross-validation was performed using simple kriging. This procedure drops a single data point, uses the surrounding data to estimate the value at that location, then compares the true value to the estimated one. The simple kriging method also provides a measure of uncertainty in the form of an estimation variance, so it is possible to judge whether the uncertainty in the estimates is being accurately assessed.

Figure 23 shows a crossplot of the true data values, in normal-score units, versus the estimated values. The mean values are both near zero, reflecting the normal-score transformation and the match, on average, of the estimates to the true values. The standard deviation of the estimates is lower than

that for the true values due to the smoothing effect of kriging (and other interpolation methods).

The correlation between the true and estimated values of about 0.46 reflects the overall ability to predict areas of high or low sandiness in the Paskapoo Formation, but it also reflects the difficulty in predicting exact values due to the heterogeneous nature of the formation and sparse data relative to the size of the area under consideration.

Aside from predicting the sandiness values, the uncertainty in the predictions is also an important consideration. Figure 24 shows an accuracy plot of the cross-validation results. This plot shows the width of the uncertainty distributions on the horizontal axis and the fraction of true values found within that width of distribution from the

cross-validated estimates. If the uncertainty of the estimates were perfectly predicted as measured by variance/standard deviation, all of the points would fall on the 45° line. The points are slightly below the line, which suggests that the uncertainty in normal-score units is being slightly understated. This effect is not too great and is larger near the tails of the uncertainty distributions. Also, when transformed back to original units, the wider distributions are truncated at 0 and 1, which increases the 'fraction within' value. Overall,

the assessed uncertainty is within an acceptable limit as compared to typical geostatistical modelling practices.

### 5.3.4 Simple Kriging

With the model parameters validated, the sandiness of the entire volume of the Paskapoo Formation was estimated. Figure 25 shows a map of the estimated sandiness, in normal-score units, in the bottom slice of the model. The high and low areas

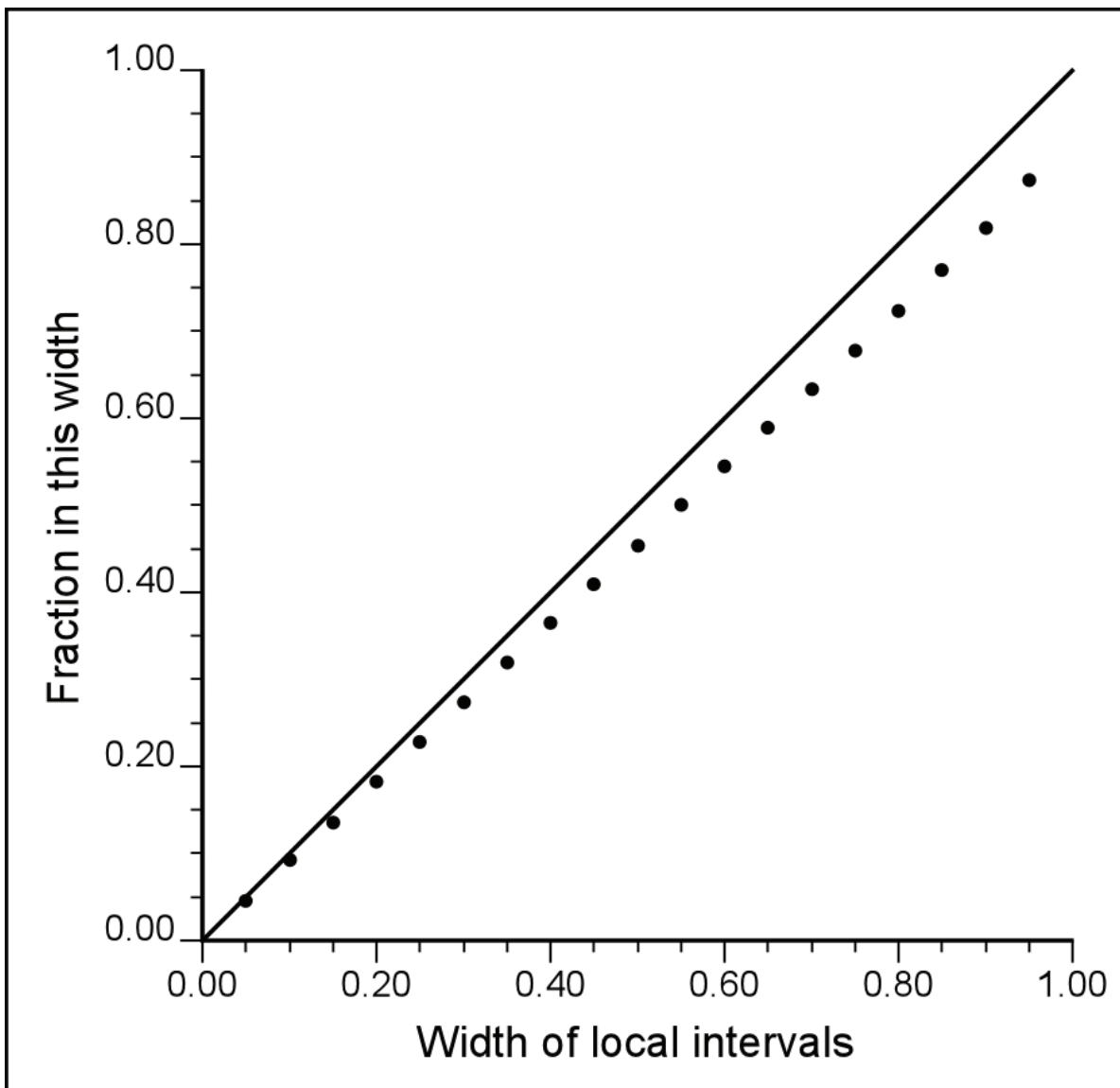


Figure 24. Accuracy of the sandiness cross-validation.

are easy to identify, with sparsely sampled regions tending toward the mean (0.0). Figure 26 is a map of the kriging variance values in the bottom slice of the model. It shows that the variance is low nearest to locations with a high density of data and high in sparsely sampled regions. Along the eastern edge of the Paskapoo Formation, the variance is low due to the high density of water wells near the subcrop edge; to the west, numerous GR logs contribute to lower variance. In areas to the north and south, where data are sparse, the best estimate is the mean of the distribution and the variance is 1.0.

### 5.3.5 Back Transformation

After the creation of the model in normal-score units, the kriged estimates were back transformed into the original units of proportion of sandstone. One of the properties of the back transformation is that the local distributions (at any single location) are no longer symmetrical. Therefore, the kriging estimate, once back transformed, corresponds to the median (P50) sandstone value of the back-transformed probability distribution and is no longer equal to the arithmetic mean. Figure 27 shows a map of the back-transformed sandstone estimates in the bottom slice of the model. Figures 76–80 in Appendix 2 show all of the back-transformed sandstone slice maps.

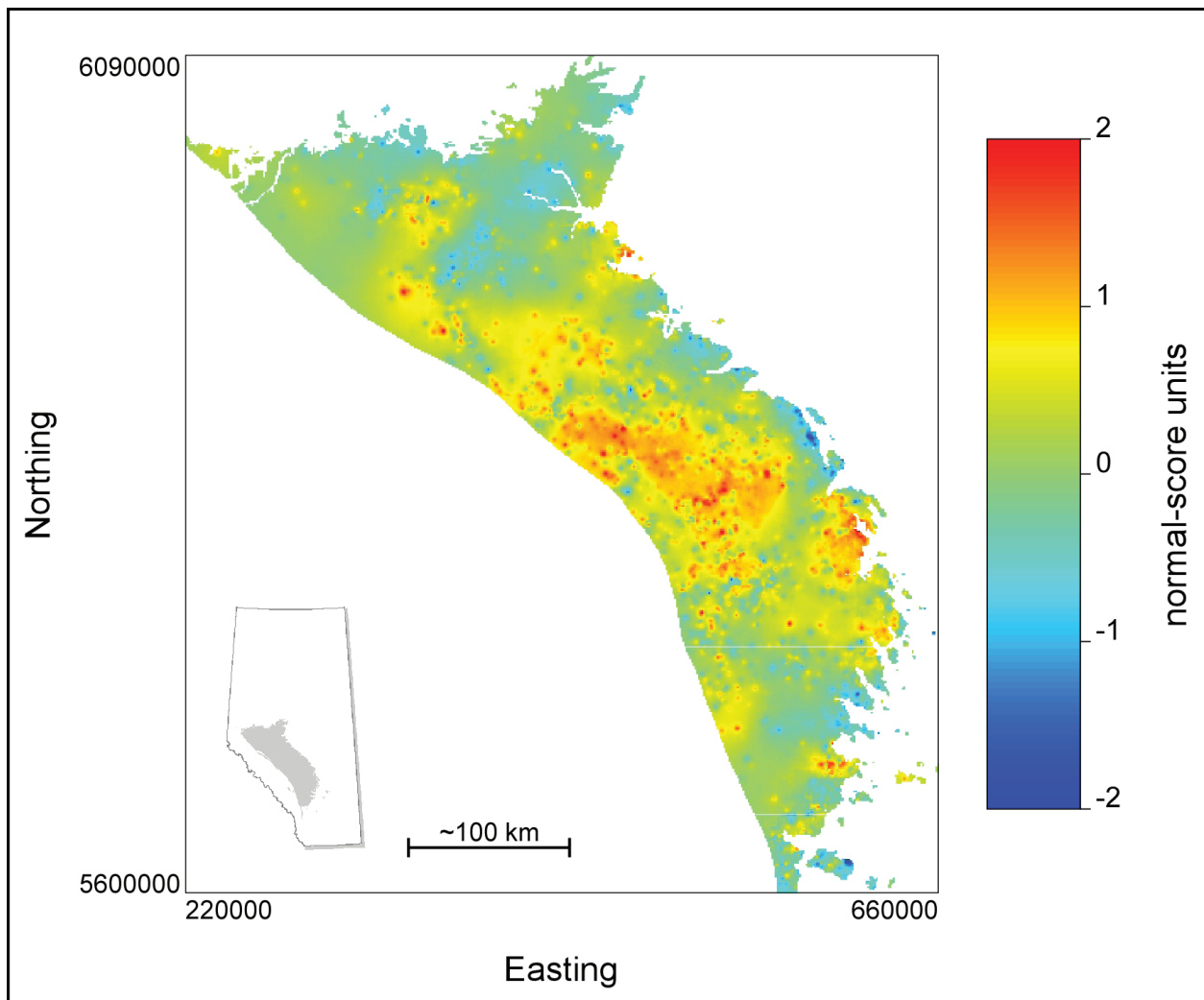


Figure 25. Kriging estimates in the bottom slice of the sandiness model, Paskapoo Formation, central Alberta.

Using the mean and variance of the estimates, any desired quantile of the local distribution can be back transformed. A standard practice is to use the P10 (tenth percentile, low) and P90 (ninetieth percentile, high) values as a measure of the spread. Figure 28 shows a map of the back-transformed P10 values, and Figure 29 shows a map of the back-transformed P90 values. High sandiness on the P10 map identifies very sandstone-dominated areas, and low sandiness on the P90 map identifies very mudstone-dominated areas.

### 5.4 Stochastic Simulation

The kriged model from the previous section can be used to create maps and cross-sections of the local

uncertainty. In this report, the best-estimate, high-case, and low-case values for each location were generated. However, the maps produced are not representative of the true lithological heterogeneity present in the subsurface. An estimation or interpolation method naturally produces smoother results than the actual data, with a lack of extreme high and low values. In a case such as this, where connected high and low permeability (or hydraulic conductivity) conduits or baffles drive the behaviour of the system, an assessment of the global uncertainty is needed.

Stochastic (or random) simulation adds random variation to a smooth map of estimates. The result restores the high and low values that are in the data but that are under-represented in the map

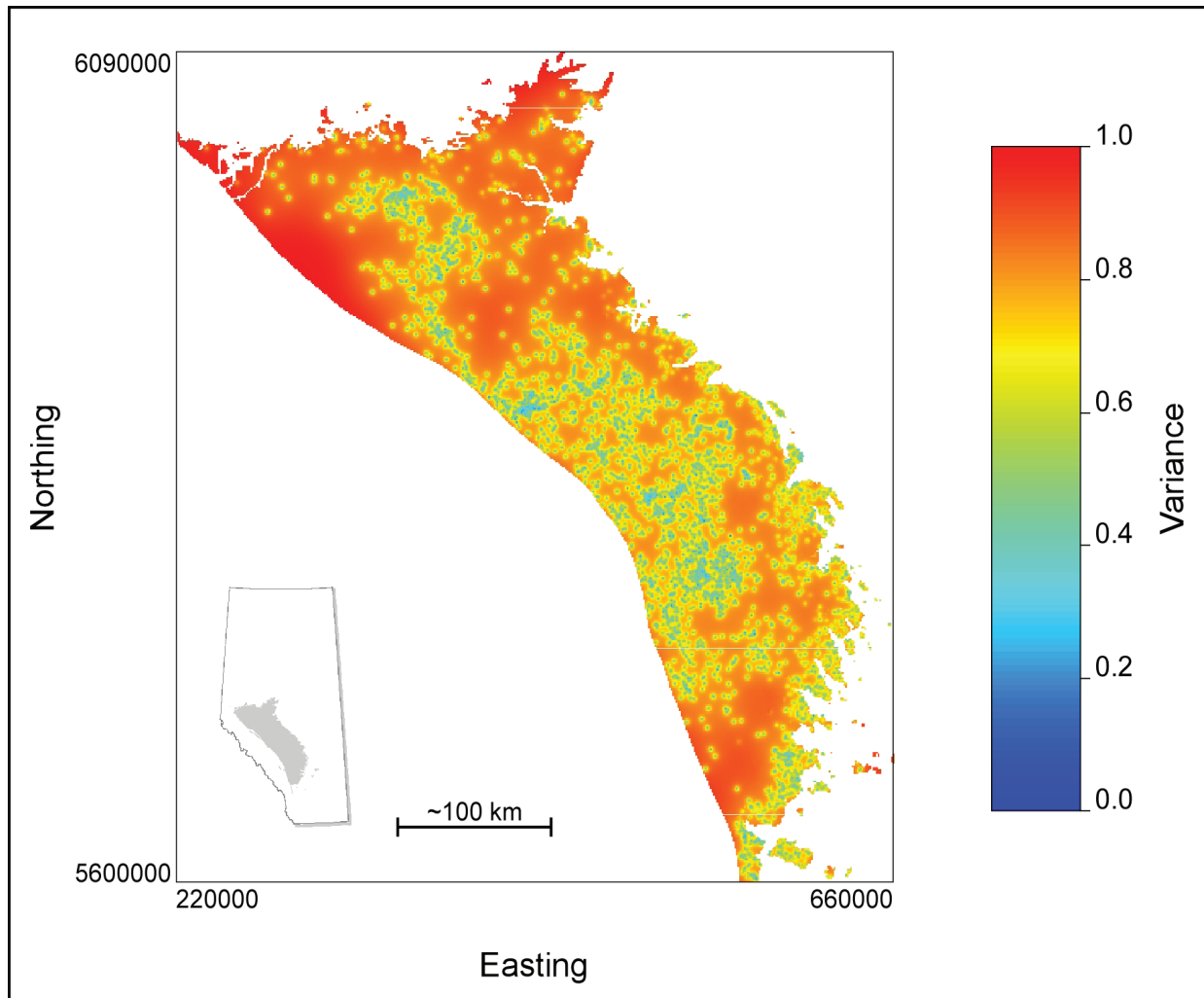


Figure 26. Kriging variances in the bottom slice of the sandiness model, Paskapoo Formation, central Alberta.

of estimates. These variations are not unique; a single case is called a realization and represents one possible outcome. The local statistics (P10, P50, P90, etc.) of a large enough number of realizations will tend to be similar to the local uncertainty assessment discussed above. An infinite number of realizations would give local statistics identical to the kriging local-uncertainty assessment. More complex, nonlinear properties of a model can be found, with uncertainty, by calculating the properties of the model on a realization-by-realization basis and then using all of the responses as the distribution of the property. This is commonly applied for properties such as recoverable reserves above a cutoff grade in mining, volume of connected pore space in petroleum applications, or probability to

exceed a contaminant threshold concentration in environmental assessments.

There are a number of different geostatistical simulation methods. The one used in this study, called p-field simulation (Srivastava, 1992), was chosen because it directly uses a previously created model of local uncertainty and is computationally efficient. The p-field uses the following workflow:

- 1) Simulate an unconditional realization in normal-score units using the variogram of the data.
- 2) Condition the values at each location using the equation  $Z_{cond} = Z_{krig} + Z_{sim} \times \sigma_{krig}$ , where  $Z_{cond}$  is the conditional simulated value,  $Z_{krig}$  is the kriged estimate,  $Z_{sim}$  is the unconditional

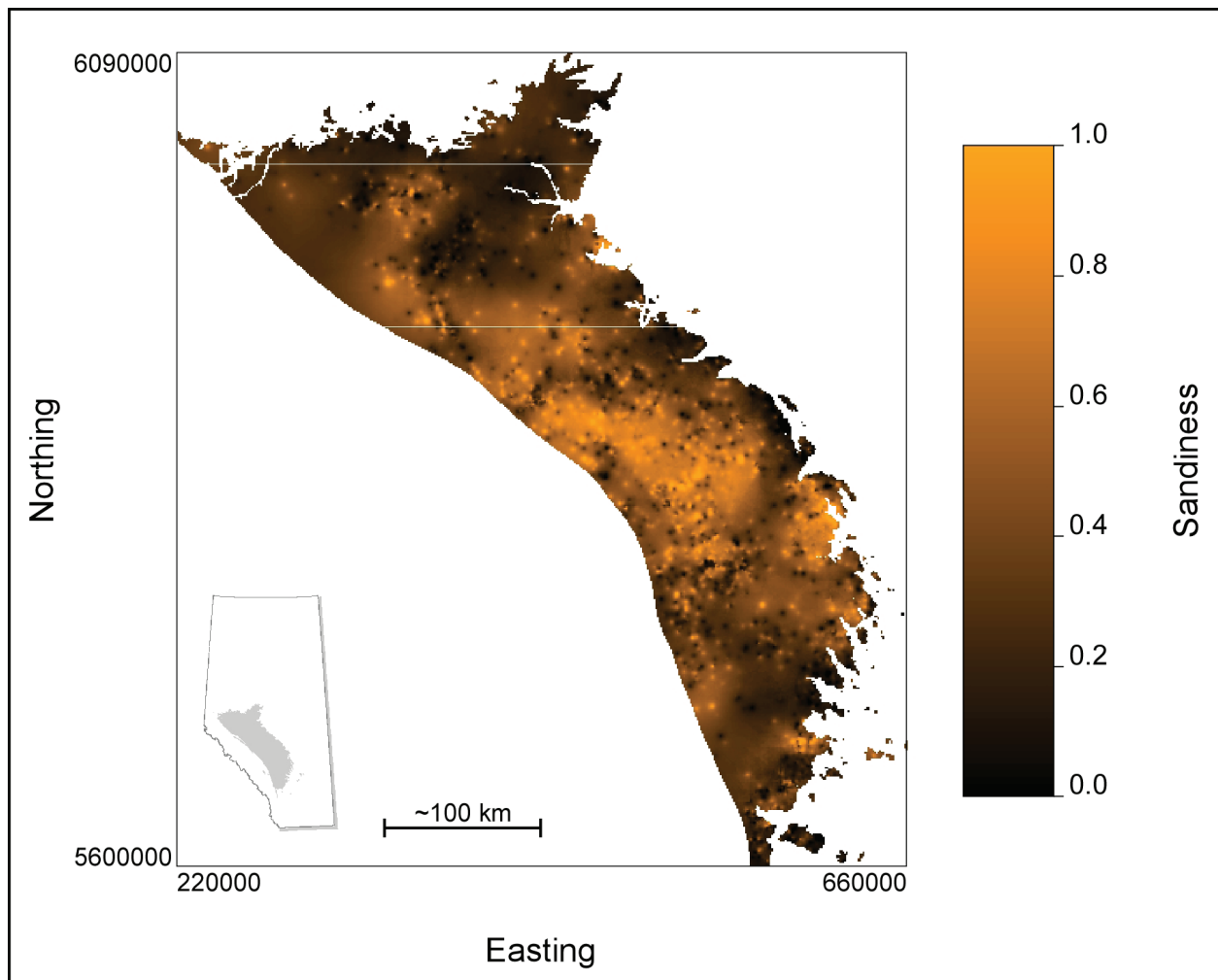


Figure 27. Back-transformed kriging estimates of sandiness values in the bottom slice of the model, Paskapoo Formation, central Alberta.

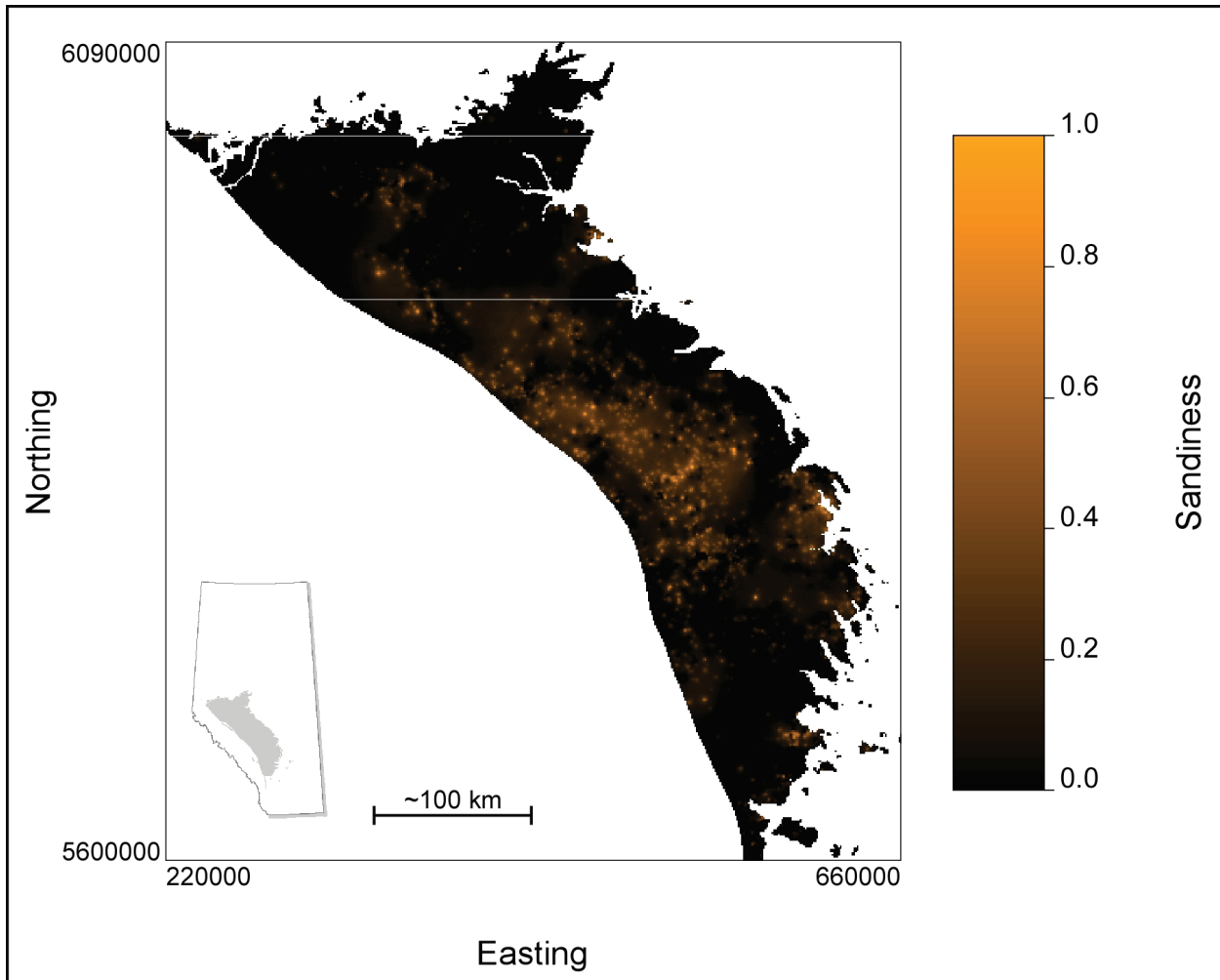


Figure 28. Back-transformed P10 (tenth percentile, low case) sandiness values in the bottom slice of the model, Paskapoo Formation, central Alberta.

simulated value and  $\sigma_{krig}$  is the kriging standard deviation.

- 3) Back transform the conditional values from normal-score units to original units.

Figure 30 shows a map of an unconditional realization in normal-score units. The high and low values do not correspond to any physical reality, but the distribution (histogram) is standard normal, and the spatial structure matches the input variogram of the data. Figure 31 shows a map of the corresponding conditional realization. The areas of high and low values correspond to sandy and muddy regions of the Paskapoo Formation, but the realization is still in normal-score units. Figure 32

shows a map of the same realization back transformed to original units. A histogram of the sandiness values in the simulated realization would be similar to that of the reference data, with the high and low values represented appropriately.

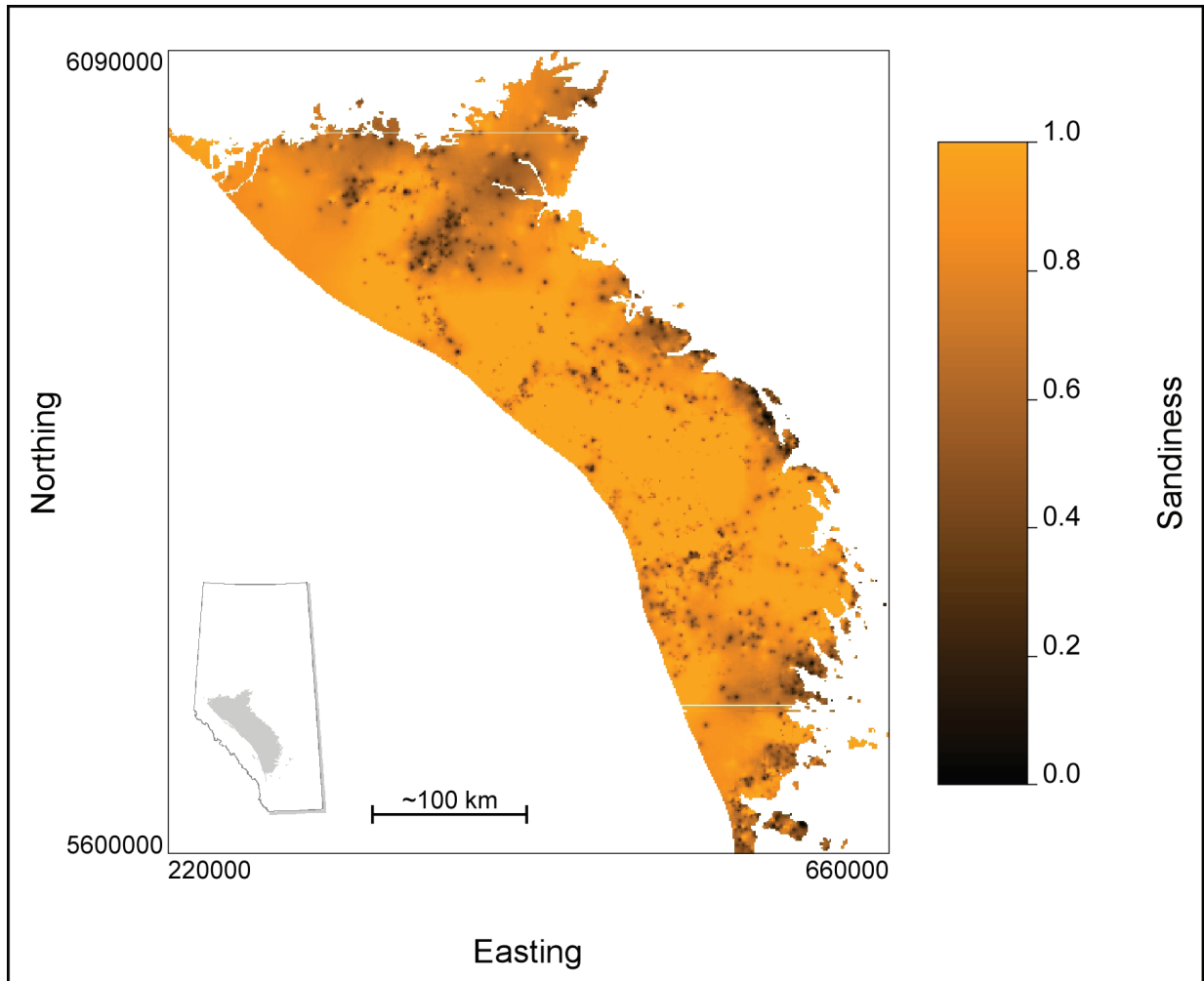


Figure 29. Back-transformed P90 (ninetieth percentile, high case) sandiness values in the bottom slice of the model, Paskapoo Formation, central Alberta.

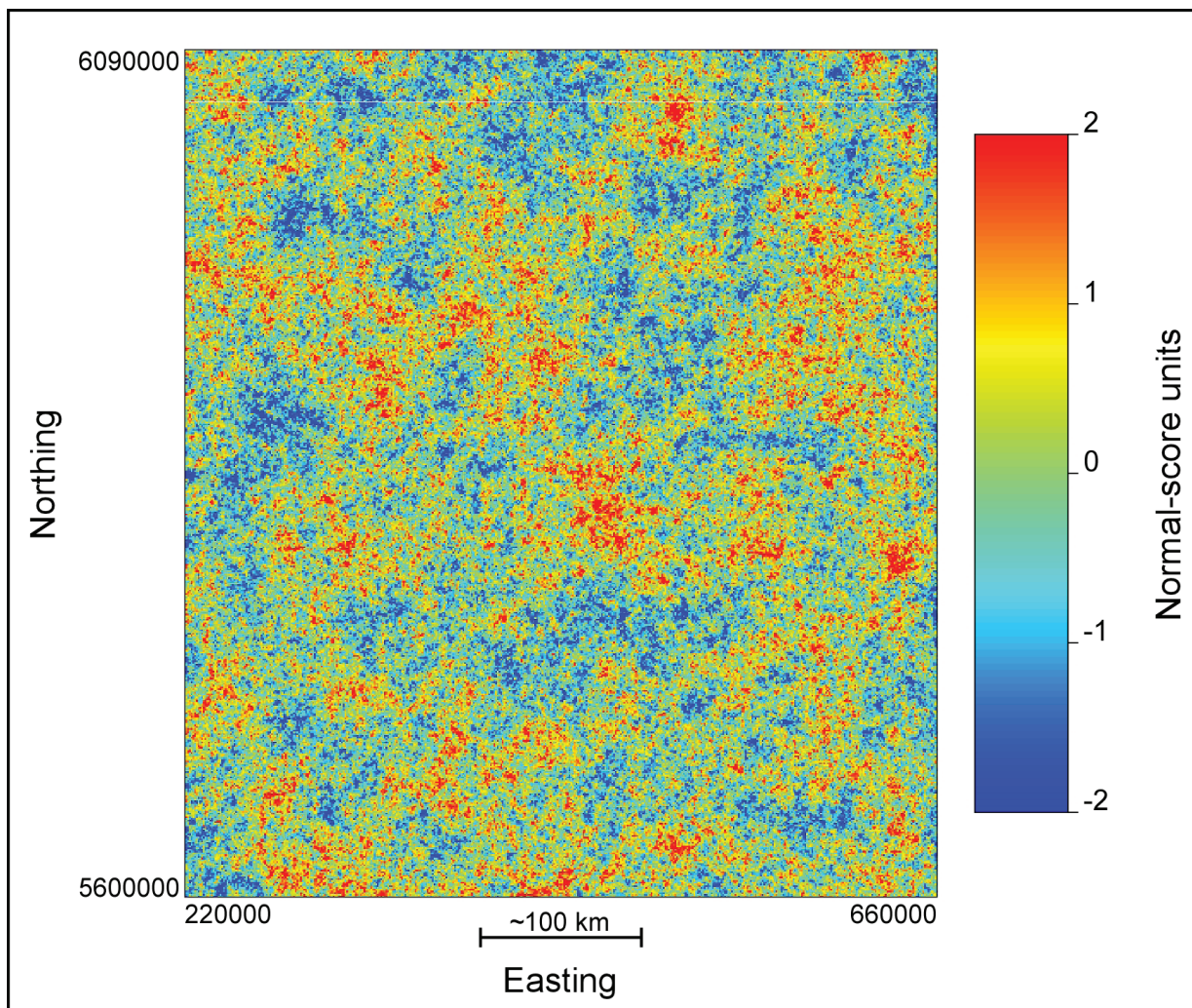


Figure 30. Unconditional simulated realization in the bottom slice of the model, Paskapoo Formation, central Alberta.

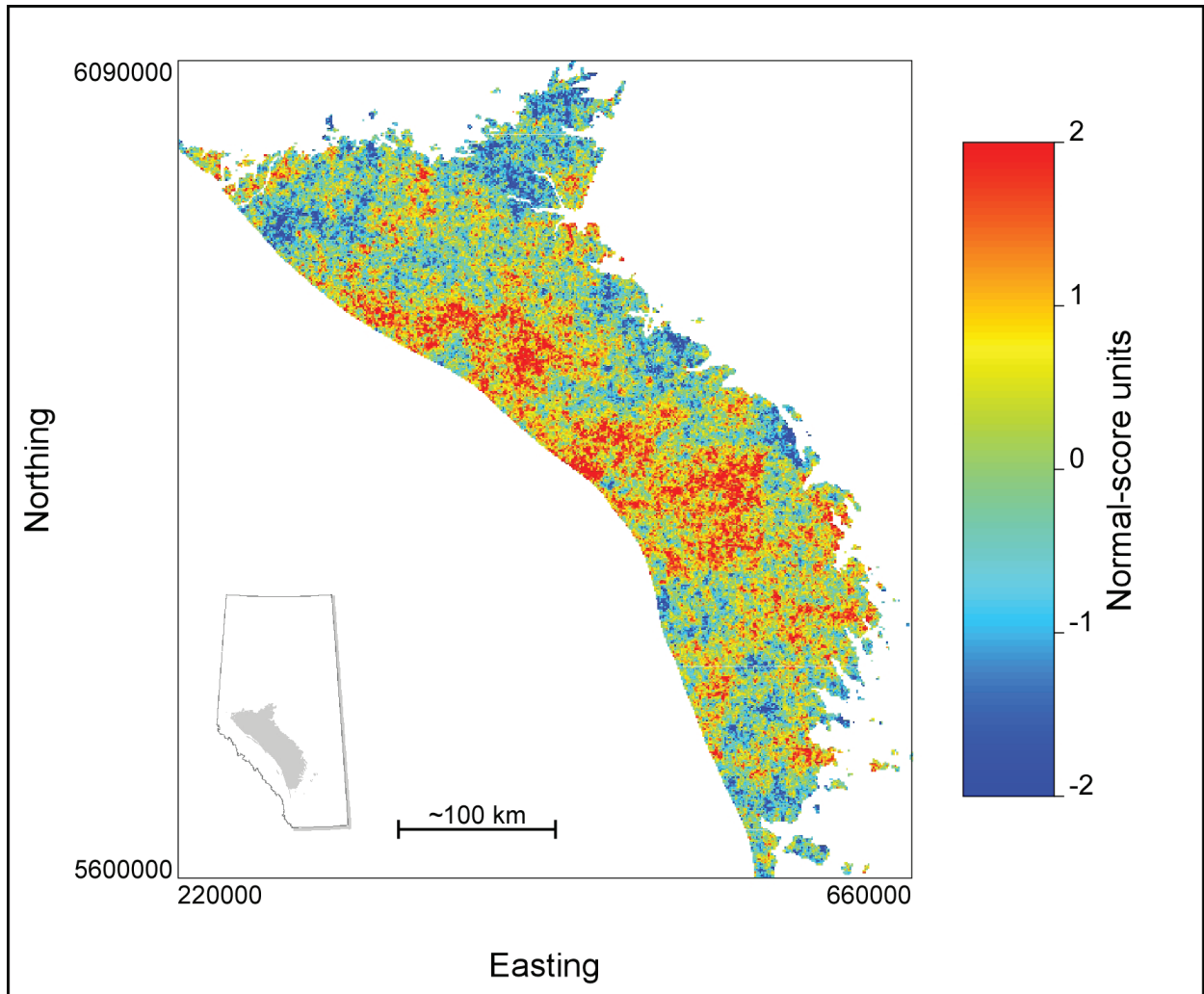


Figure 31. Conditional simulated realization in the bottom slice of the model, Paskapoo Formation, central Alberta.

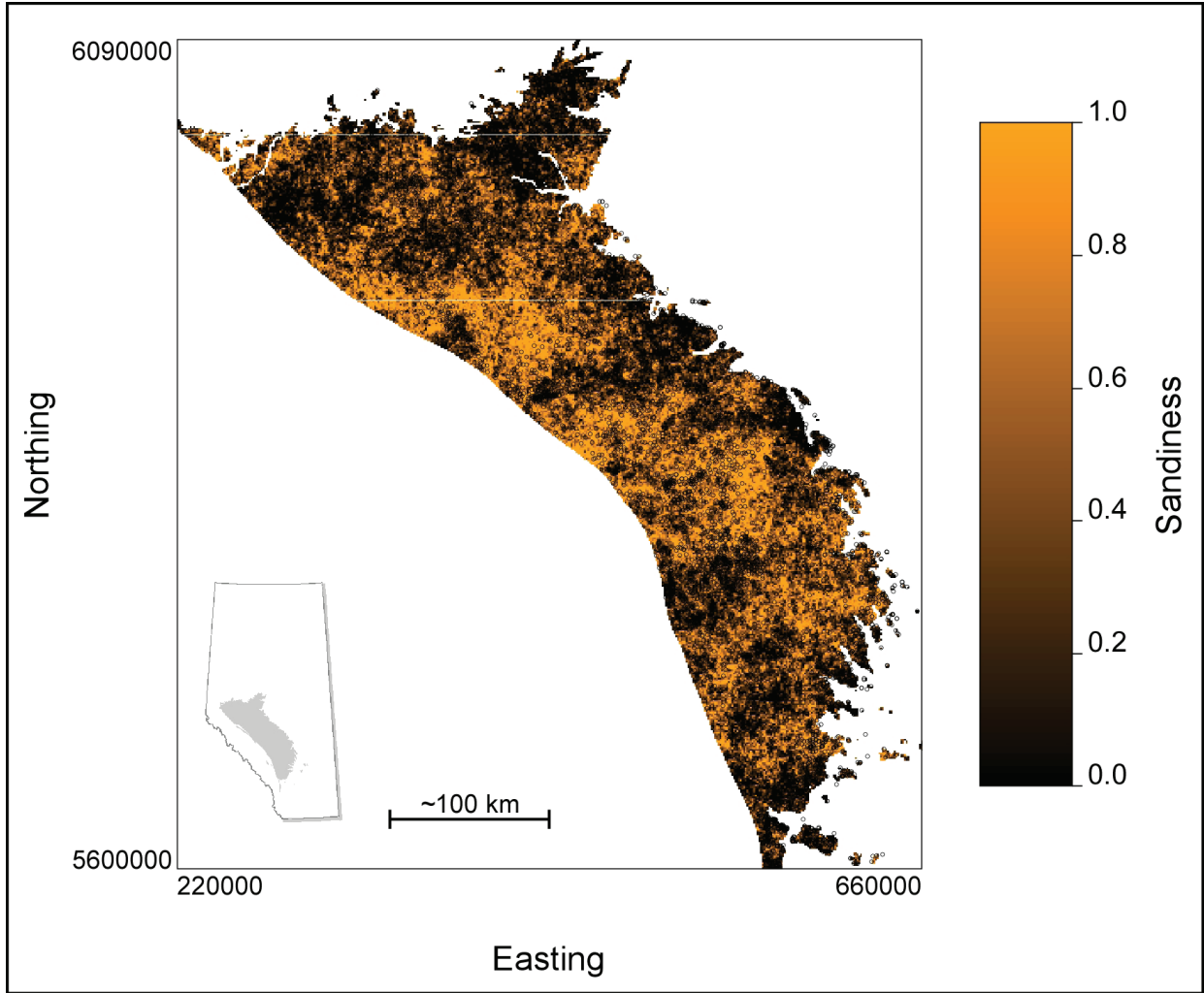


Figure 32. Back-transformed simulated realization of sandiness in the bottom slice of the model, Paskapoo Formation, central Alberta.

## 6 Geometry of Sandstone Bodies

As discussed earlier, the Paskapoo Formation is composed of isolated or stacked channel sandstone bodies and splay sandstone beds encased in a mudstone and siltstone matrix (Figure 33). The degree of connectivity between highly porous and permeable sandstone bodies primarily drives the hydraulic properties of the succession. For this reason, the spatial structure and arrangement of these sandstone bodies is an important factor in evaluating the extent and properties of hydrostratigraphic units. The spatial structure of sandstone bodies refers to the physical size and shape of the highly permeable sandstone beds. This includes the channel thickness, width, sinuosity, and the variability in these parameters. The arrangement of the sandstone bodies encompasses such features as stacking of channels, interaction between channels and splays, and connectivity of one channel system to another.

### 6.1 Previous Work

Dawson et al. (1994) concluded that individual Paskapoo Formation channel sandstone bodies were typically >15 m thick, with stacked successions commonly in excess of 60 m thick. Hamblin (2004) summarized the Paskapoo Formation channel sandstones as individual beds up to 15 m thick, typically 5 to 10 m, lenticular, and pinching out laterally over 150 m or more. Hamblin (2004) considered the stacked sandstone units to represent an interconnected network of channels in a vertically aggrading, anastomosing fluvial channel system. Grasby et al. (2008) considered the channel sandstone bodies to be generally 3 to 12 m thick, with stacked successions up to 50 m thick. According to Grasby et al. (2008) splay deposits are generally <3 m thick and typically no more than 1 m thick.

Recent studies (Burns et al., 2010a, b; Matthews, 2011) have applied 3-D, object-based, stochastic models to assess hydraulic connectivity of channel sandstone bodies and splay sandstone bodies encased in mudstone within a channel belt system in the Paskapoo Formation north of Calgary. After assigning hydraulic properties to these sandstone facies and other geometrical variables, such as

channel width, thickness, sinuosity, and meander amplitude, Burns et al. (2010a, b) conducted groundwater-flow simulations and determined that connectivity within the Paskapoo Formation is a function of channel sinuosity, which primarily affects transverse connectivity, and channel sand fraction, which influences both horizontal and vertical connectivity. Burns et al. (2010a) determined from water-well litholog data that channel sandstone beds constitute as much as 24% of the upper 100 m of the Paskapoo Formation. Citing previous studies of connectivity as a function of sand fraction (Fogg, 1986; Bridge and Mackey, 1993), they concluded that a 24% volume fraction of channel sandstone would result in relatively isolated sandstone channels that are in poor communication with each other but that have strong conductivity along the axes of the sandstone channels.

### 6.2 Local-Scale Architecture

Depending on the scale chosen, data are sampled at specific scales, and data distributions are dependent on the scale considered. Core-scale data show different characteristics than seismic data because core data represent a small volume of rock, whereas seismic profiles represent composite values of a very large volume. This phenomenon is well known in geostatistical literature. Variables that average linearly (including sandiness) will have several properties (Deutsch, 2002), such as

- the mean remains unchanged regardless of scale;
- the variance is reduced as scale increases; and
- the shape of the histogram will tend to be more symmetrical as scale increases.

To illustrate, Figure 34 shows the histograms of sandiness data calculated from GR logs at increments of 1 m (Figure 34a) and 25 m (Figure 34b), respectively. At a scale as fine as 1 m, the Paskapoo Formation is separated almost entirely into either ones (sandstone) or zeros (mudstone), with little averaging of the two. At the coarser scale of 25 m (which corresponds to the regional-scale sandiness model), there is

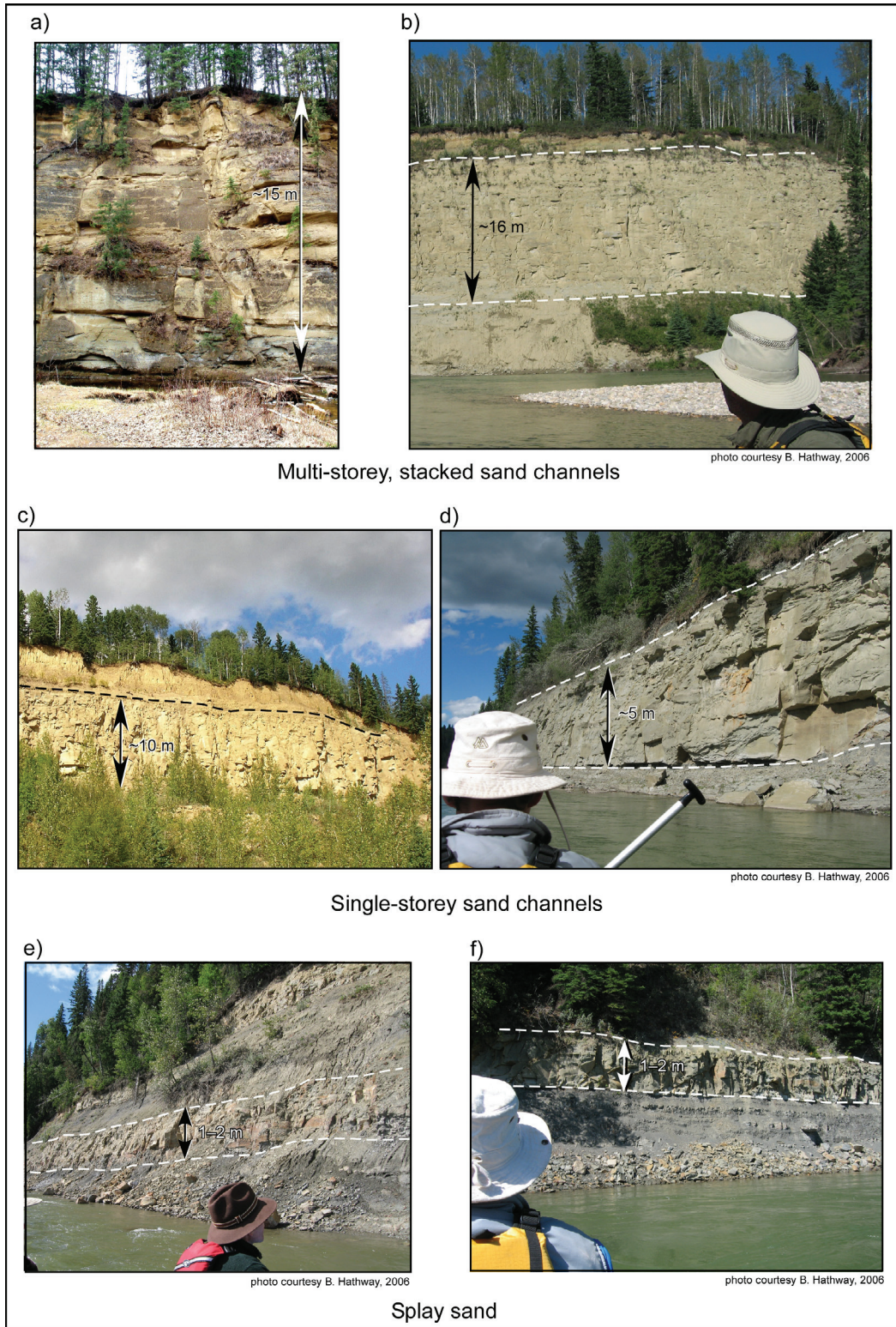


Figure 33. Outcrops of sandstone-body types within the Paskapoo Formation, central Alberta: a) Whitecourt area (Zone 11, 579594E, 5984239N); b) North Saskatchewan River (Zone 11, 635404E, 5824455N); c) North Saskatchewan River (Zone 11, 623068E, 5853349N); d) North Saskatchewan River (Zone 11, 622862E, 5852491N); e) North Saskatchewan River (Zone 11, 629811E, 5841462N); f) North Saskatchewan River (Zone 11, 629118E, 5844863N).

very little discrete sandstone or mudstone across the entire 25 m interval. The mean represents the proportion of sandstone within the Paskapoo Formation and does not change between scales, but at larger increments the data are closer to the central value and farther away from values of 0.0 and 1.0 and, correspondingly, the variance is reduced.

A significant factor in determining the thickness of a geological body from log data is the difference between true thickness and apparent thickness. The apparent thickness of any given sandstone interval recorded by a log is not necessarily representative of the true maximum thickness of the geological body. Where channel sandstone bodies form the strata, the true maximum thickness is unlikely to be seen because of variations in thickness along the cross-section. Figure 35 shows how a log can record sandstone bodies in the subsurface with apparent thicknesses different from the true maximum thickness of an individual channel sandstone body. Figure 35a shows a single channel with associated splay sands. Only a single well intersects the channel at its maximum vertical extent, whereas the others record the thicknesses of either the splays or the channel margins. Figure 35b illustrates a stacked sequence of five channels and three wells; the logs record six sand intervals: four are channel margins, one is near the maximum thickness of a single channel, and one is a very thick stacked channel structure. To determine the true thickness of individual channel sandstone bodies, the distribution of apparent thicknesses needs some interpretation.

### 6.3 Geostatistical Methods

Several geostatistical methods can infer the size of channel or splay sands. Indicator variograms may be used to infer the extent of geological bodies (Guo and Deutsch, 2010) but the variogram method does have limitations. The size of different facies bodies may also be determined by using runs (Boisvert, 2007; Boisvert et al., 2007; Lyster, 2009). Runs are the probability of a certain facies (sand/mud) occurring consecutively for a given distance or number of data points. As all of the data used in this study are from vertical logs and boreholes, the thickness of the sandstone bodies is the only property that can be directly inferred; other parameters are found by methods that are more indirect.

The first geostatistical method discussed here, the variogram, measures the variability between different locations separated by a lag vector. For a vertical lag vector, the variogram is a measure of the spatial variability along boreholes or geophysical logs. An indicator variogram is the variogram of an indicator variable that consists of ones and zeros, which in this case represent sandstone and mudstone, respectively. An indicator variogram is related to the probability of transitioning from one indicator value (or facies type) to another at the lag vector distance.

Figure 36 shows the vertical variogram calculated from the GR log data represented in Figure 34a. Though this is not exactly the same as a true sandstone/mudstone indicator, it is a close enough

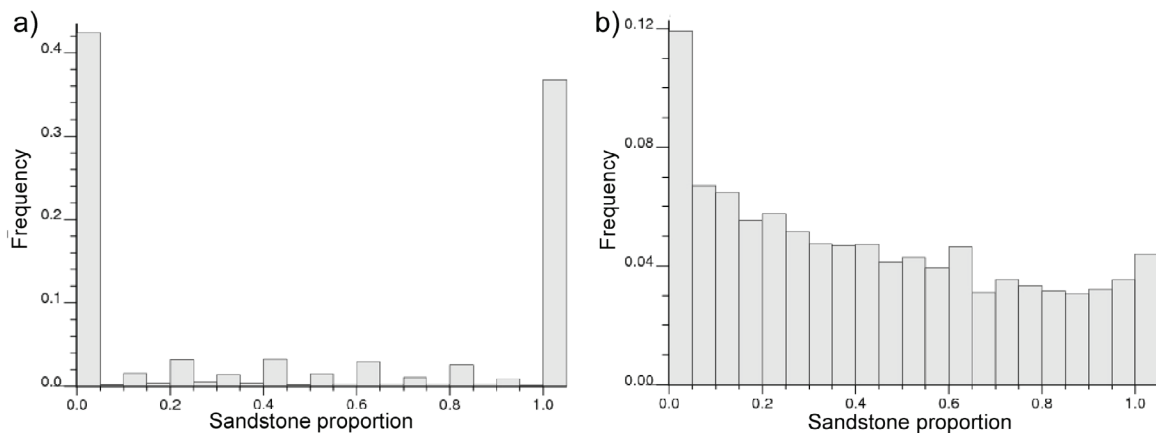
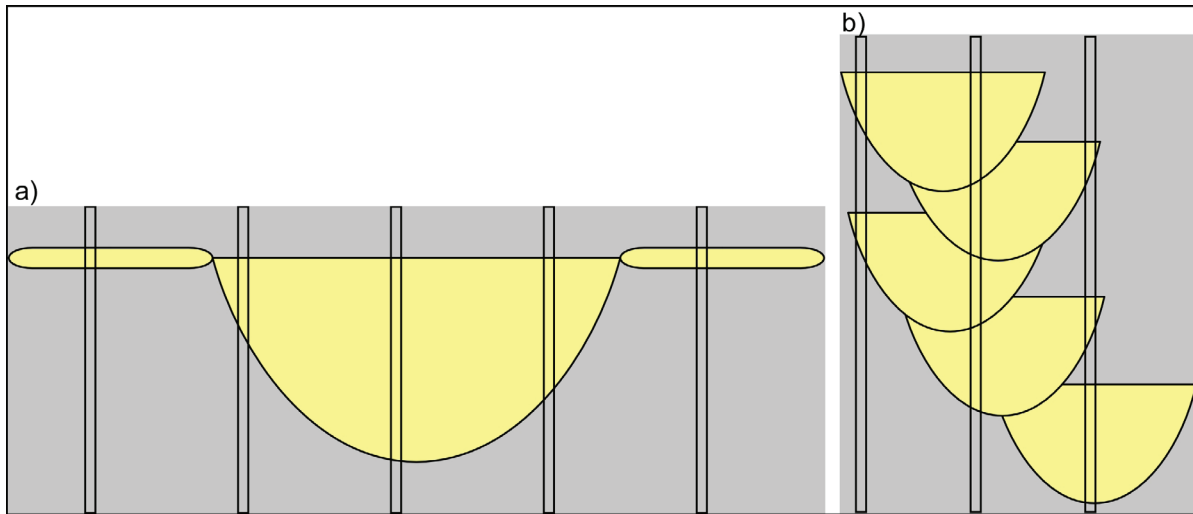


Figure 34. Data histograms for the gamma-ray log data at a) 1 m increments and b) 25 m increments.



**Figure 35. Examples of logs intersecting sandstone geobodies: a) logs intersecting splays and a single channel sandstone body (both shaded yellow) where only a single log intersects the full vertical extent of the largest sandstone body; b) logs intersecting a stacked channel sequence with small and large sandstone intervals encountered.**

approximation for our purposes. At a short range of a few metres, there is an abrupt increase in the variogram. This is attributed to the thin splay sands. The longer-range structure of the variogram reaches the sill at a range of about 25 m. This is the approximate maximum vertical extent of the sandstone bodies, which in this case is the thickness of the channels.

Although a vertical variogram is useful for a quick analysis of major and minor structures, the variogram is a second-order statistic, and so only captures the spatial structure represented by the endpoints of a lag vector. Runs are a higher-order (or multiple-point) statistic and can give greater insight into the distribution of sizes of geological bodies.

Figure 37 shows the distribution of sandstone body thicknesses extracted from the GR logs. The horizontal axis in Figure 37 shows the thickness of individual continuous sand intervals from the GR logs; the left vertical axis shows the probability that an individual sand interval is a given thickness, weighted for sand volume; and the right vertical axis shows the cumulative proportion of sand. This chart reveals that a significant proportion of sandstone within the Paskapoo Formation resides in beds 1 to 3 m

thick, likely representing splay sands with limited areal extent. At thicknesses between about 3 and 6 m, the amount of sandstone declines rapidly. This is interpreted as representing those parts of a channel where the full thickness is not intersected by a log (the margins). The long plateau in the curve, from about 7 to 23 m thick, is interpreted to represent single-storey channels that are intersected by logs at or near the thickest part of the sand deposit. At sandstone thicknesses >23 m, the long declining tail on the chart is interpreted to represent progressively larger multi-storey channel successions. Overlap between these interpretations is to be expected; a thick splay and the thin edge of a channel are indistinguishable by this method, but a typical channel, splay, or stacked sequence will be identifiable.

Figure 38 shows the same distribution chart as Figure 37, but with the cumulative distributions highlighted. Based on this interpretation, splay sands make up about 25% of the total sandstone within the Paskapoo Formation, single-storey channels about 45%, and multi-storey channels about 30%. Even though there are relatively few sequences of stacked channel intervals thicker than 50 m, the great thickness of these stacked channel sandstone bodies means they contain about 5% of the total sandstone within the formation. Based on

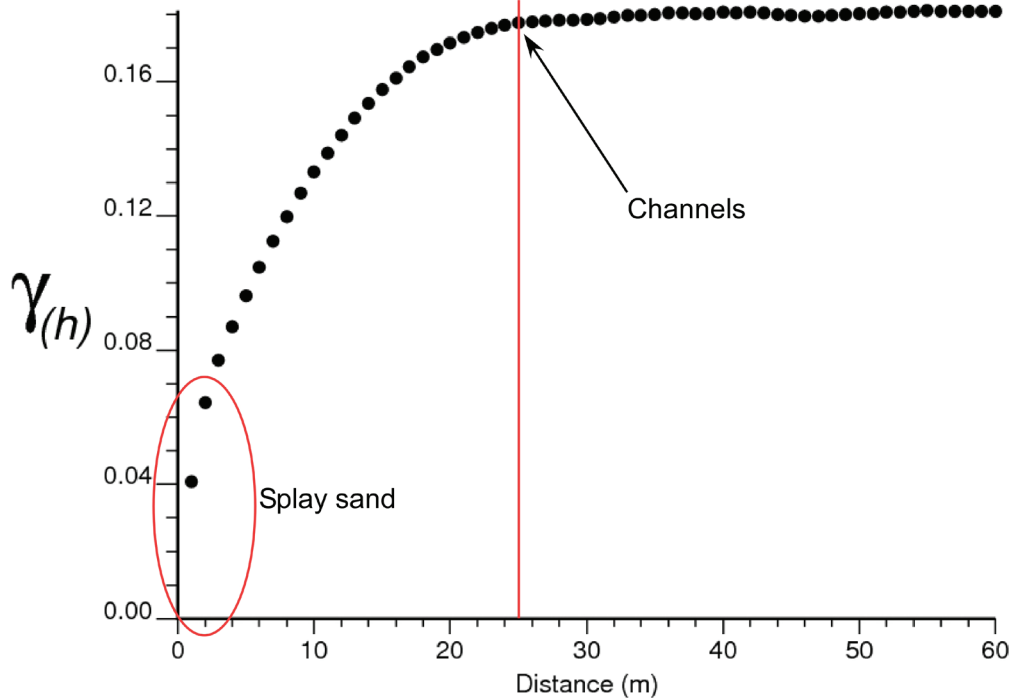


Figure 36. Vertical variogram of the gamma-ray log sandiness data at 1 m intervals.

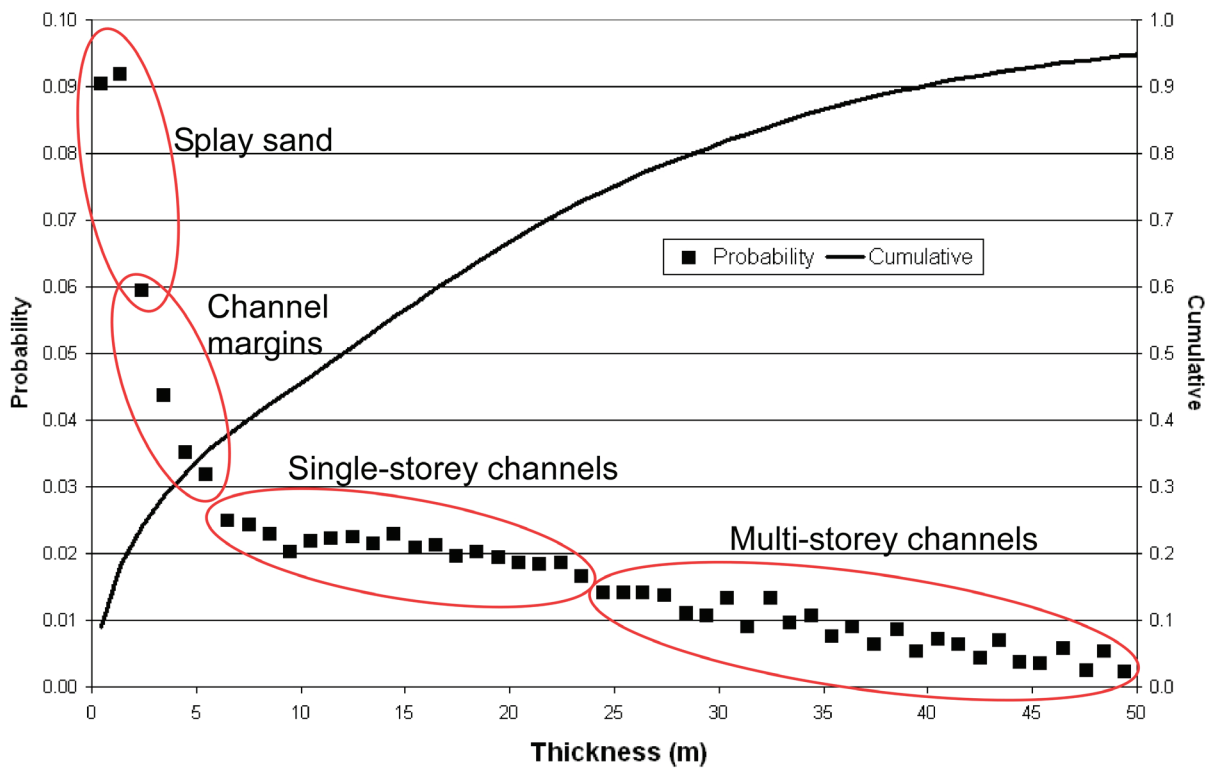


Figure 37. Distribution of sandstone body thicknesses encountered in the gamma-ray log data showing the interpreted sandstone-body type corresponding to the different thicknesses.

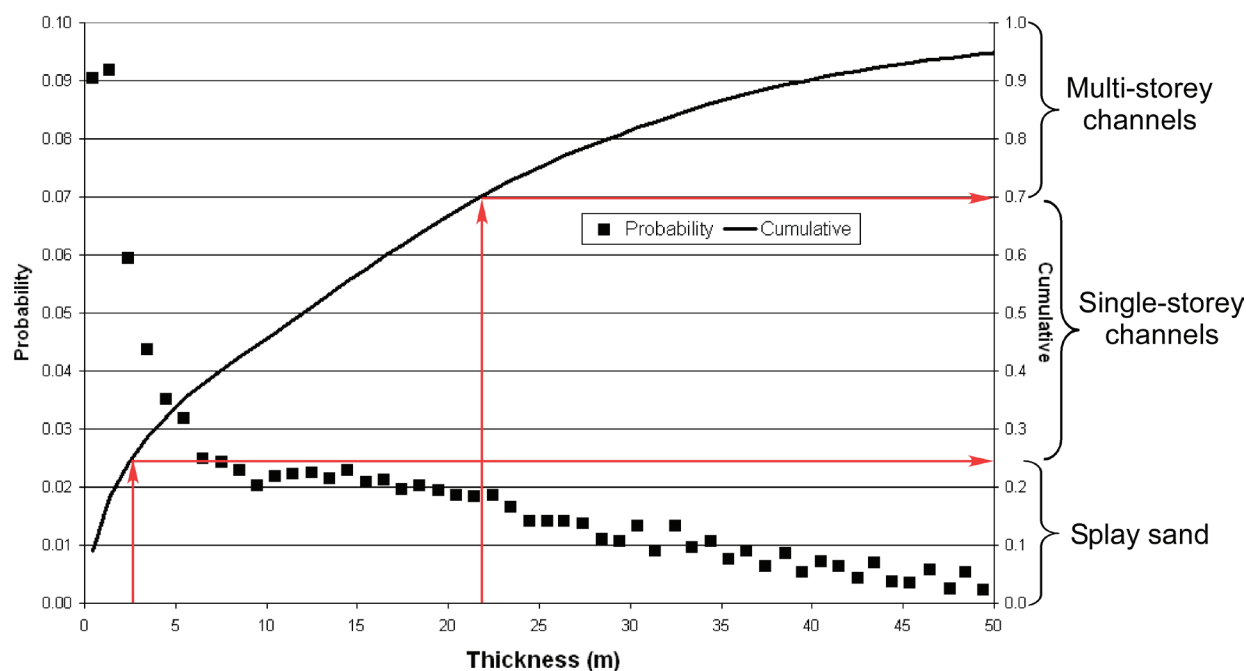


Figure 38. Distribution of sandstone body thickness encountered in the gamma-ray log data showing the interpreted proportion of sandstone corresponding to each type of sandstone body.

our estimate that sandstone makes up 40% of the Paskapoo Formation, we conclude that single- and multi-storey channel sandstone bodies constitute about 30% volume of the entire Paskapoo Formation. This is somewhat greater than the 24% volume estimate of Burns et al. (2010a). We believe their estimate to be lower because their study area was more limited in scope (both in areal extent and depth) and was geographically located in the southern, muddier parts of the Paskapoo Formation.

### 6.3.1 Mini-Modelling

Only the vertical dimensions of the sandstone bodies in the Paskapoo Formation can be directly inferred from the data. To determine horizontal extents, a procedure called mini-modelling was used (McLennan et al., 2006), with the modelling parameters matched to the data in a method similar to training image selection (Boisvert, 2007; Boisvert et al., 2007; Lyster, 2009).

Mini-modelling is a process that simulates the fine-scale structure of a formation for the purpose

of defining the relationship between simple properties (such as porosity or, in this case, sandiness) and more complex properties (such as permeability or hydraulic conductivity) at a larger scale. The simulation can use any appropriate algorithm and can incorporate any important structures or statistics. After generation of the simulated realizations, complex properties, such as flow response, may be calculated.

In some geostatistical simulation methods, a training image is used to infer spatial statistics rather than inferring it directly from the data. A training image is a 3-D model that represents the conceptual geology being modelled while not being conditional on the available data. Because a training image is a fully populated 3-D model with the spatial structure of the volume of interest, any desired spatial statistics can be inferred easily, which is not possible when using sparse and scattered field data. To create a training image, object-based simulation methods (Deutsch and Tran, 2002) create realistic geological patterns in a fully populated grid. Any training images

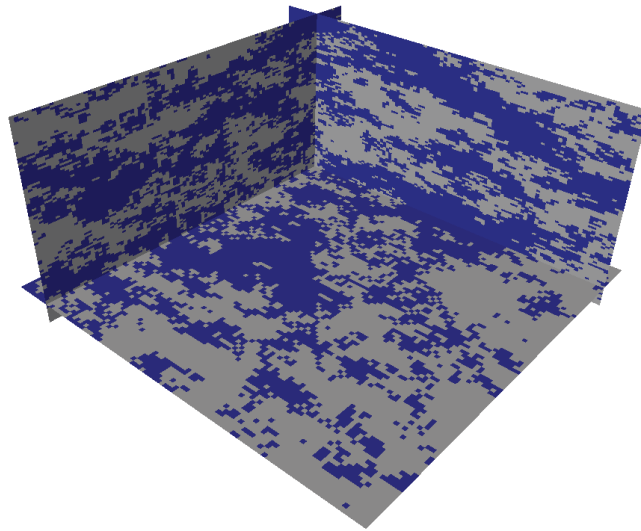


Figure 39. Fence diagram of a mini-model created using the SISIM program. Blue is sandstone, grey is mudstone.

generated need to be checked that they match both the geologist's conception of what the structure looks like and the statistical spatial structure inferred from the data.

By combining these two concepts (mini-modelling and conceptual models of geology through training images), other geometrical parameters of the sandstone bodies in the Paskapoo Formation can be calculated. As a first-pass proof of concept, two relatively simple geostatistical programs were used to generate mini-models that honour the variogram structure but not any conceptual model of geology. The size of the cells in the mini-models is 100 by 100 by 2.5 m, which is exactly 1/10th the size, in each dimension, of the cells in the regional-scale sandiness model. This makes upscaling properties relatively easy. Each mini-model is 100 by 100 by 100 cells, so there are 1000 regional-scale sandiness cells represented in each mini-model. The sandiness data was recalculated at a 2.5 m scale instead of the previous 25 m scale. Because of the difference in scale between the mini-model cells and the regional-scale model cells, the variogram is different. The variogram model at a 2.5 m scale is:

$$\gamma(h) = 0.176 + 0.616 \cdot \text{Exp}_{\substack{ax=1147.5 \\ ay=719.45 \\ az=23.737}}(h) + 0.208 \cdot \text{Sph}_{\substack{ax=82328 \\ ay=61952 \\ az=27.37}}(h)$$

This variogram model was used for pure sandstone and mudstone at a 2.5 m scale. All cells in the mini-model were assigned values of 0 (pure mudstone) or 1 (pure sandstone).

The first simulation program we tested is called SISIM and uses sequential indicator simulation (SIS; Deutsch and Journel, 1998). SIS is a purely variogram-based indicator simulation method that honours only the input proportions of the indicators and variograms. Figure 39 shows a fence diagram of a mini-model created using SISIM; the mini-model reproduces the vertical as well as the horizontal (sparsely sampled) variograms of sandiness. The patchiness seen in Figure 39 is typical of variogram-based methods because of the property of maximum entropy or randomness.

The second program tested is called ELLIPSIM (Deutsch and Journel, 1998). ELLIPSIM randomly places overlapping ellipsoids in a simulation grid until ellipses populate a target proportion of the grid. An input variogram can be honoured by setting the ellipse dimensions to the ranges of the

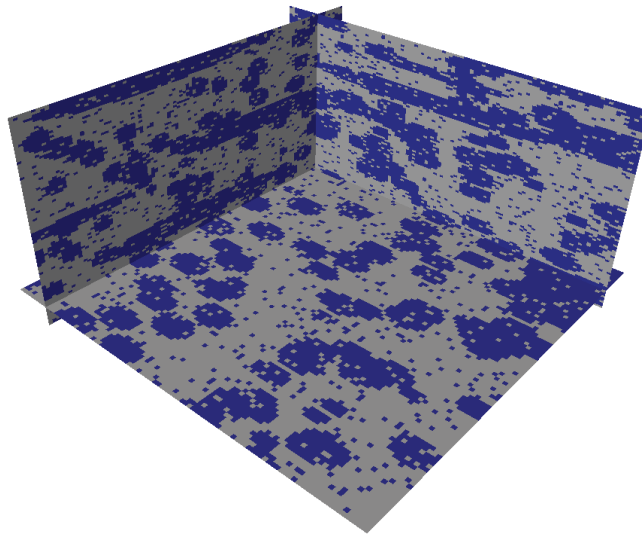


Figure 40. Fence diagram of a mini-model created using the ELLIPSIM program. Blue is sandstone, grey is mudstone.

variograms structures; in this case, the nugget effect was reproduced by adding random noise to the simulated grid. Figure 40 shows a fence diagram of a mini-model created using ELLIPSIM.

The most realistic mini-modelling algorithm is found in a program called FLUVSIM (Deutsch and Tran, 2002). FLUVSIM randomly places channel and (optionally) crevasse splay and levee structures of user-defined dimensions within the simulation grid until target proportions are met; it then modifies the structures to better match the target facies proportions. In this case, the conceptual model of geology within the Paskapoo Formation is sandstone channels and splays, therefore, FLUVSIM is well suited to mini-modelling. Although mini-modelling is normally used for upscaling properties, the primary goal in this case was to determine the sandstone-body geometry by iteratively simulating until a reasonably close match to the data statistics (proportions and variogram) was found.

FLUVSIM needs channel and splay geometries as input parameters. The thicknesses were previously determined, but initial estimates for the width to

thickness ratio and other parameters were needed. Gibling (2006) compiled an extensive review of fluvial channel body widths and thicknesses, which was a valuable resource in choosing a starting point. Because FLUVSIM uses properties that are more complex than the variogram, the initial assignments of channel and splay geometries did not match the data variogram shown above. The parameters were changed, and the mini-modelling was repeated until a closer match was achieved. The complex interactions between the parameters make this process difficult, and the solution that was found is not unique because there are many different geometrical parameters that could match the input variogram. The final parameters found with the closest match are

- channel thickness of 20 m,
- channel width of 400 m,
- width to thickness ratio of 20:1,
- average departure from centreline of 1200 m,
- sinuosity length scale of 6000 m,
- splay thickness of 2 m, and
- splay diameter of 500 m.

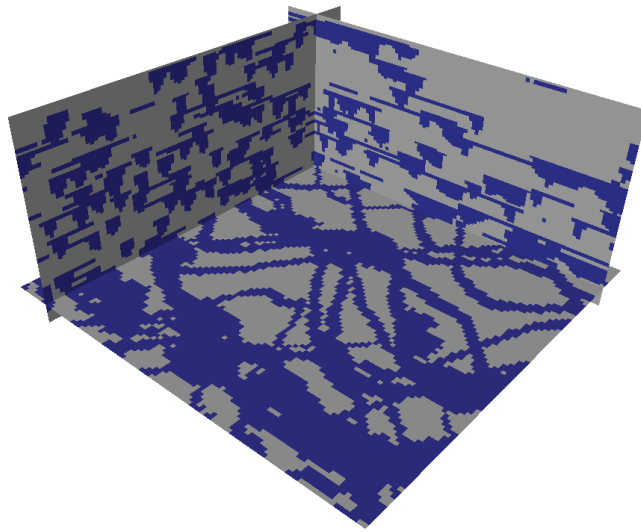


Figure 41. Fence diagram of a mini-model created using the FLUVSIM program. Blue is sandstone, grey is mudstone.

Figure 41 shows a fence diagram of a mini-model created using FLUVSIM. The channels and splays are evident in plan, cross-section, and long-section view.

Figures 81–89 in Appendix 3 show detailed mini-modelling results for all three algorithms.

A number of assumptions and simplifications were made to allow for the mini-modelling process. Every channel and splay in the model was assigned the same geometrical parameters, so the variation that is always present in natural geological systems is absent. All of the channels are aligned along the same axis as the simulation grid, again with no variation. The direction of transport and channel orientation in the Paskapoo Formation is assumed to be generally outward from the mountains and, in a local area, is assumed to be relatively constant, but over the entire area there would certainly be variations.

Finally, the geometrical parameters found by mini-modelling are not unique. A variogram is too simple to capture complex features and, as such, many different sets of fluvial geometries could reproduce the modelled variogram.

### 6.3.2 Sandiness-Flow Relationships

In this study, mini-modelling mainly determined channel and splay geometry, although the original purpose was to upscale properties that do not average linearly, in particular, flow properties such as permeability or hydraulic conductivity. Other studies have examined the relationship between architecture and flow response in the Paskapoo Formation (c.f. Burns et al., 2010a, b). With the mini-models already created, it was relatively simple to perform upscaling to relate sandiness of a regional-scale modelling cell to permeability. The program FLOWSIM (Deutsch, 1999) solved the steady-state flow equations with no-flow boundary conditions to take a number of small grid cells and determine the effective permeability of an upscaled grid cell. In each mini-model, there is the equivalent of 1000 regional-scale sandiness cells and ten mini-models were generated, so there are 10 000 data points relating sandiness to permeability.

Figure 42 shows the sandiness–horizontal permeability relationship for the FLUVSIM models, and Figure 43 shows the sandiness–vertical permeability relationship. Permeability values

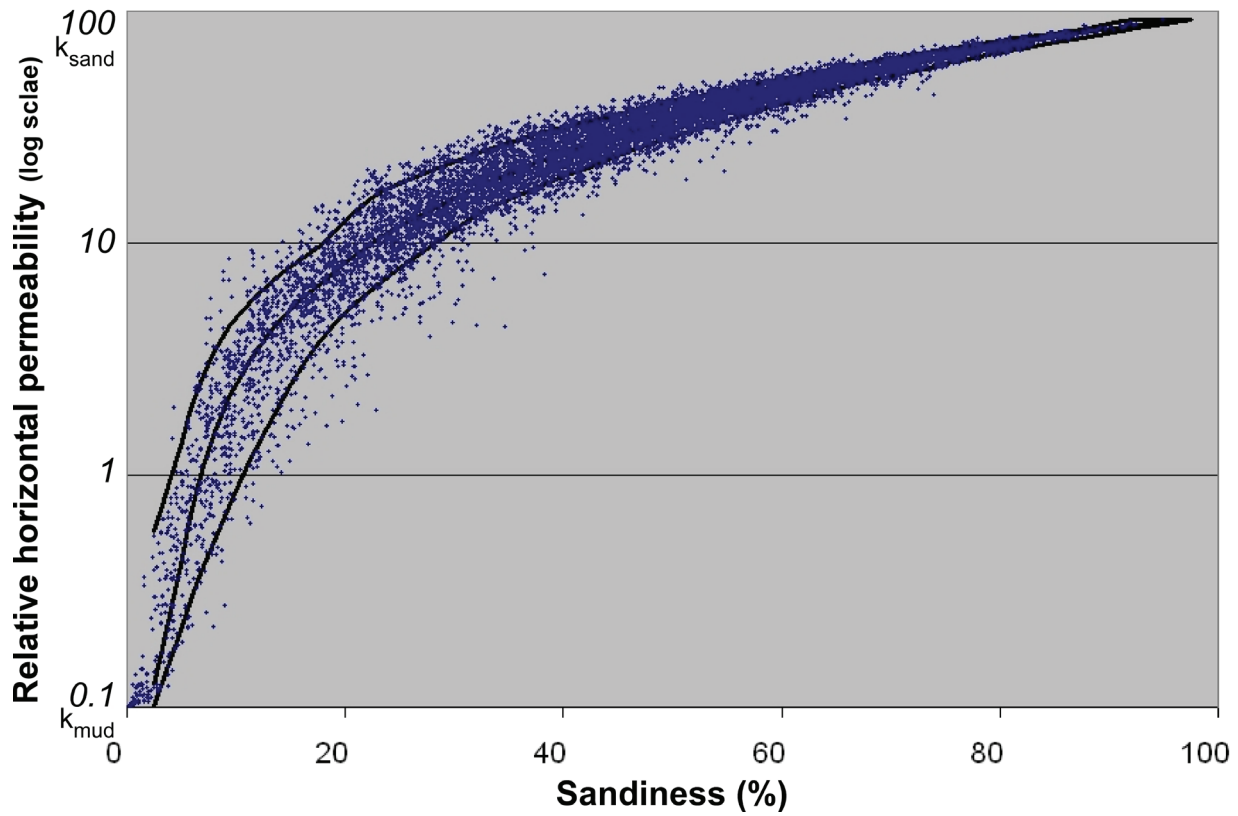


Figure 42. Per cent sandiness versus horizontal permeability relationship derived from the FLUVSIM mini-modelling results.

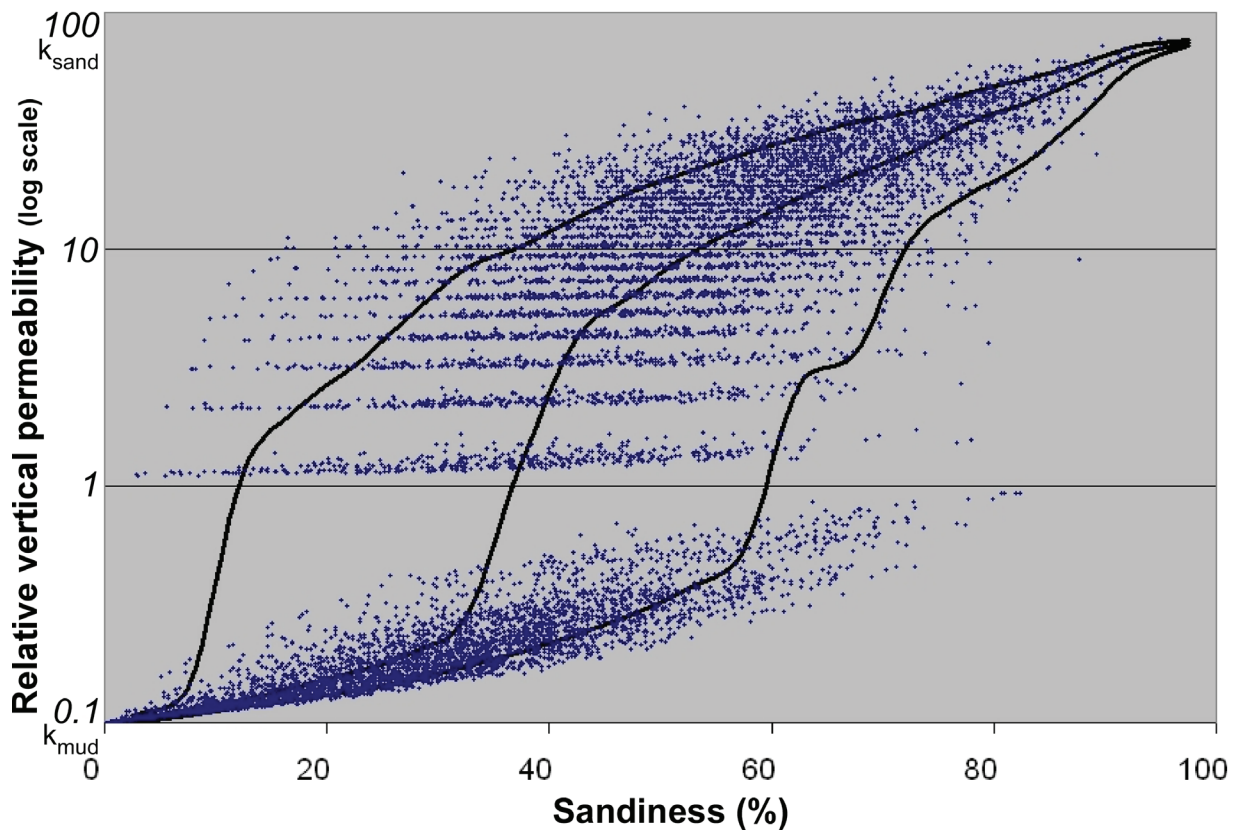


Figure 43. Per cent sandiness versus vertical permeability relationship derived from the FLUVSIM mini-modelling results.

for sandstone and mudstone were 100 and 0.1 millidarcies (mD), respectively. These are average values taken from air-permeameter test results on Paskapoo Formation cores drilled by the AGS (Riddell et al., 2009), which are consistent with published data from other Paskapoo Formation cores (Grasby et al., 2008; Burns et al., 2010a). The figures show all 10 000 data points on a semilog scale as well as P10, P50, and P90 quantile lines. From the relationships, it can be seen that, for the volume of a regional-scale model cell (1 km by 1 km by 25 m), relatively little sand is needed for horizontal connectivity, whereas more is needed for vertical connectivity. There is also more spread in the permeability distribution in

the vertical direction. The interpretation section of this bulletin contains further details on these and other observations.

The sandiness–permeability relationships allow multivariate simulations to be performed. Even though these simulations are not used for anything more than a proof of concept in this bulletin, the permeability values could be used if more complex flow simulation were to be done in the future. Figures 44 and 45 show horizontal and vertical permeability simulations, respectively, which are conditional to the sandiness realization shown in Figure 32. The high and low values occur in similar locations as the sandiness simulation, which is expected.

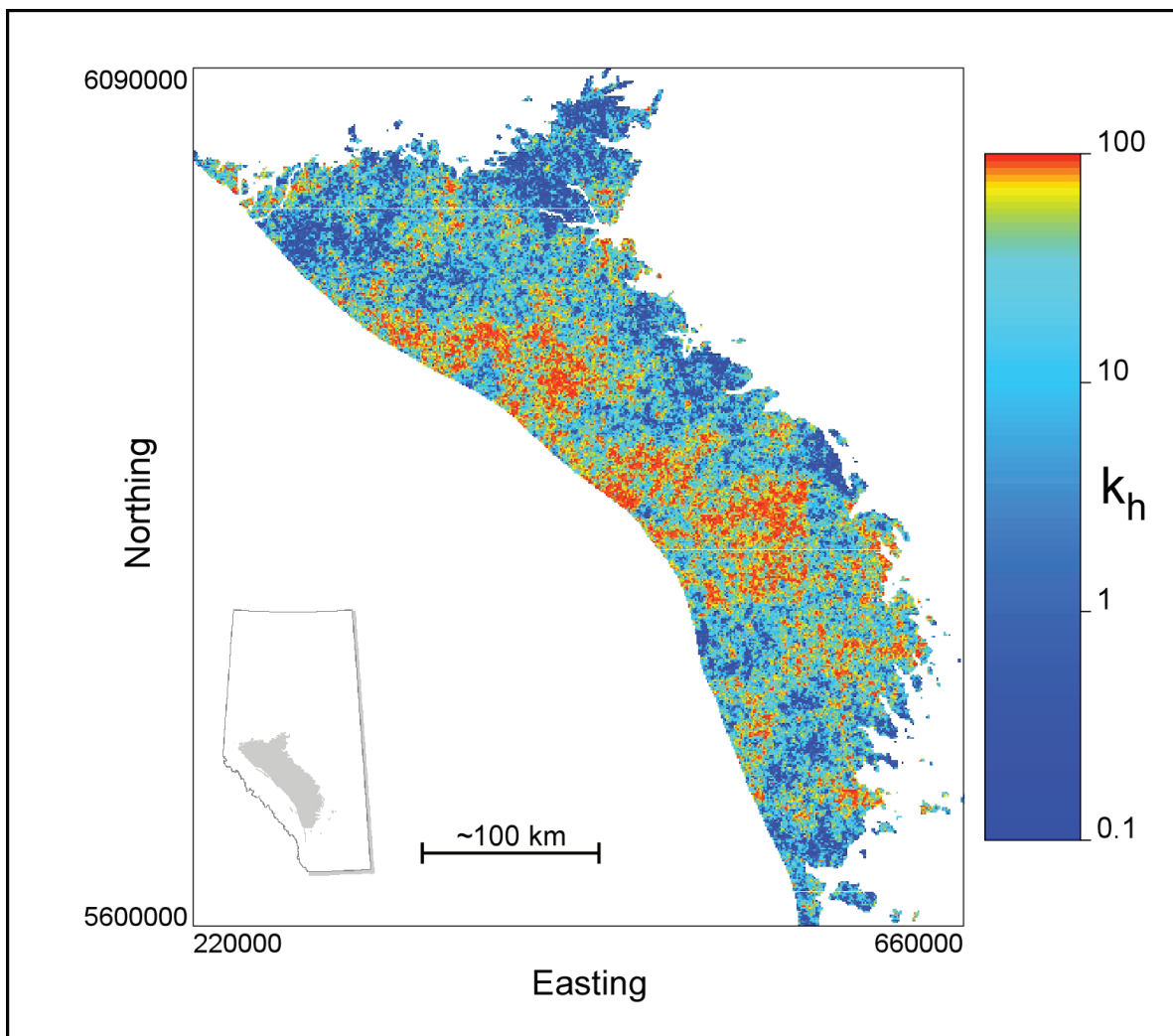


Figure 44. Simulated realization of horizontal permeability ( $k_h$ ) in the bottom slice of the model.

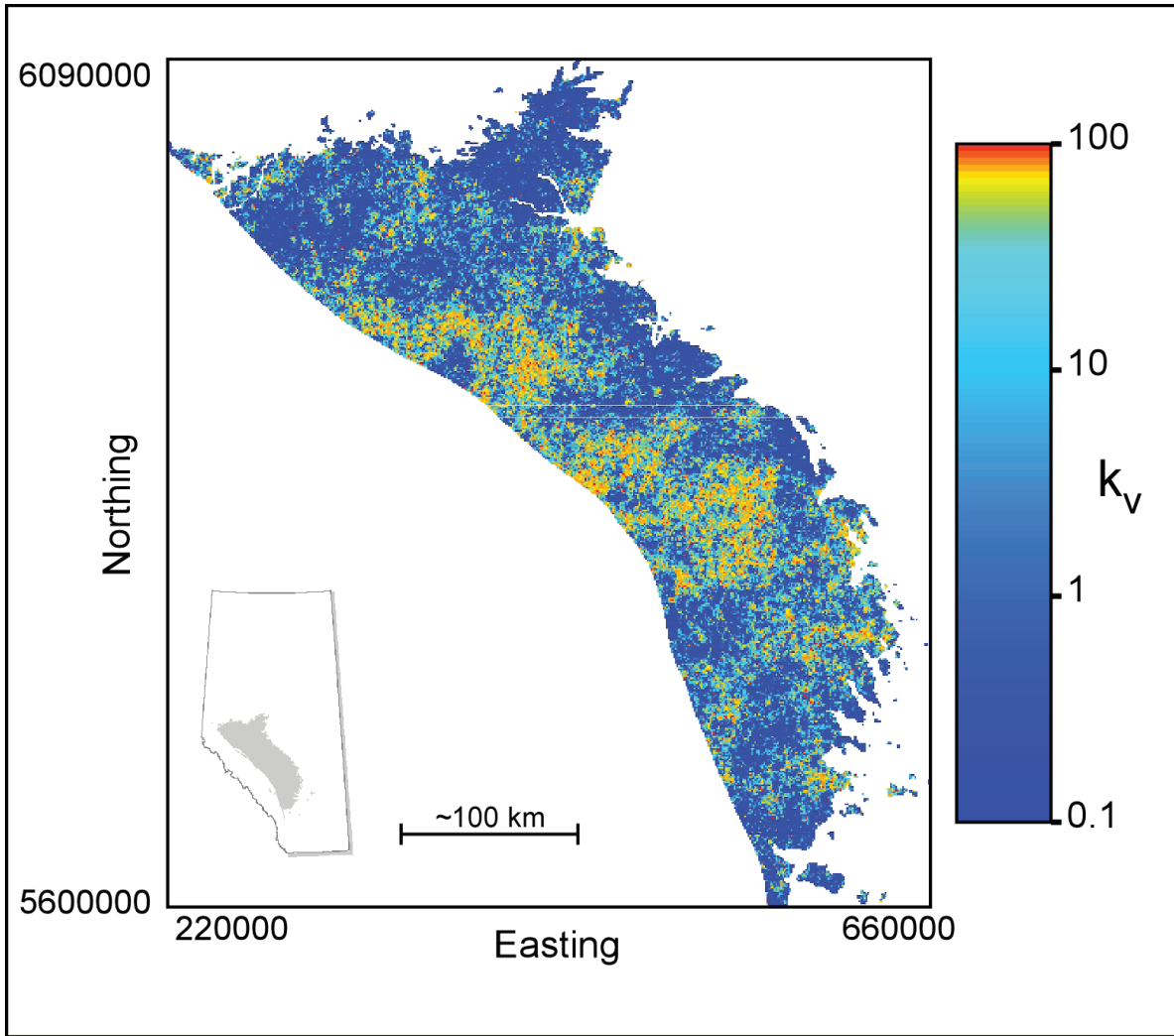


Figure 45. Simulated realization of vertical permeability ( $k_v$ ) in the bottom slice of the model.

## 7 Interpretation of Model Results

### 7.1 Distributions of Sandstone and Mudstone

Voxler<sup>®</sup> renderings illustrate the modelled 3-D distribution of sandstone and mudstone abundance within the Paskapoo Formation (Figures 46 and 47). Figure 46 shows the sandstone abundance modelled to a flattened base of the Paskapoo Formation, whereas Figure 47 shows the results modelled to a sea-level datum and reflect the present-day structure of the base of the Paskapoo Formation (Figure 6). At first glance, both figures reveal a non-uniform 3-D distribution of sandstone and mudstone that is consistent with deposition of a fluvial system in a foreland basin. However, closer examination of the internal architecture of the model reveals trends in regional sandstone/mudstone distributions.

For purposes of discussion of the internal geometry, the distribution of the sandstone and mudstone/siltstone abundance is depicted sequentially in thirty 25 m thick slices (Figures 76–81). Three regional sandstone/mudstone trends can be recognized from the series of stacked slices. The first trend consists of a large, >50 m thick, southeast-trending sandstone body that lies at the base of the Paskapoo Formation in the area between Red Deer and northwest of Edson (slices 1 and 2, Figure 76). The areal extent of this sandstone body is largely confined to a westward-dipping depression on the structure surface of the underlying Scollard Formation, as illustrated in a vertical slice of the model along its western edge (Figure 47). Slices 3 to 5 (Figure 76) show that west of Red Deer, elements of this sandy trend extend vertically to at least 125 m above the base of the formation, at which point the Paskapoo Formation becomes progressively more mudstone dominated. Outcrops along the eastern edge of this sandstone trend correlate with exposures of sandstone assigned to the Haynes Member of the Paskapoo Formation (Demchuk and Hills, 1991).

A 225 to 250 m thick interval represents the second regional trend (slices 6–14, Figures 76–78), where sandstone abundance is relatively low, and mostly mudstone and siltstone dominate the Paskapoo Formation. This largely fine-grained interval makes up the bulk of the Paskapoo Formation and likely correlates to the Lacombe Member of Demchuk and Hills (1991). Although areas of high sandstone abundance are present within this finer-grained trend, they generally occur as isolated bodies and lack regional connection with other sandstone bodies. This is particularly true in the area south of Red Deer to Calgary, where sandstone bodies are few and where muddy sedimentary rock dominates. One exception is in the region west of Drayton Valley along the western boundary of the study area, where high sandstone abundance persists through almost all slices, from the base to the top of the Paskapoo Formation.

The third discernable trend is characterized by an approximately 300 to 400 m thick interval in which areas of high sandstone abundance appear to be regionally interconnected (slices 15–30, Figures 78–80). This sandstone trend appears to have significant variability in 3-D space and is expressed in the present-day landscape as an area with prominent scarped, high relief topography in the western part of the study area (Figure 5). Although incised and modified by modern drainage, this upper sandstone-dominated system appears fan-like and shows no evidence of sand deposition constrained by a pre-existing basin or depression in the underlying surface. This upper sandstone-dominated trend likely encompasses elements of the Dalehurst Member sandstone (Figure 7; Demchuk and Hills, 1991), but there is no direct correlation implied here. More details on stratigraphic correlations follow later.

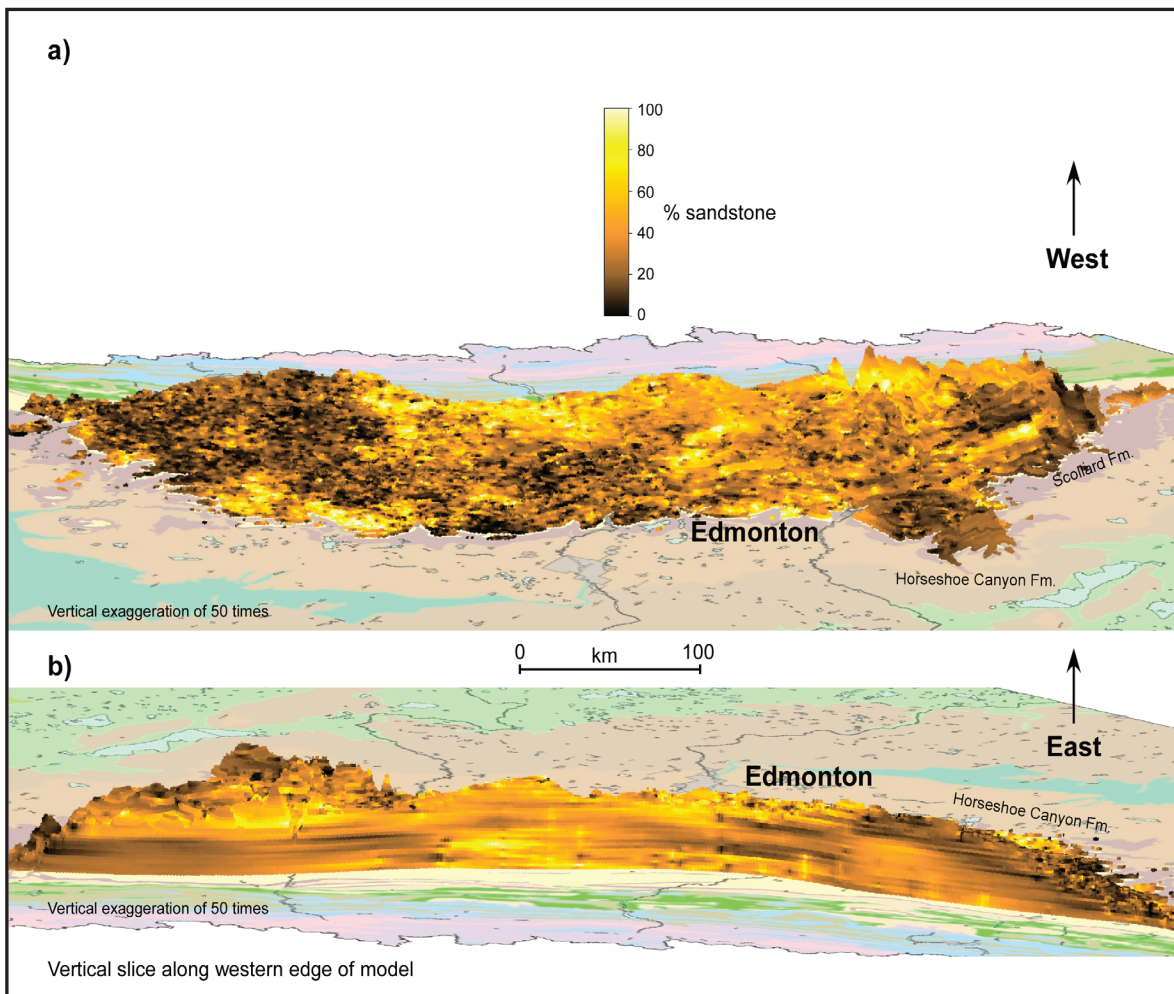


Figure 46. Modelled 3-D distribution of sandiness within the Paskapoo Formation flattened to base of formation: a) oblique aerial view to west of modelled Paskapoo Formation and b) view to east of vertical slice along the undeformed western edge of the Paskapoo Formation.

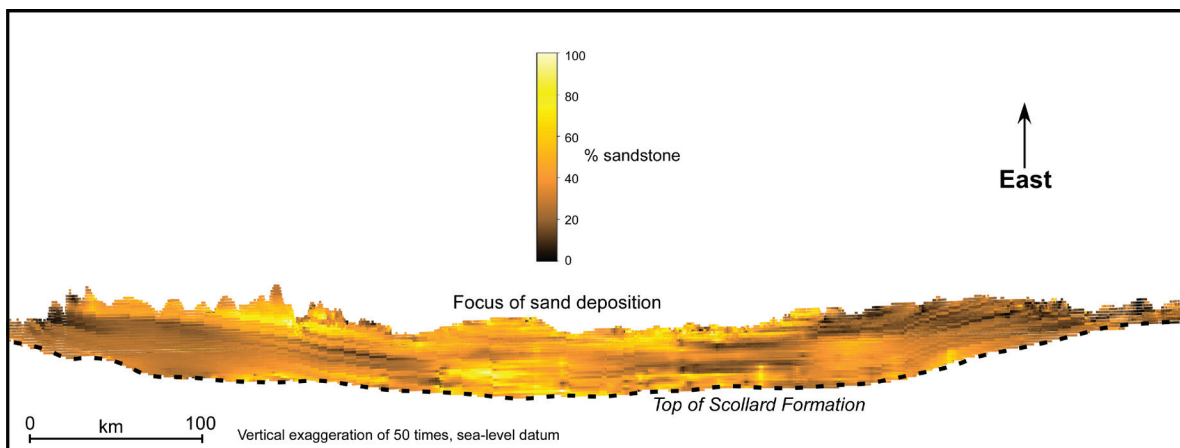


Figure 47. Modelled 3-D distribution of sandiness within the Paskapoo Formation referenced to sea level. View to east of vertical slice along western edge of the undeformed edge of the Paskapoo Formation.

## 7.2 Hydrostratigraphic Framework

### 7.2.1 Sandstone Thresholds and Permeabilities

Even though the above description of modelled sandstone trends within the Paskapoo Formation is useful for understanding lateral variations in properties and their distribution, it does not provide insight into the 3-D relationships of interconnected sandstone bodies that might form regional aquifers. Furthermore, even though the model clearly illustrates areas that are predominantly sandstone or predominantly mudstone/siltstone, it does not readily illustrate the geometry of those areas of medium sandiness values, which may be connected with areas of higher sandstone values to form a connected network. Nor does it address the question of what is the threshold of sandstone required to consider a body of rock a regionally extensive aquifer.

To select an appropriate cutoff value of sandiness, which would help define an aquifer, we were guided by the results of the mini-modelling that relate horizontal and vertical permeability to sandstone abundance in a rock volume. Figure 48 shows the sandiness versus permeability plots from the three mini-model simulations described in Section 6. The three P50 curves on the left side of the figure illustrate the change in horizontal permeability with change in sandstone abundance. The three P50 curves on the right illustrate the change in vertical permeability with change in sandstone abundance. The mini-modelling results show that horizontal permeability increases by two orders of magnitude with the addition of just 20% to 30% sandstone. At these amounts, there is a relatively high probability (shown by the relatively narrow range in values between the P10 and P90 curves in Figure 42) that sandstone bodies can be considered to be connected locally and primarily in the horizontal direction. In contrast, changes of the same magnitude in vertical permeability

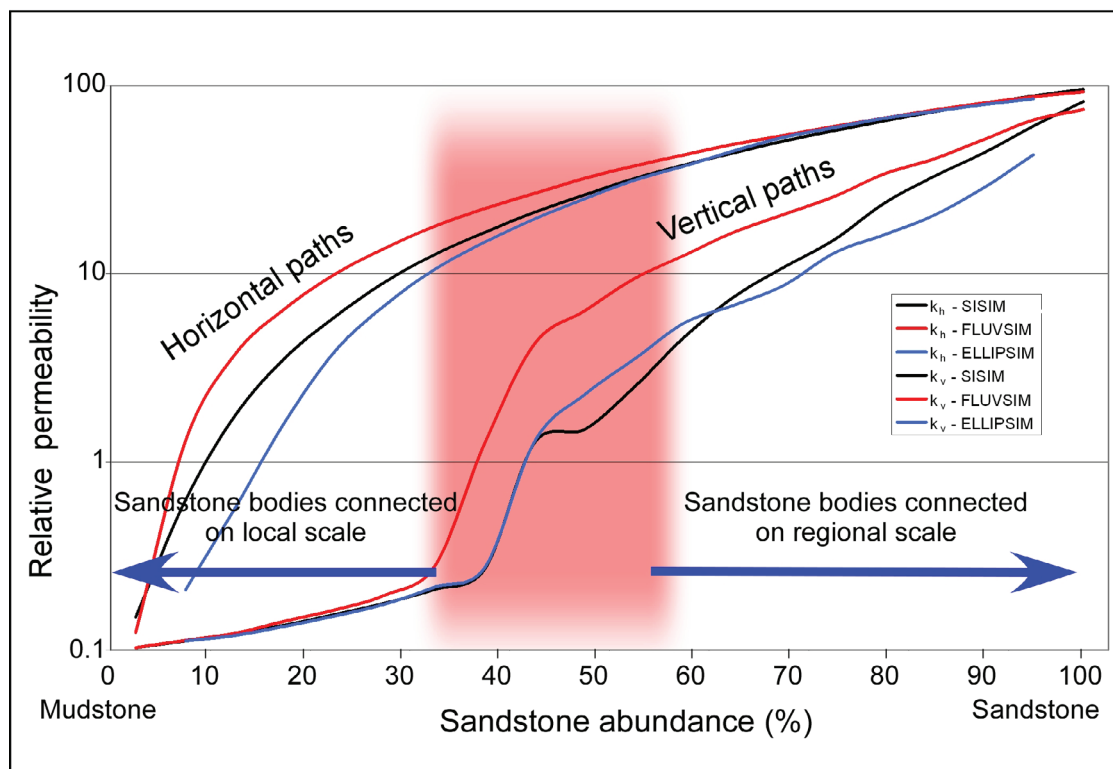


Figure 48. Probability of connected hydraulic paths with increase in sandstone abundance from three mini-model simulations (P50 curves) of the Paskapoo Formation. At about 55%–60% sandstone abundance in the FLUVSIM model, the probability that local sandstone bodies become vertically connected to form a regional system increases significantly.

only occur at higher sandstone-abundance values, somewhere around 55% in the FLUVSIM model and higher yet, around 65% to 70%, in the SISIM and ELLIPSIM models (though the relatively large range between the P10 and P90 curves shown in Figure 43 indicates vertical connections can occur at much lower or at much higher values). We can conclude, therefore, that at sandstone-abundance levels of >55%, the probability of sandstone bodies being hydraulically connected in three dimensions at the regional scale increases significantly. The red shading on Figure 48 represents sandstone-abundance values in the range of 35% to 60% sandstone and reflects the transition where the probability of sandstone bodies being connected at a regional scale changes from low to high. It is noteworthy that Parks and Andriashek (2009) used percolation theory results to predict similar transition values between local-scale connections and regional-scale connections.

The FLUVSIM model appears to represent best the internal structure of beds within the Paskapoo Formation, and we concluded that when sandstone abundance exceeds 55%, individual sandstone bodies in the Paskapoo Formation have a significant probability of being both horizontally and vertically connected. On this basis, we consider areas of >55% sandstone abundance in our model to represent regional aquifers. Conversely, we consider areas of <35% sandstone (>65% mudstone/siltstone) to represent regional aquitards.

## **7.2.2 Regional Hydrostratigraphic Units in the Paskapoo Formation**

### **7.2.2.1 Introduction**

The application of sand threshold values enables the rendering of the 3-D architecture of regional aquifers and aquitards, which are nested within the sand-slice model of the Paskapoo Formation. A series of Voxler® views of sandstone/mudstone isovalues (Figure 49) show the distributions of >55% sandstone (regional sandstones, shown in yellow) and <35% sandstone (regional mudstones, shown in brown). Not highlighted are those areas where the average value of the model cell falls

between 35% sandstone (65% mudstone) and 55% sandstone (45% mudstone), represented by the red-shaded area on Figure 48.

Figure 49a and b are west and east views, respectively, of the volumetric distribution of the previously discussed three sandstone/mudstone trends interpreted from the individual depth slices. The lowermost sandstone-dominated trend is herein referred to as the Haynes aquifer; the regionally extensive mudstone trend, which forms the bulk of the Paskapoo Formation, is herein named the Lacombe aquitard; and the uppermost sandstone-dominated unit is herein named the Sunchild aquifer. In Figure 49c and d, the removal of the Lacombe aquitard highlights the nature of superposition of the Sunchild aquifer atop the Haynes aquifer. The model also illustrates that local sand connections extend from the lowermost Haynes aquifer through the muddy sediments of the Lacombe aquitard to connect with the Sunchild aquifer. The following sections describe this in more detail.

### **7.2.2.2 Haynes Aquifer**

Plan and cross-section views of the distribution and extent of the >55% sandstone isovalues (Figures 50 and 51) show that the main body of sandstone in the Haynes aquifer forms a relatively extensive southeast-trending system in the central part of the study area, with isolated segments in the north and west (Figure 52). The top of the aquifer occurs as high as 1000 m asl, but the surface dips westward to 450 m asl along the edge of the deformation belt (Figures 51 and 53). Parts of the aquifer are up to 100 m thick, particularly in the west near the deformation belt and in a region west of Red Deer (Figure 54), although elsewhere the unit averages about 50 m thick. Although the Haynes aquifer outcrops along its eastern edge, east of Red Deer, most of the aquifer is overlain by thick muddy sedimentary rocks of the Lacombe aquitard, as illustrated in Figure 55.

The ability to query the 3-D model of sandiness by selecting different isovalue cutoffs provides an opportunity to explore the outcomes of applying conservative or liberal threshold values to define an aquifer. Figure 56 illustrates the difference in

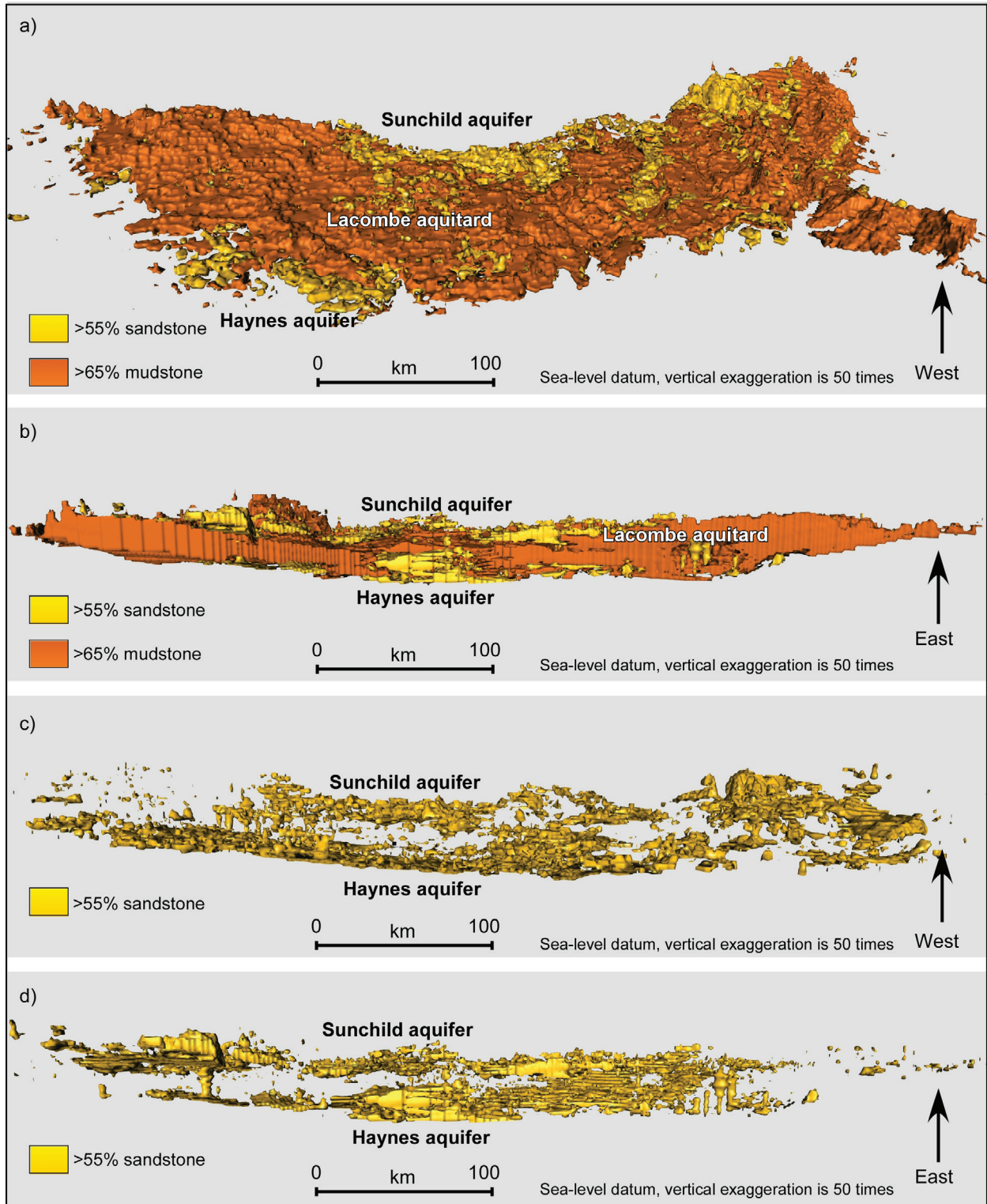


Figure 49. a) West and b) east views showing the combined distribution of >55% sandstone isovalues and >65% mudstone isovalues in the Paskapoo Formation. c) West and d) east views showing only those parts of the Paskapoo Formation where sandstone isovalues are >55%.

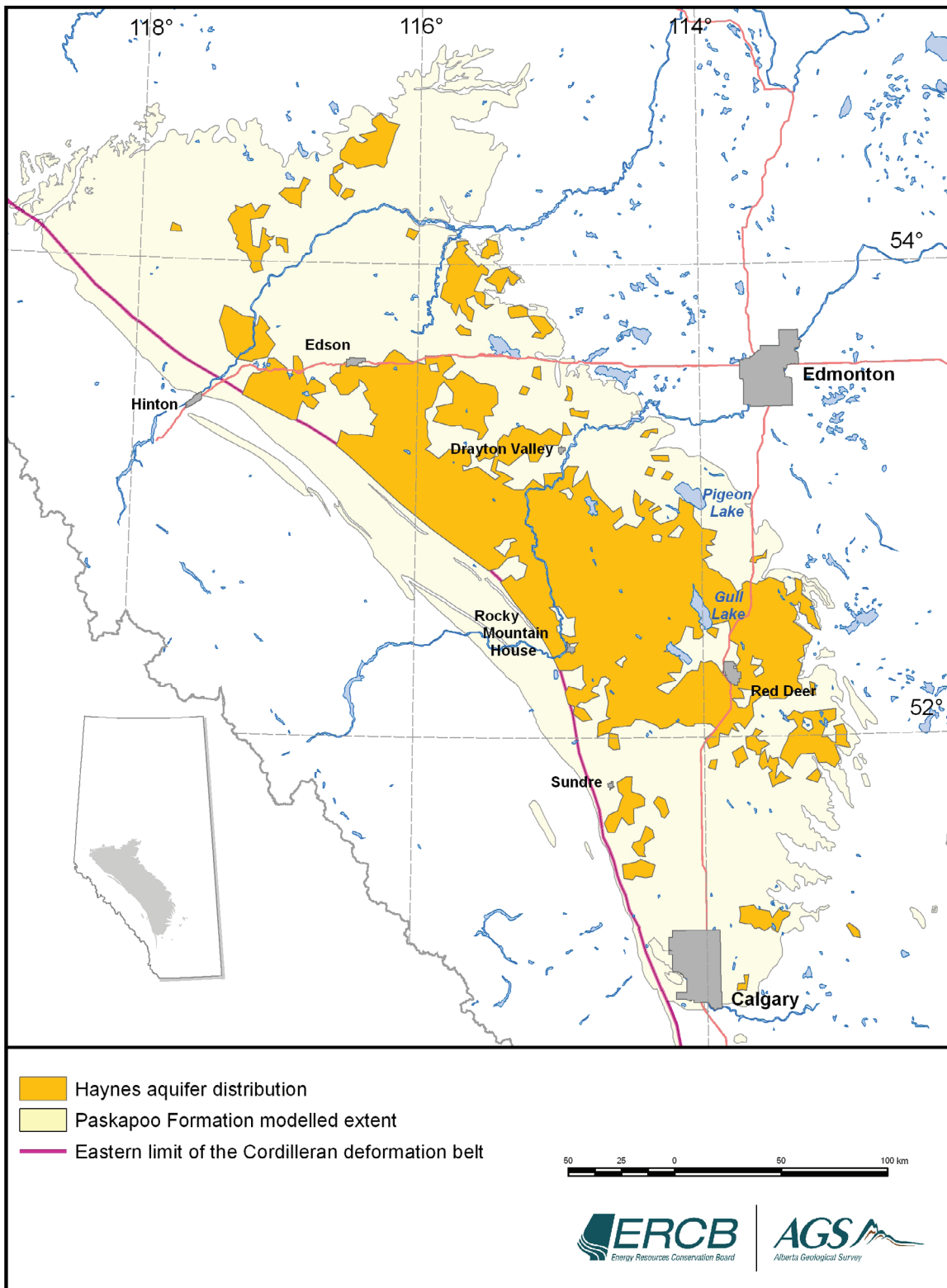


Figure 50. Distribution of the Haynes aquifer. The figure is a composite of the >55% sandstone distribution of the first five 25 m thick slices above the base of the Paskapoo Formation.

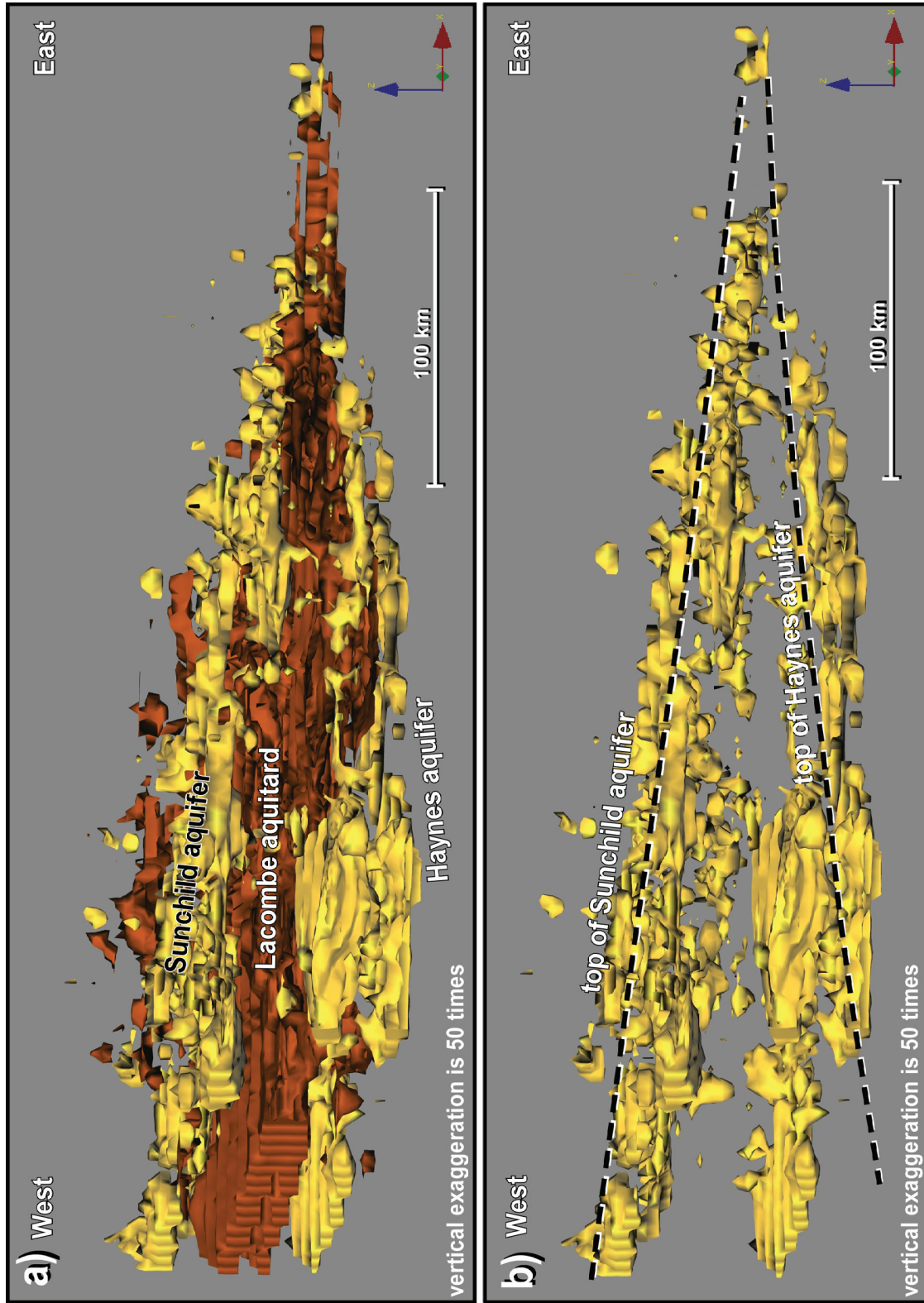


Figure 51. a) Edge-on, section view of the Sunchild aquifer, Lacombe aquitard, and Haynes aquifer and b) structural surfaces of the tops of the Sunchild and Haynes aquifers. Remnants of the Sunchild aquifer almost overlap the Haynes aquifer as the wedge of muddy sediments of the Lacombe aquitard thins to the east.



Figure 52. Outcrop of stacked channel sandstone (interpreted as part of the Haynes aquifer within the Paskapoo Formation), Hard Luck Canyon, Whitecourt area (Zone 11, 579594E, 5984239N, elevation top ~815 m asl).

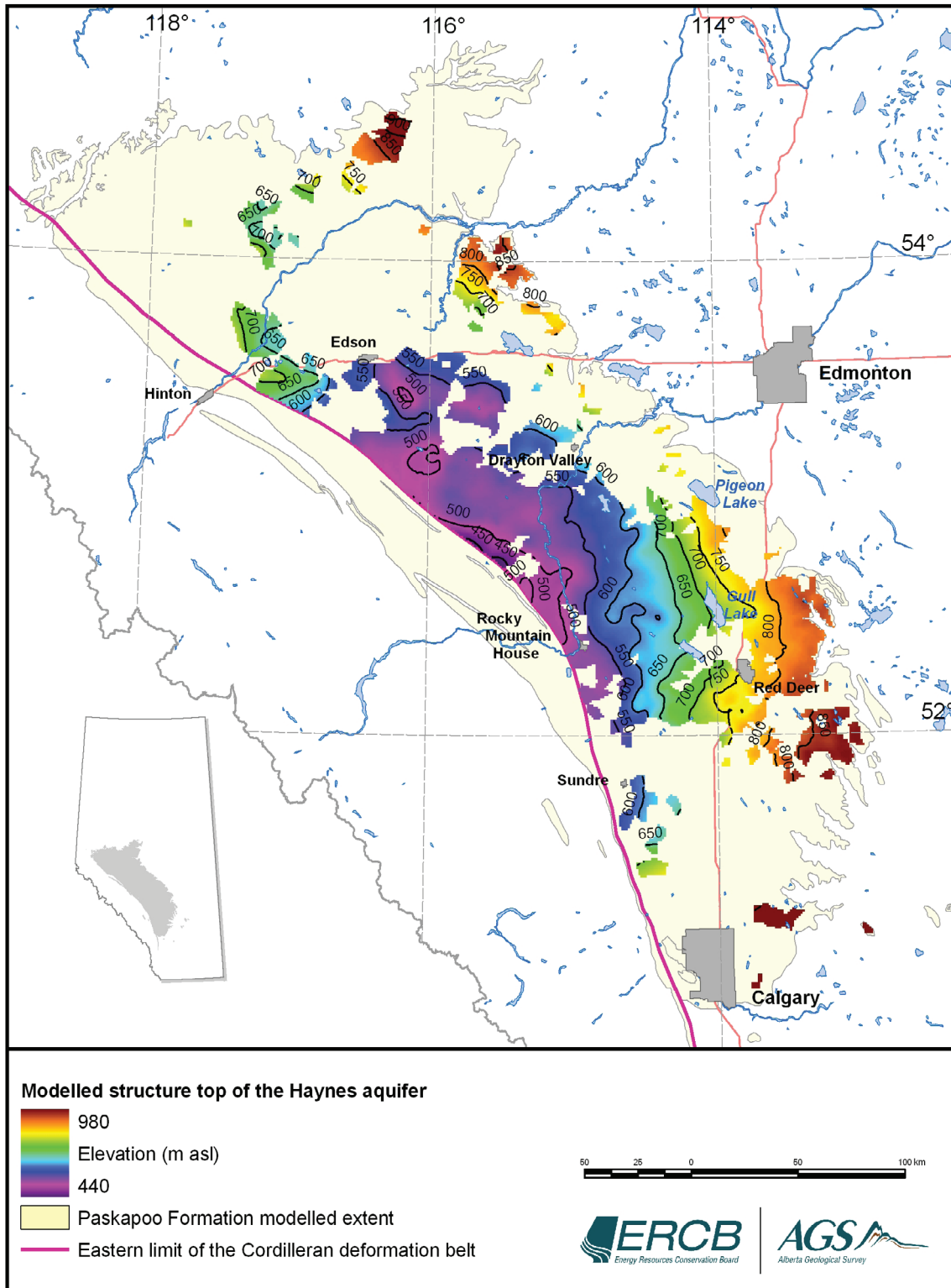


Figure 53. Elevation of the upper surface of the Haynes aquifer.

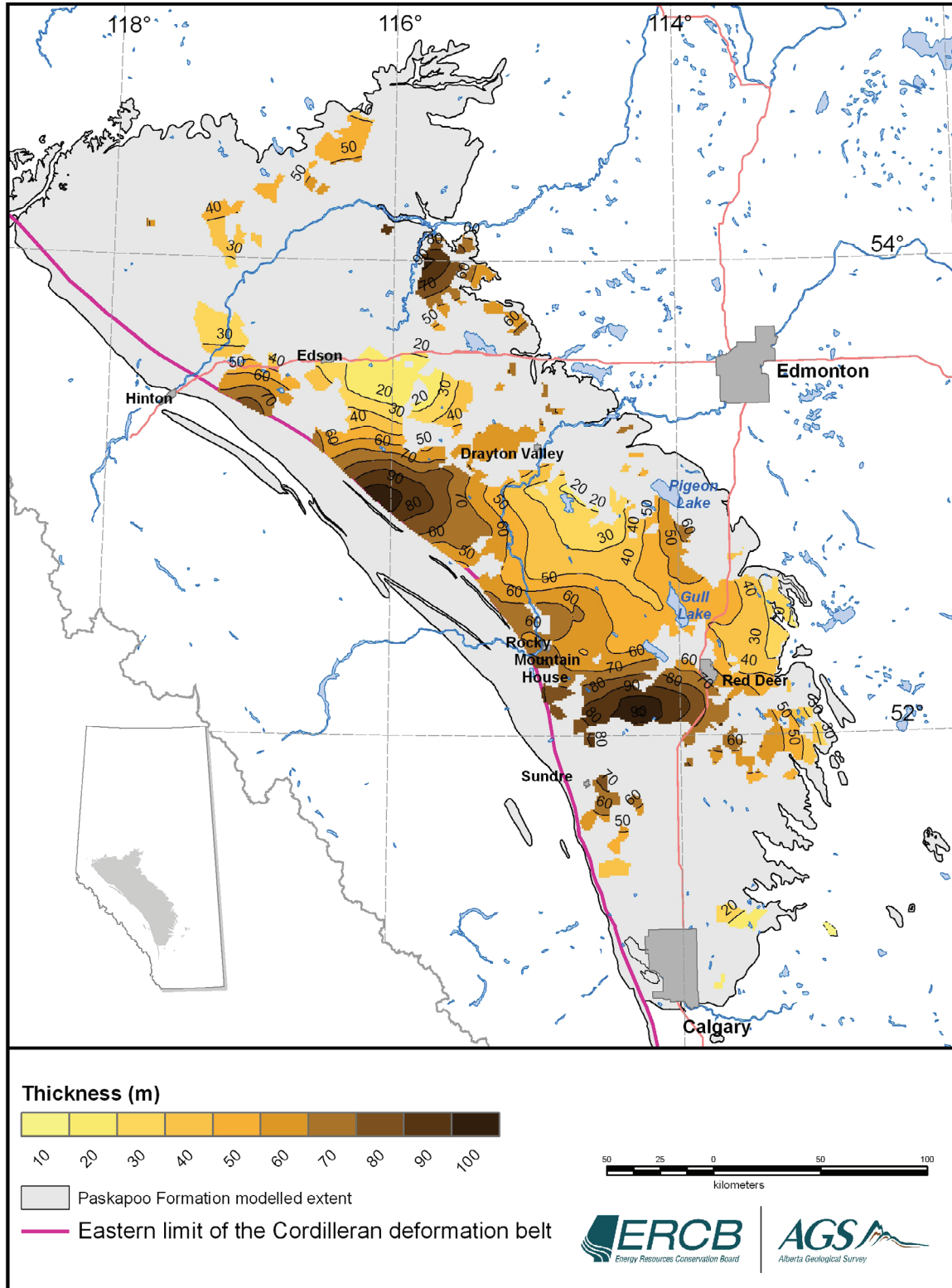


Figure 54. Thickness (isopachs) of the Haynes aquifer.

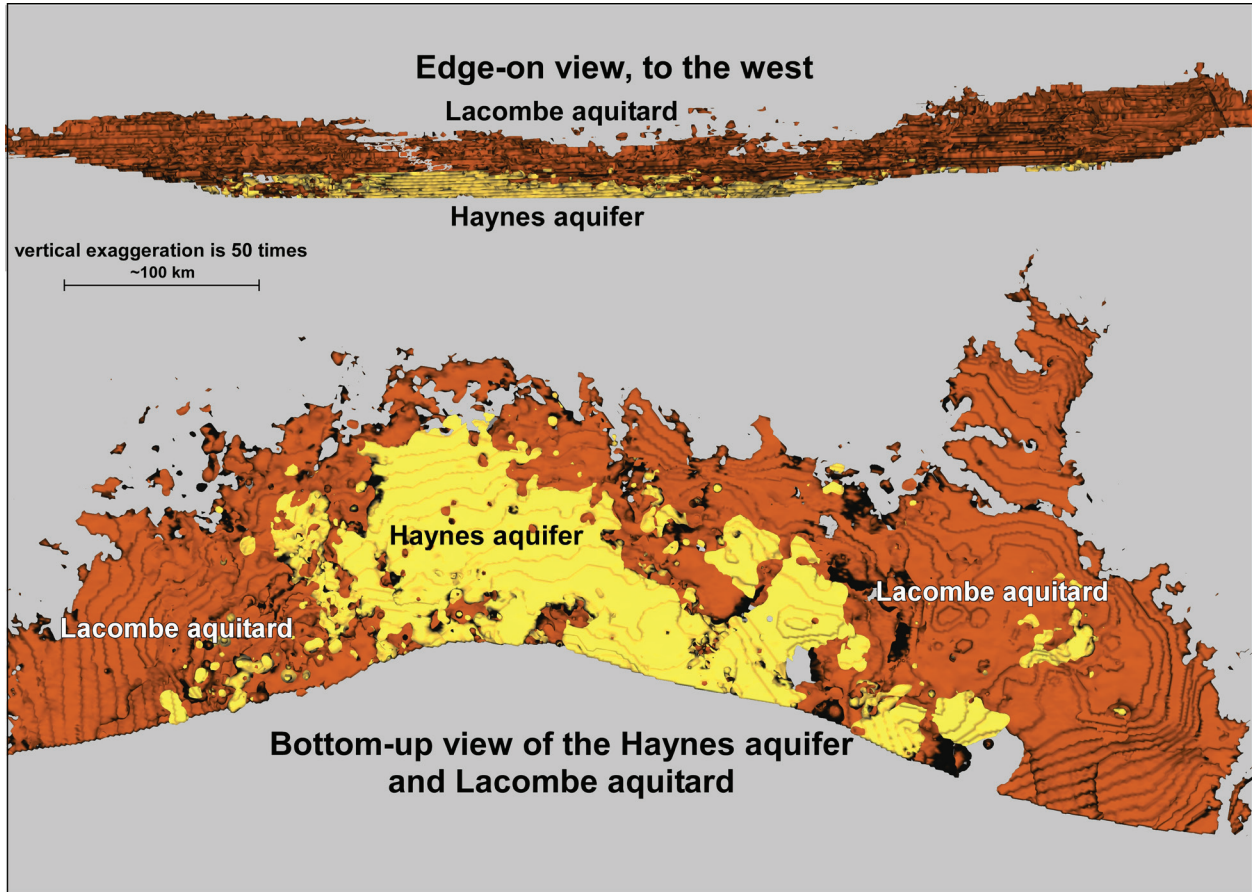


Figure 55. Stratigraphic relationship between the Haynes aquifer and the overlying Lacombe aquitard.

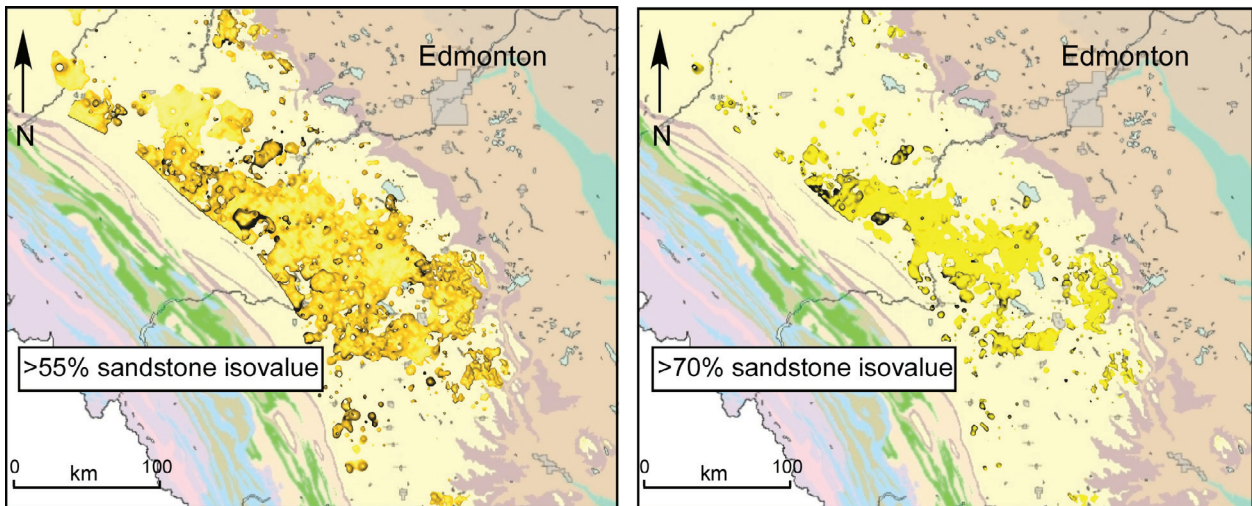


Figure 56. Distribution of Haynes aquifer at >55% and >70% sandstone isovalue thresholds.

geometry of the Haynes aquifer when the >55% sandstone cutoff value (determined from the FLUVSIM mini-model; Figure 48) is applied versus the more conservative >70% sandstone cutoff value (determined from the ELLIPSIM and SISIM mini-models). Although the size of the modelled aquifer is reduced with the >70% sandstone cutoff, applying this more conservative value makes it possible to identify those parts of the aquifer that are likely to be the most permeable and therefore most productive in terms of supplying groundwater.

### 7.2.2.3 Lacombe Aquitard

Although the Paskapoo Formation is commonly referred to as the Paskapoo Aquifer, this study and those of Demchuk and Hills, 1991; Jerzykiewicz, 1997; and Grasby et al., 2008 show that much of the formation is composed of muddy sedimentary rocks. These rocks comprise the Lacombe aquitard (Figure 57), which overlies

either sandstone of the Haynes aquifer or the Scollard Formation where the Haynes aquifer is absent (Figure 55).

We have defined the extent of the Lacombe aquitard to be those areas in our model where >65% of a 25 m thick cell consists of nonsandy material (siltstone and/or mudstone) or, conversely, where the sandstone is <35%. A query of the model to identify the cells that meet the >65% cutoff criteria and have the highest elevations, combined with a visual examination of slices in the Voxler<sup>®</sup> 3-D model, enables the construction of an approximation of the upper surface (Figure 58), and a plan view (Figure 59) of the distribution of mudstone-dominated strata of the Lacombe aquitard. The upper surface of the Lacombe aquitard is mostly erosional, forming the bedrock topography across much of the study area, except in the west, where the dominantly sandstone deposits of the Sunchild aquifer overlie finer-grained deposits.



Figure 57. Outcrop of mudstone, minor sandstone and ironstone (interpreted as part of the Lacombe aquitard within the Paskapoo Formation), Dickson Dam location (Zone 11, 690340E, 5765105N, NAD83, elevation top ~935 m asl).

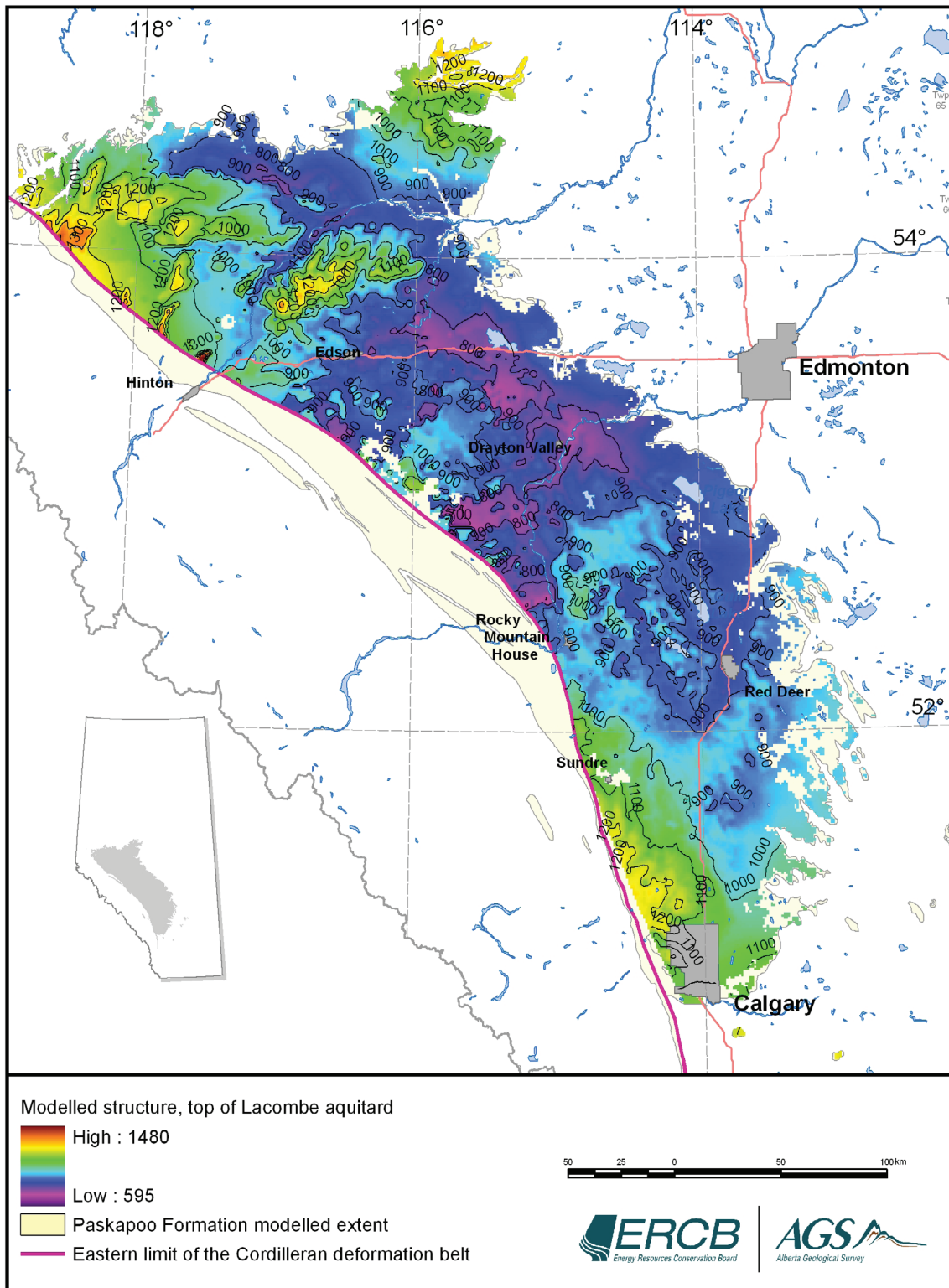


Figure 58. Elevation of the upper surface of the Lacombe aquitard.

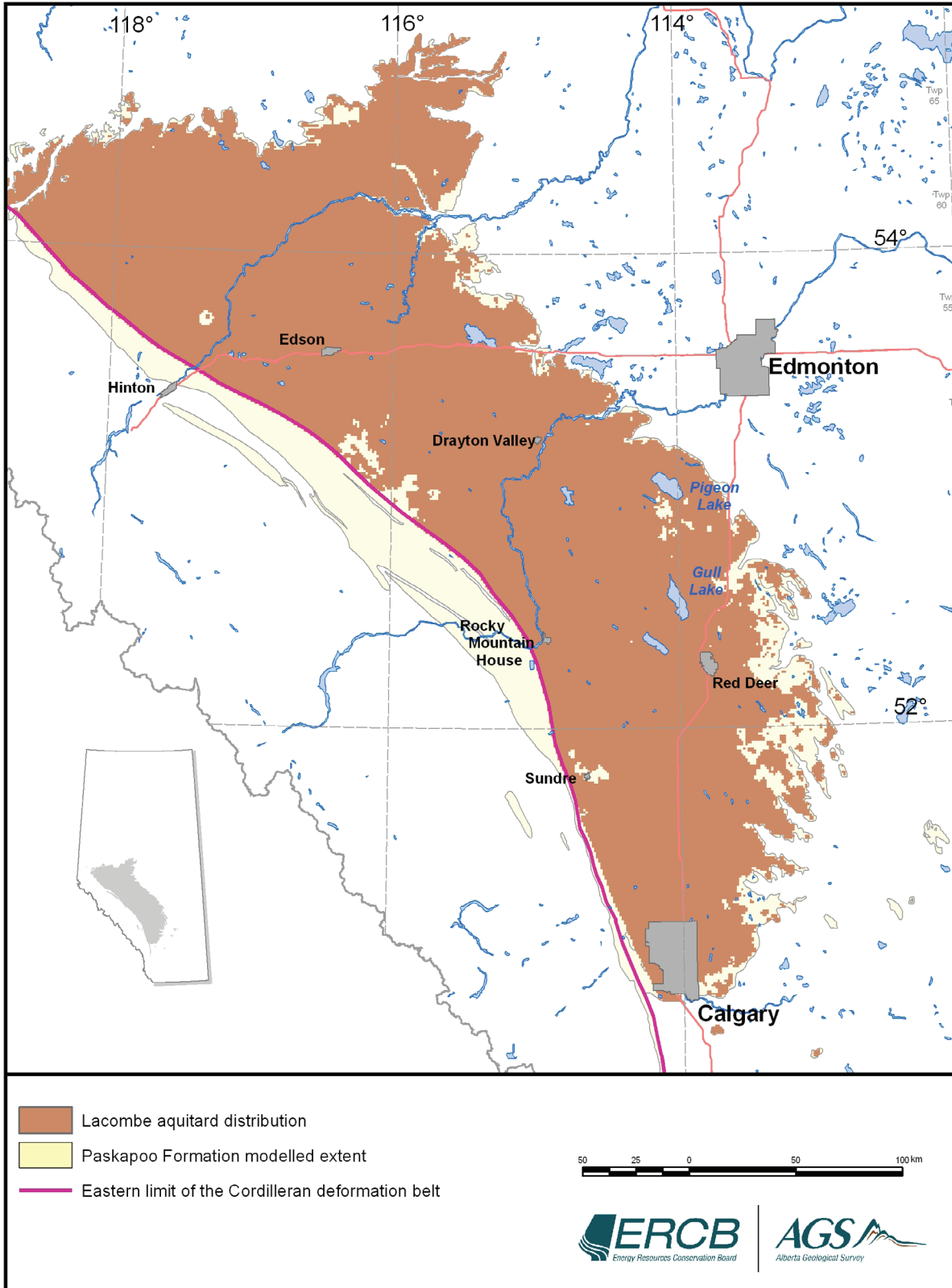


Figure 59. Distribution of the Lacombe aquitard. The figure is a composite distribution of >65% clayey sedimentary rock from 25 m thick slices, encompassing a thickness of as much as 350 m of muddy sedimentary rock.

The Lacombe aquitard constitutes a clastic wedge (Figures 49 and 51) which thins from about >500 m near the deformation front to <50 m close to its eastern edge (Figure 60). The overall fine-grained composition of the unit, as determined from geophysical logs and outcrop observations, suggests a fluvial to lacustrine depositional environment. Although sandstone bodies may be present in the Lacombe aquitard, they tend to be isolated and poorly connected at the regional scale. Of interest is the persistence of sandstone along the deformation front, west of Drayton Valley, and south of Sundre, which propagates upward from the Haynes aquifer and into the overlying Lacombe aquitard (Figures 49b, 78, 79). These areas appear to be the loci for the influx of much of the coarse sediment transported eastward into the foreland basin. The absence of a continuous Lacombe aquitard in these areas suggests time-transgressive deposition of coarse sediment, creating an apparent step-like connection through the finer-grained Lacombe aquitard, potentially connecting the underlying Haynes aquifer with the overlying Sunchild aquifer.

#### 7.2.2.4 Sunchild Aquifer

The Sunchild aquifer consists of a step-like connection of sandstone bodies (Figure 61) spanning an elevation range of 600 m. It overlies the regional mudstone and siltstone of the Lacombe aquitard in the central and western part of the Paskapoo Formation (Figure 62). Sandstone bodies within the Sunchild aquifer subcrop over most of the aquifer's extent and, because overlying Neogene sediment is relatively thin in the western part of the study area, the unit expresses itself in the present-day topography. Because of their proximity to surface, the sandstone bodies in the Sunchild aquifer can be well recognized by their highly resistive signature in airborne electromagnetic surveys. Figure 63 is a comparison of the modelled distribution of near-surface sandiness of the Paskapoo Formation from well data, and the distribution of high resistivity values ( $\geq 20 \text{ ohm}\cdot\text{m}$ ) of the ground to a depth of 20 m below surface from the airborne survey data (Barker et al., 2011). The general similarity in distribution of the high resistivity

(sandy materials) areas to that of the modelled distribution of sandstone bodies in the Sunchild aquifer confirms the regional extent of a near-surface, sandstone-dominated system within the upper parts of the Paskapoo Formation. Though perhaps once continuous and more extensive, both patterns show that the Sunchild aquifer now has a fragmented distribution, mainly due to paleostream and present-day stream incision. The easternmost extent of the aquifer occurs as isolated remnants, which form the topographic highs southwest of Pigeon Lake as well as other topographic highs near Red Deer in the central part of the study area. These eastern remnants are possibly correlative to locations of 'Middle Paskapoo Escarpments' described by Campbell (1967). The lower boundary of the Sunchild aquifer is more difficult to define, particularly in the east, where intervening muddy sediment of the Lacombe aquitard is thin to absent and where remnants of sandstone of the Sunchild aquifer are almost superposed on the Haynes aquifer (Figure 51). Because of fragmentation by stream incision, groundwater-flow systems within the Sunchild aquifer are likely to be semiconfined and local compared to flow in the underlying Haynes aquifer.

Figure 64 shows the elevation of the uppermost surface of the sandstone bodies that make up the Sunchild aquifer. This surface also represents the bedrock topographic surface. The construction of the Sunchild aquifer thickness map was somewhat problematic primarily because of the difficulty of mapping the step-like distribution and connection of sandstone bodies, which in places are laterally adjacent to mudstone-dominated intervals. The resultant isopach shown in Figure 65 was generated by subtracting the elevation of the Lacombe surface from that of the Sunchild surface to yield an approximation of Sunchild aquifer thickness. The Sunchild aquifer thickens from <50 m in the east to >300 m in the west. The thickness (~600 to 700 m) of this aquifer along the deformation front southwest of Drayton Valley is attributed to the stacking of coarse fluvial deposits extending from the base of the Paskapoo Formation almost to surface.

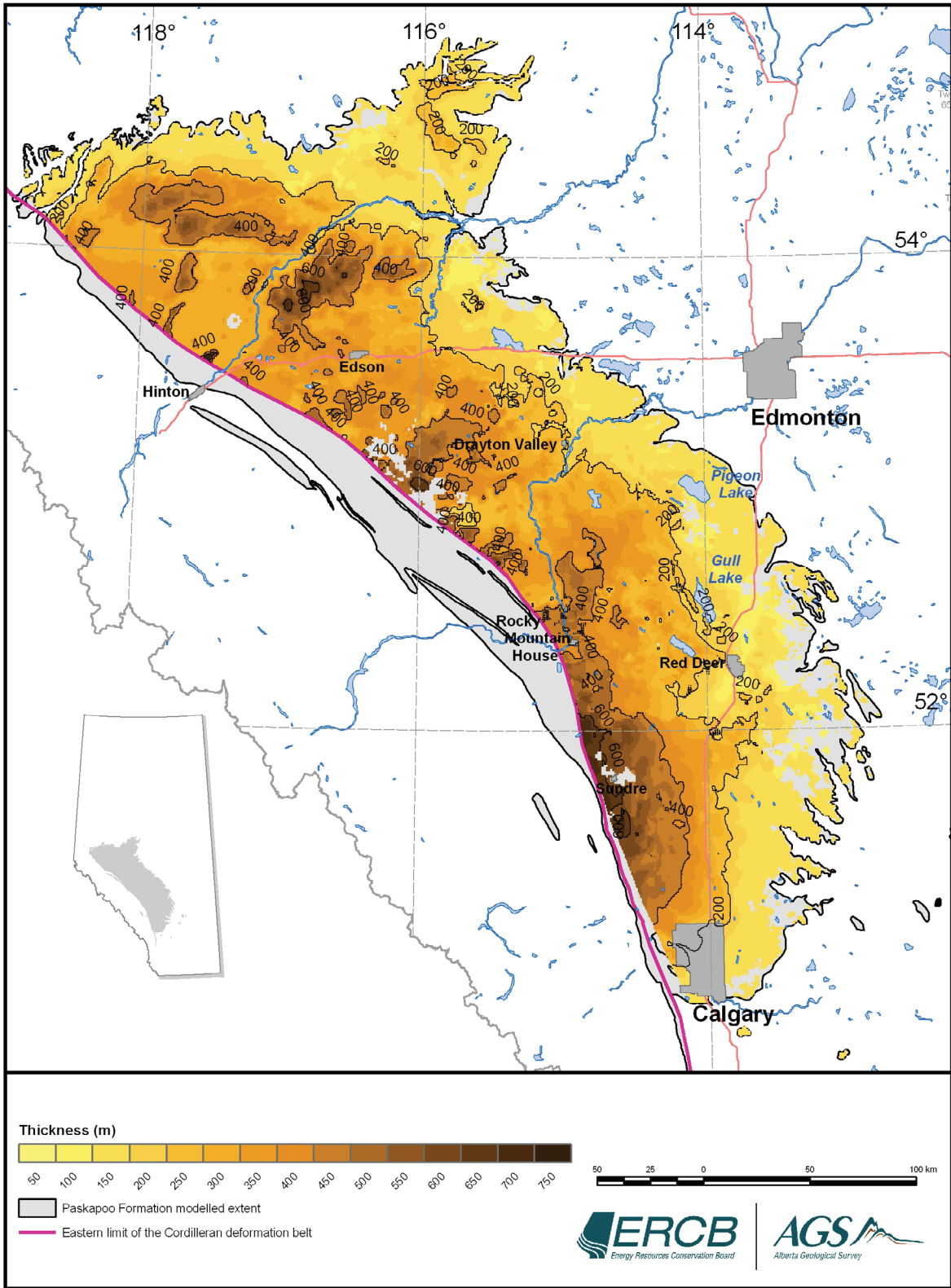


Figure 60. Thickness (isopachs) of the Lacombe aquitard.

Unlike the Haynes aquifer, deposition of sandstone bodies within the Sunchild aquifer does not appear to have been constrained to a foreland depression. Rather, the aquifer extends as an eastward-sloping clastic wedge onto relatively flat-lying muddy sediments that make up the Lacombe aquitard (Figures 51 and 62). Given its geographic and stratigraphic position, the Sunchild aquifer can be considered correlative to the uppermost Dalehurst Member of Demchuk and Hills (1991), as was the case in a previous hydrogeological study, which introduced the term “Dalehurst Aquifer” (Hydrogeological Consultants Ltd., 1999). Although the Dalehurst Member appears to be dominantly sandstone and siltstone at the type location (Demchuk and Hills, 1991), the defining characteristics of the Dalehurst Member (thick coal seams in the Obed-Marsh area) could not be applied to describe the occurrence and distribution of the mappable upper aquifer in our model, nor is it possible to correlate the Dalehurst Member strata away from the Obed-Marsh area

(Demchuk and Hills, 1991, p. 279). Hence, a new name, the Sunchild aquifer, was chosen to define the uppermost regional sandstone-dominated unit, independent of the Dalehurst Member–defining criteria.

### 7.2.3 Hydrogeological Aspects

The construction of the 3-D aquifer model enables the incorporation of other subsurface hydraulic information, such as well-water production rates, into the hydrogeological framework of the Paskapoo Formation. Figure 66 shows the 3-D distribution of the midpoint of screen intervals in high-producing licensed water wells. High-producing wells are located throughout the Paskapoo Formation, including some within the Lacombe aquitard, but most tend to be completed within the lower parts of the Sunchild aquifer or upper parts of the Haynes aquifer, along its eastern margin. The absence of numerous high-producing wells completed in the central and western parts



Figure 61. Outcrop of sandstone along the Obed mine road (interpreted as part of the Sunchild aquifer, Zone 11, 470934E, 5936971N, elevation ~1300 m asl).

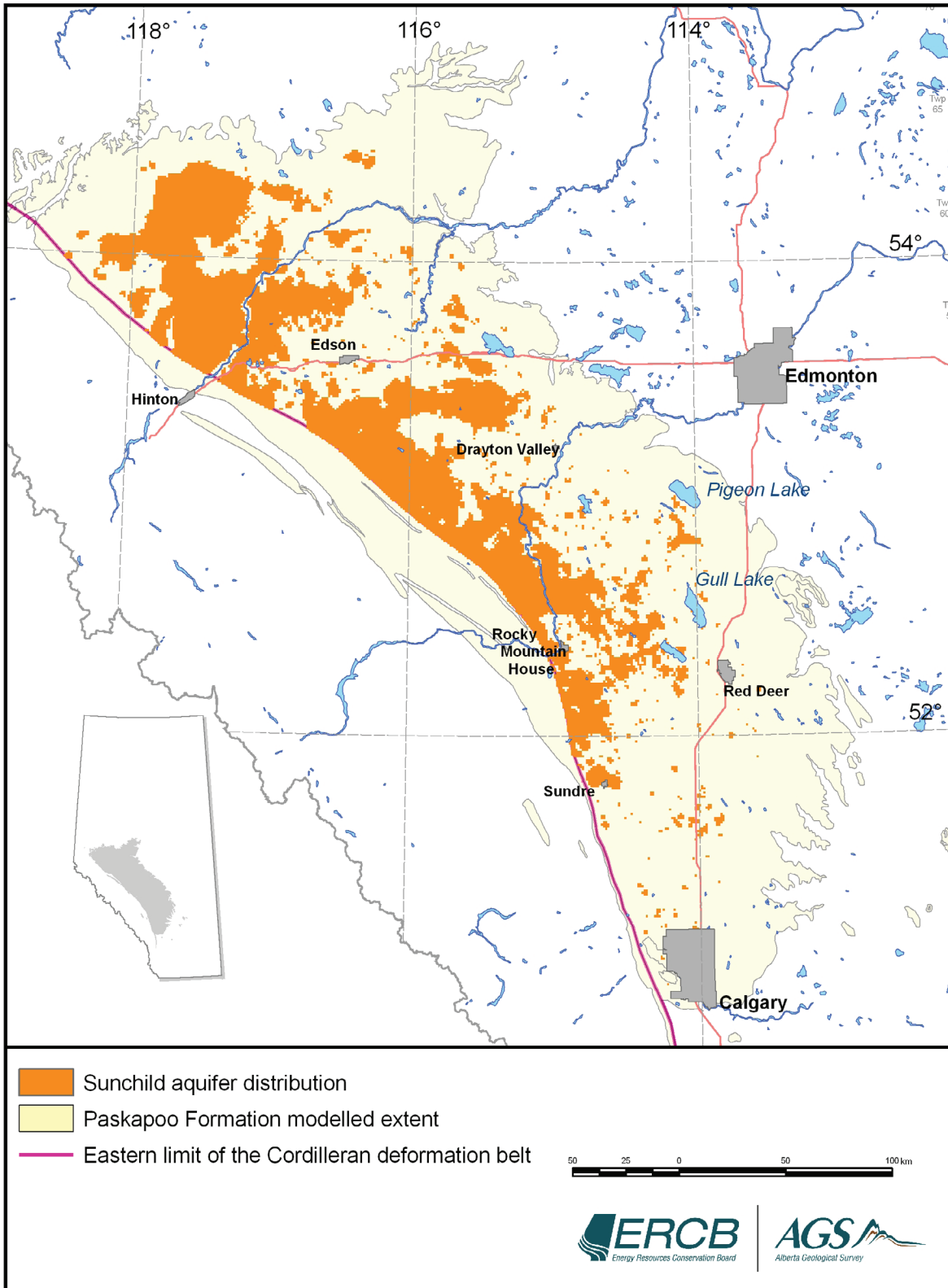


Figure 62. Distribution of the Sunchild aquifer. The figure is a composite of the >55% sandstone distribution from 25 m thick slices, encompassing an elevation range of as much as 600 m within the Paskapoo Formation.

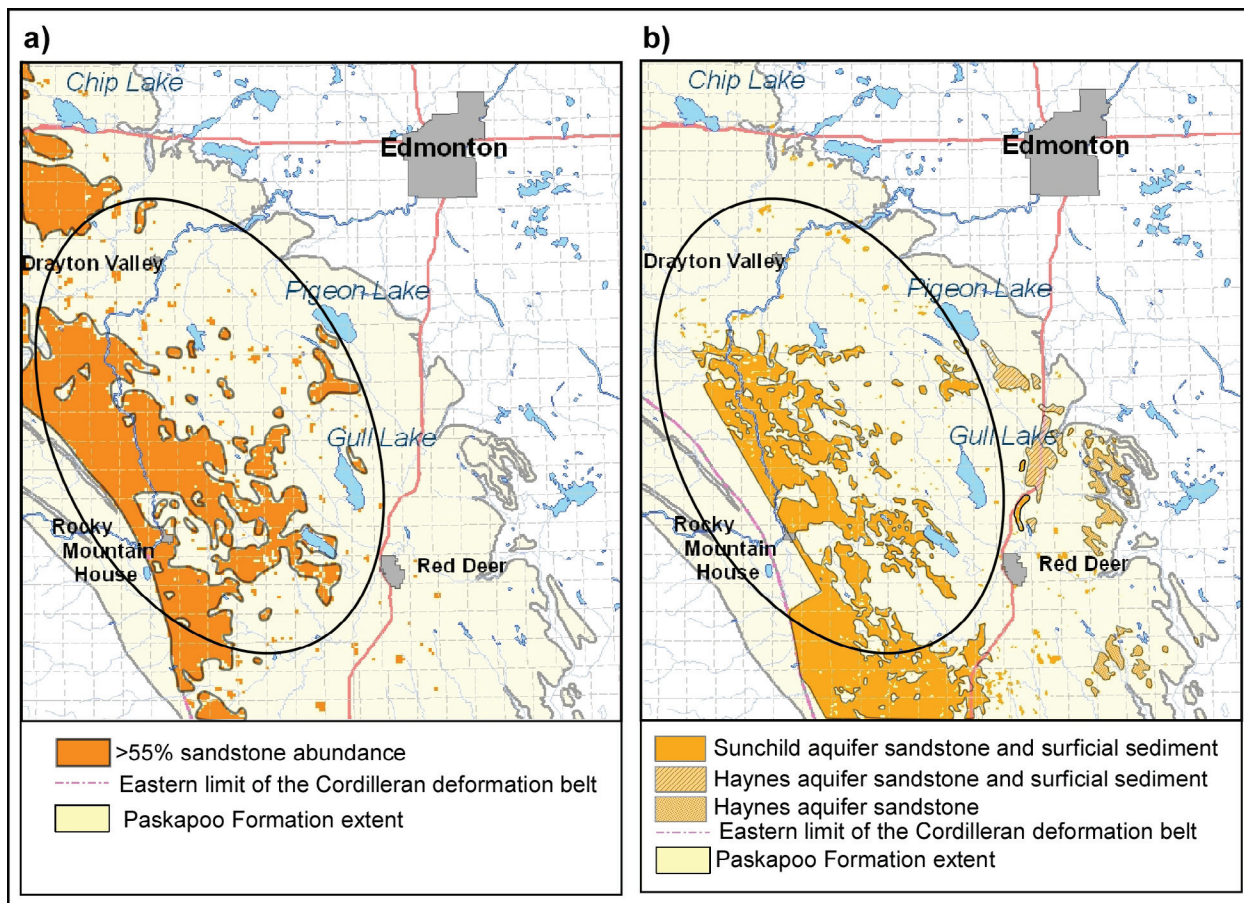


Figure 63. Comparison of the modelled distribution of the Sunchild aquifer with the sandiest areas of the upper 20 m of ground, as interpreted from airborne resistivity surveys. The regional pattern of sandiness in the airborne resistivity survey northeast of Rocky Mountain House is similar to that of the modelled Sunchild aquifer, and highlights the near-surface expression of sandstone-dominated bodies that comprise the Sunchild aquifer.

of the Haynes aquifer can likely be attributed to greater depth of burial and higher associated costs or difficulty to produce, rather than to diminished capacity of the aquifer to yield water to a well. Groundwater yield to wells completed in both aquifer systems may be prolific, but because of lateral discontinuity resulting from paleoerosion and present-day erosion, groundwater-flow systems in the Sunchild aquifer are likely to be of a more local scale than flow systems within the Haynes aquifer.

In evaluating the success of our approach and its suitability for future hydrostratigraphic characterizations of the Paskapoo Formation, we believe the architecture can be further refined if the sandstone-abundance calculations are constrained

by geologically defensible stratigraphic surfaces. In Section 4, we described the appropriateness of geological datum(s) for depth-slice methodologies and concluded that, in the ideal case, the datum would reflect the surface of a geological process or depositional event so that the analysis contained the averages of more closely related data. The construction of structural surfaces for the Haynes and Lacombe aquifers from the 3-D model of sandiness provides those appropriate datums that were not available for this study. With these newly defined control surfaces, we believe we can reduce the variances in the sandstone-abundance calculations and generate more geologically valid interpretations using computer-enabled data analysis methods.

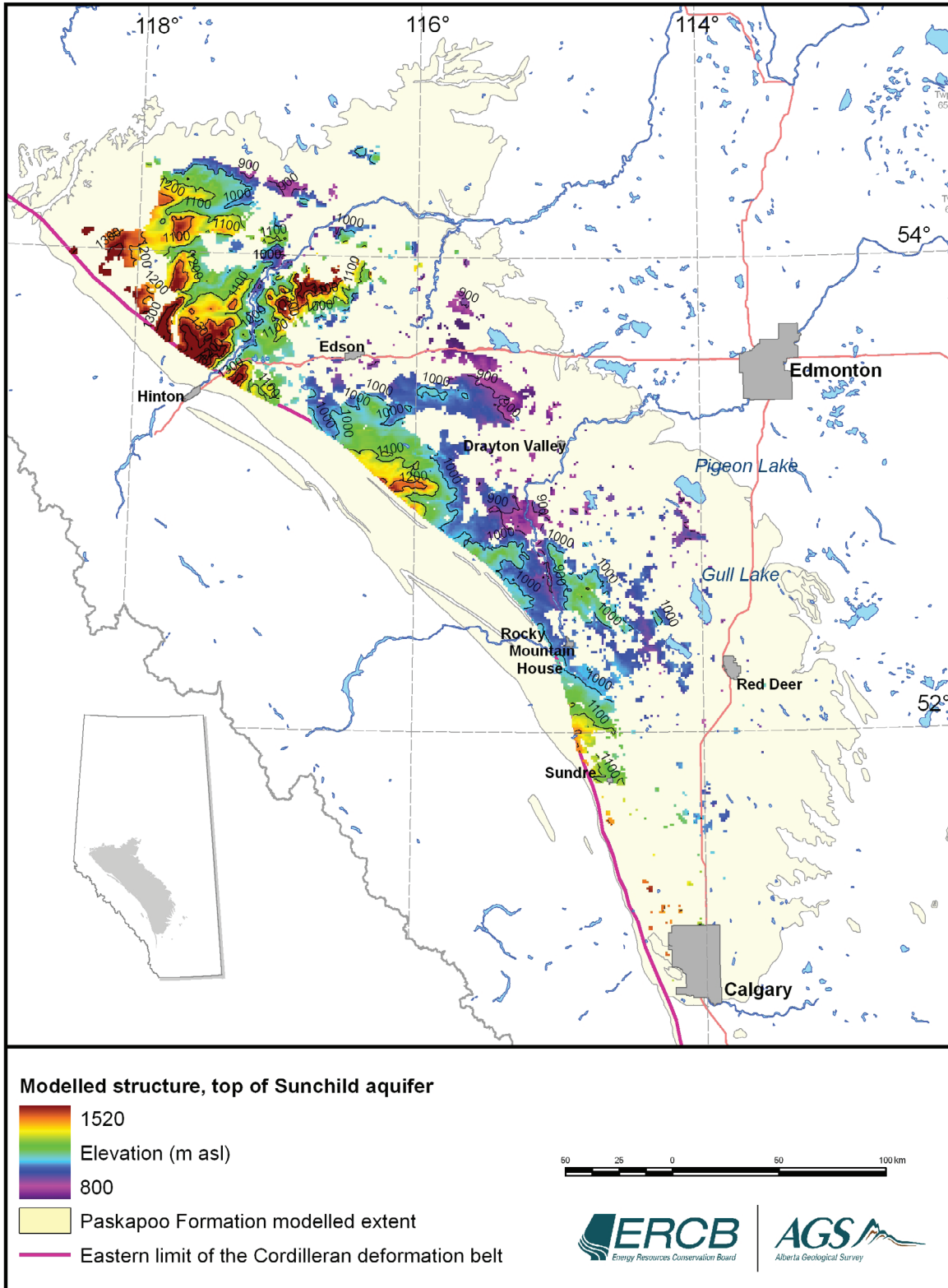


Figure 64. Elevation of the upper surface of the Sunchild aquifer.

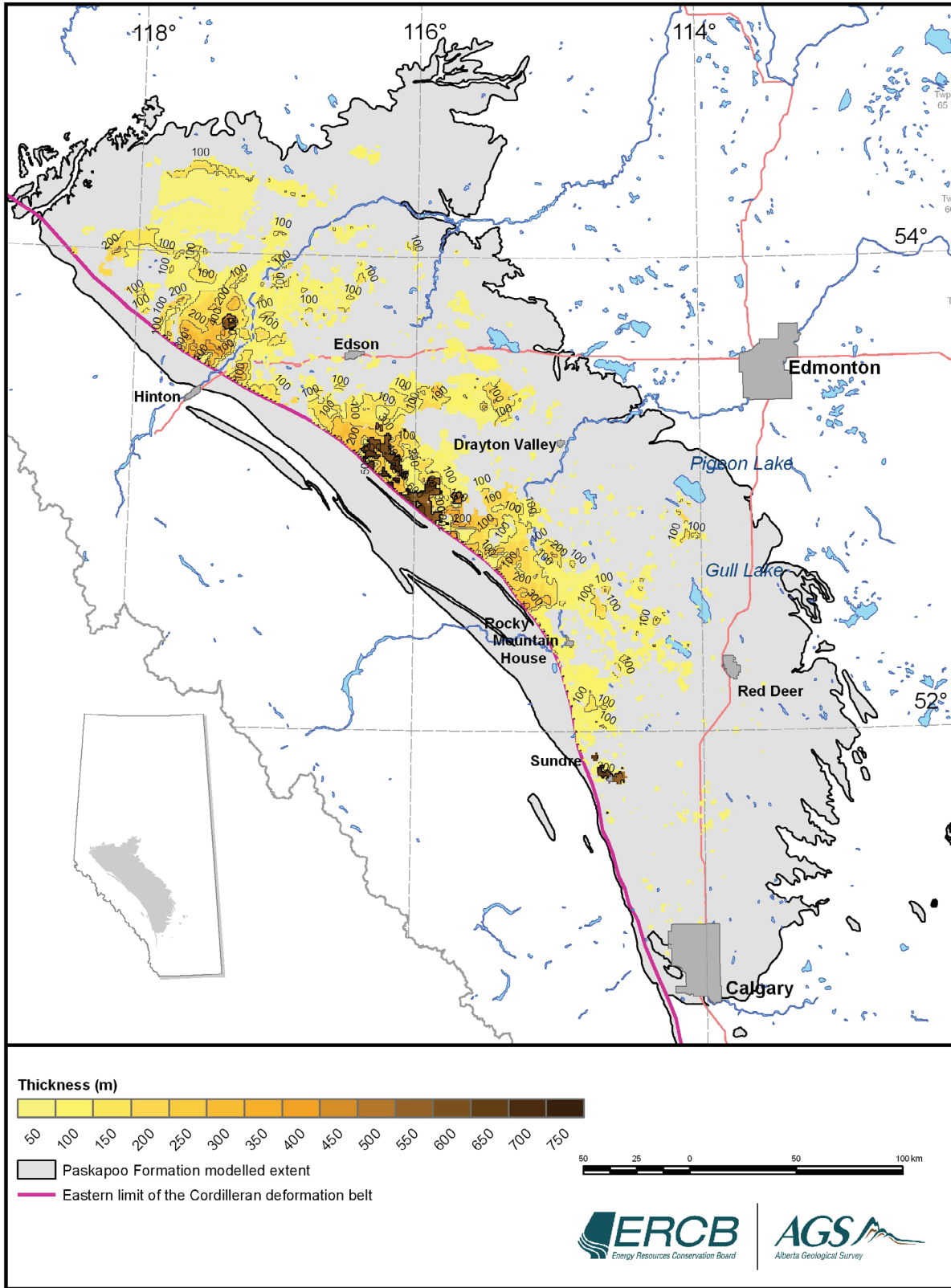


Figure 65. Thickness (isopachs) of the Sunchild aquifer.

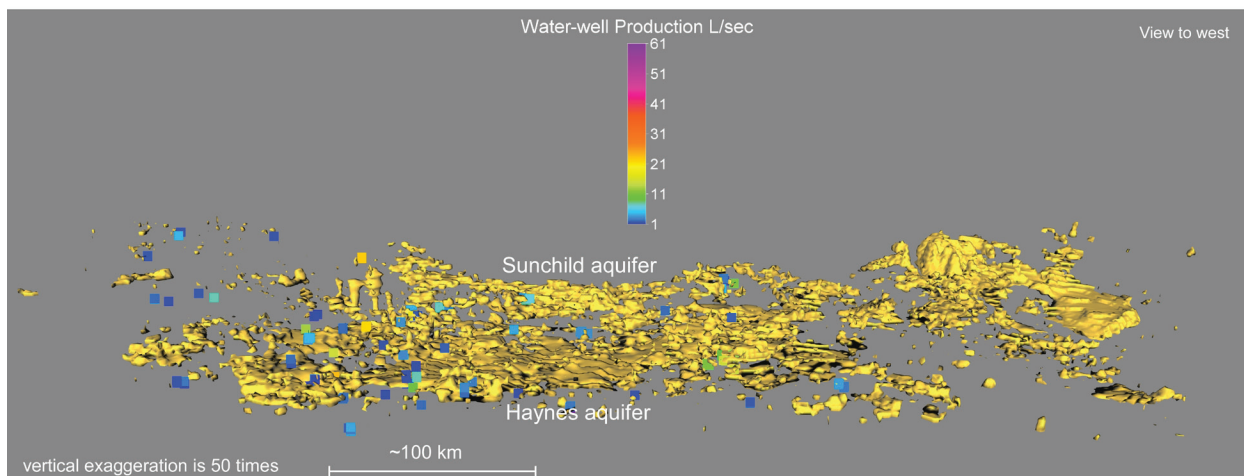


Figure 66. Location of high-producing licensed water wells within aquifers of the Paskapoo Formation.

### 7.3 Discussion of Geological Interpretations

The hydrostratigraphic architecture of the Paskapoo Formation, which evolved from our analysis and modelling of sandstone abundance, can be summarized as two regional, mappable, sandstone-dominated aquifer units separated by a mudstone-dominated aquitard. In assessing our hydrostratigraphic framework against models proposed in previous lithostratigraphic studies, we find that our framework is consistent with most of that proposed by Demchuk and Hills (1991). As a consequence, we have adopted their nomenclature for two of our hydrostratigraphic units. The sandstone-dominated Haynes Member and the overlying mudstone-dominated Lacombe Member can be clearly recognized and mapped from our modelled results. The major difference between the two models is the lack of agreement on the uppermost unit; there are insufficient criteria to permit the correlation of the Sunchild aquifer with the Dalehurst Member, as defined by its type section in the Obed-Marsh area near Hinton (Demchuk and Hills, 1991).

We believe our model provides new insights into the subsurface and surface distribution and geometry of the geological units that define the previously named Haynes and Lacombe members, as well as the possibility for the occurrence of a new sandstone-dominated unit that comprises the Sunchild aquifer.

#### 7.3.1 Speculations on Genesis and Sequential Development of the Internal Architecture of the Paskapoo Formation

##### 7.3.1.1 Introduction – Architectural Models for Continental Strata

The purpose of this study was to construct a model of the 3-D distribution of sandiness within the Paskapoo Formation to define regional hydrostratigraphic units. However, as the model generated interpretive products, inferences could be made not only about the spatial relationships of sandstone and mudstone within the Paskapoo Formation but also about the genesis and evolution of depositional settings. Although preceding sections addressed aspects of these hydrostratigraphic units, they are re-appraised here in the context of a predictive stratigraphic architecture.

In their discussion of a sequence-stratigraphic framework for continental strata, Shanley and McCabe (1994) related changes in the architecture of fluvial deposits to the interplay between allocyclical (e.g., tectonism, climate, changing base level) and autocyclical (e.g., channel avulsion) processes. The relationship between accommodation space, particularly its rate of change, and sediment supply plays an important role in shaping the architecture of stratigraphic patterns in continental settings (Figure 67). When

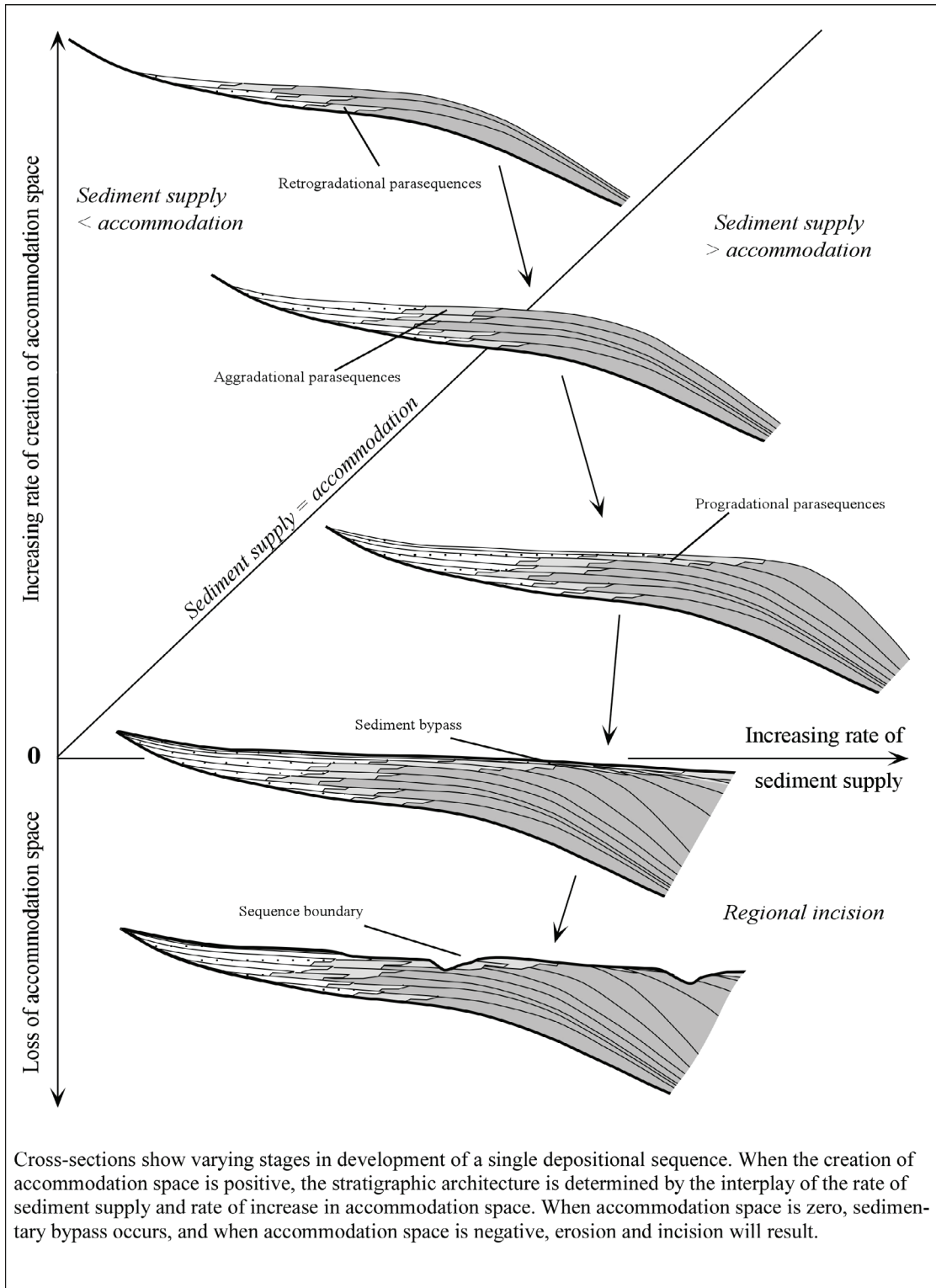


Figure 67. Interplay between accommodation space and sediment supply resulting in stratigraphic stacking (modified from Shanley and McCabe, 1994, Figure 2, reprinted by permission of the American Association of Petroleum Geologists, whose permission is required for further use).

considering those parts of interior basins in nonmarine settings, changes in stratigraphic base level and accommodation space will be influenced more by tectonic (e.g., source-area uplift and basin subsidence) and climatic cycles and less by eustatic changes in sea level.

Drawing on examples of sedimentary sequences in fluvial deposits from numerous locations, including those of interior basins in Argentina, Shanley and McCabe (1994) demonstrated there is a predictive pattern in fluvial architecture as accommodation space is created due to a change in stratigraphic base level. Although their examples illustrate how sedimentary architecture develops in response to changes in base level due to rise and fall in eustatic sea level, the principles can be applied to changes in stratigraphic base level and accommodation space due to tectonism. Where sediment supply is constant or increasing, a slow rate in the creation of accommodation space will result in stacked channel sand belts where repeated channel migration cannibalizes most of the fine-grained floodplain sediment. The result is widespread, amalgamated, multi-storey and multilateral sandstone units, which may be laterally constrained by the basin flanks. With increasing rates in the growth of accommodation space, both bedload and suspension sediments prevail, and the architecture evolves into more widely spaced meander-belt channel sandbodies and an increase in mud content. The areal extent of these strata is generally broader. As accommodation space and surface gradient decrease, the strata will consist mainly of suspension sediments.

Autocyclical processes, styles of avulsion in particular, may also leave their imprint on the architecture of fluvial deposits. Mackey and Bridge (1995) developed a model to simulate the distribution, proportion, and connectedness of coarse-grained channel belts as a function of changes in floodplain and channel-belt geometry, location and frequency of avulsions, sedimentation and compaction rates, and tectonism. Their model shows that the distribution of channel belts, and the dimensions and degrees of connectedness of sandbodies within, vary as a function of distance

from avulsion nodes and cross-section orientation. In systems experiencing slowly rising stratigraphic base levels and greater downvalley aggradation, avulsion points systematically shift upvalley with greater frequency to produce avulsion sequences of numerous channel belts and interconnected sandbodies (Figure 68a). Within each sequence, laterally constrained channel belts grade upwards into thinner, more broadly distributed channel belts. As regional avulsions shift the locations of channel deposition across the floodplain, another sequence initiates. With progressive migration of avulsion points upvalley, the resulting geometry evolves into vertical succession of sequences, each thinner than the last (Figure 68b). Where aggradation is greater in upvalley locations, such as in alluvial fans in foreland settings or with falling base level, avulsions and interconnected sandbodies are more likely to occur in the upvalley part of the floodplain (Figure 68c).

Hajek et al. (2010) cautioned against over-interpreting the paleotectonic or climatic environments from the architecture and distribution of channel-belt sandstone bodies. Using fluvial tank experiments, in which variables such as sediment and water supply were held constant, they determined that a cyclical stacking of channel sandbodies can form entirely by autogenic avulsion processes, independent of changes in external controls, such as accommodation space or sediment supply.

### **7.3.1.2 Deposition of the Paskapoo Formation**

#### **Creation of Accommodation Space and Deposition of the Haynes Aquifer Sandstone Bodies**

There are parallels between our model of the architecture of the Paskapoo Formation and that described for continental strata by Shanley and McCabe (1994) and Mackey and Bridge (1995). The regional distribution and internal geometry of the Haynes aquifer suggests it formed by the amalgamation of multi-storey and multilateral, coarse-grained, channel-belt deposits occupying a broad depression on the surface of the underlying Scollard Formation (Figure 69). Shanley and McCabe (1994) proposed that stacked channel

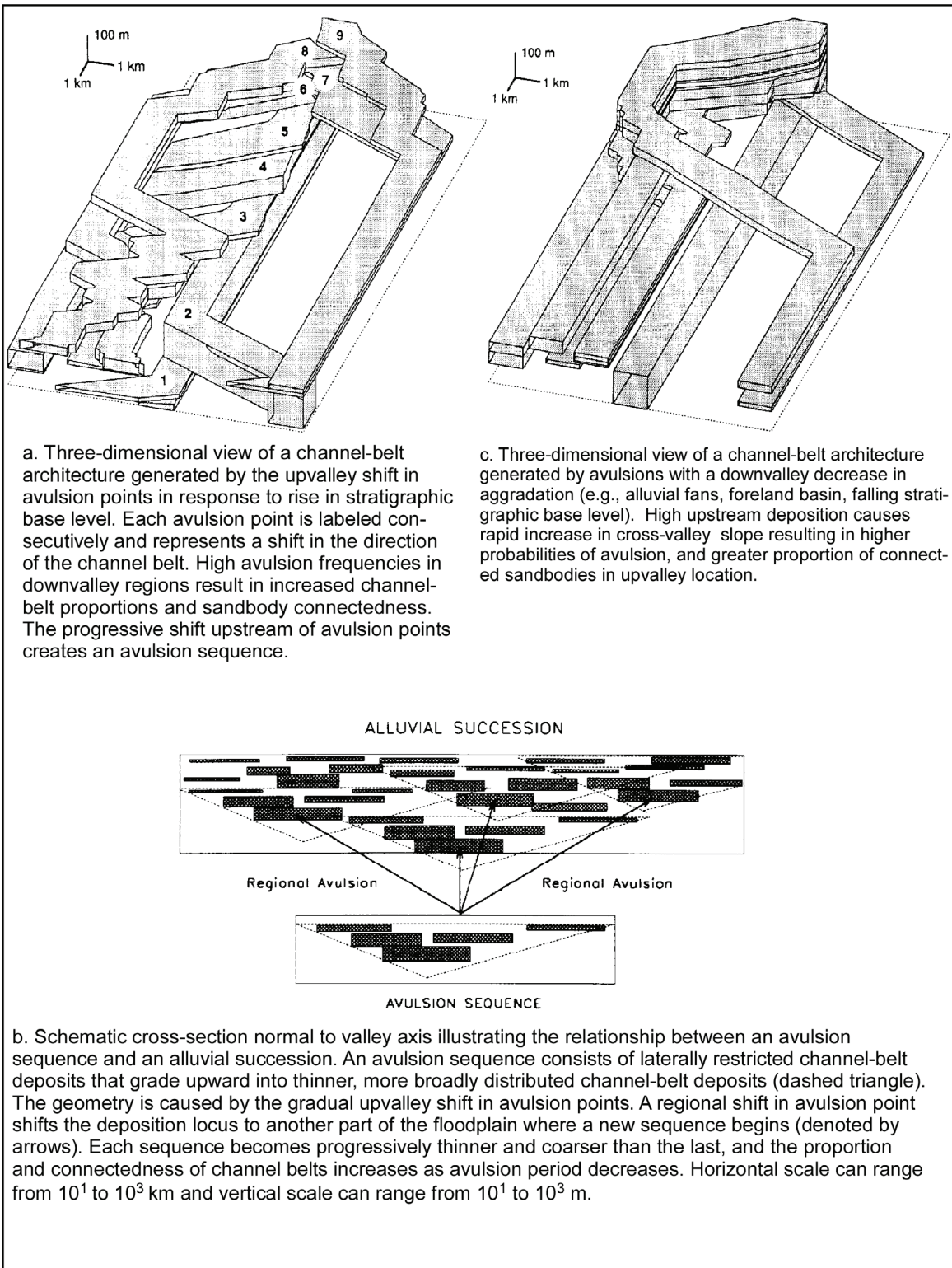


Figure 68. Influence of avulsion styles on the architecture of channel sandstone bodies (modified from Mackey and Bridge, 1995, Figures 13–15, copyright permission granted by Society for Sedimentary Geology).

sandstone belts develop in those settings where a slow rate of rise in base level creates accommodation space. In the case of the Haynes aquifer, change in the relative base level most likely resulted from foreland subsidence due to tectonism and sediment loading rather than rising sea level.

Others have proposed that the associated Haynes Member represents an interconnected network of stacked channel sandstone bodies deposited in an anastomosing fluvial system (Demchuk and Hills, 1991; Jerzykiewicz, 1997; Hamblin, 2004). Jerzykiewicz (1997) believed the unit represented widespread flash-flood deposits. The base of the Paskapoo Formation (Haynes Member sandstone) generally has an erosional contact with the Scollard Formation, sometimes marked by cobble lags. Previous studies have determined this basal sandstone unit is generally no more than 100 m thick. This is consistent with the modelled results in our study, which show that most of the sandstone averages about 50 m thick (Figure 54).

A generally southeast trend to the most sandy parts of the unit in central Alberta (Figure 56) suggests regional flow was southeast, subparallel to the axis of the deformation front, an interpretation supported by some previous studies (Hamblin, 2004). Given the range in elevation of the top of the unit and the unit's relatively uniform thickness, we infer that most of the Haynes aquifer was deposited prior to major deformation, since only its westernmost parts show evidence of infill within enhanced accommodation space. The relatively uniform thickness of the Haynes aquifer also suggests that the rate of sediment influx was at least equal to, or slightly greater than, the rate of growth in accommodation space. An exception is the accumulation of thicker deposits east of the deformation front in the area west of Drayton Valley and in the area southwest of Red Deer (Figure 54), which may define the locus of stream and sediment emergence eastward from the mountain front (Figure 70). These sites may represent a nodal style of avulsion typical of foreland settings where aggradation rates are high (Figure 68c).

### **Increase in Rate of Growth of Accommodation Space and Deposition of Lacombe Mudstone-Dominated Complex**

We speculate that active tectonism and thrusting deformed the western edge of the Haynes Member and increased the rate of growth of accommodation space in the foreland basin. Previous studies suggested that at maximum subsidence, infilling occurred through the accretion of thick, dominantly fine-grained, alluvial floodplain and lacustrine deposits (Jerzykiewicz, 1997; Hamblin, 2004). Where deposition of both bedload and suspension sedimentation prevail, Shanley and McCabe (1994) suggest the resulting architecture will consist of isolated high-sinuosity channels encased in silt and mud. This characterizes both the composition and architecture of the Lacombe aquitard, which our model demonstrates consists of a westward-thickening wedge of dominantly fine-grained deposits with isolated sandstone bodies lacking regional connectedness. Our model reveals that during basin infill, coarse fluvial sediment continued to be deposited into the basin proximal to the thrust front west of Drayton Valley, in the same location as the depocentre of the Haynes aquifer sandstone complex (Figure 70).

### **Deposition of the Sunchild Sandstone-Dominated Complex**

It is unknown if a hiatus occurred following the deposition of fine-grained sediments of the Lacombe aquitard. However, a decrease in the rate of growth of accommodation space coupled with another influx of coarse fluvial sediment into the foreland basin initiated a new depositional sequence marked by the sandstone bodies of the Sunchild aquifer (Figure 69). Jerzykiewicz (1997) also recognized aspects of this event in the stratigraphic record; he attributed coarse sand and conglomerate beds (which mark the boundary of his upper and lower members in the Entrance area, west of Hinton) to flash floods. Unlike the relatively uniformly thick sheet deposits that make up the Haynes aquifer, our model shows that sandstone bodies of the Sunchild aquifer system have a varied thickness and a more fragmentary, step-like vertical distribution. This

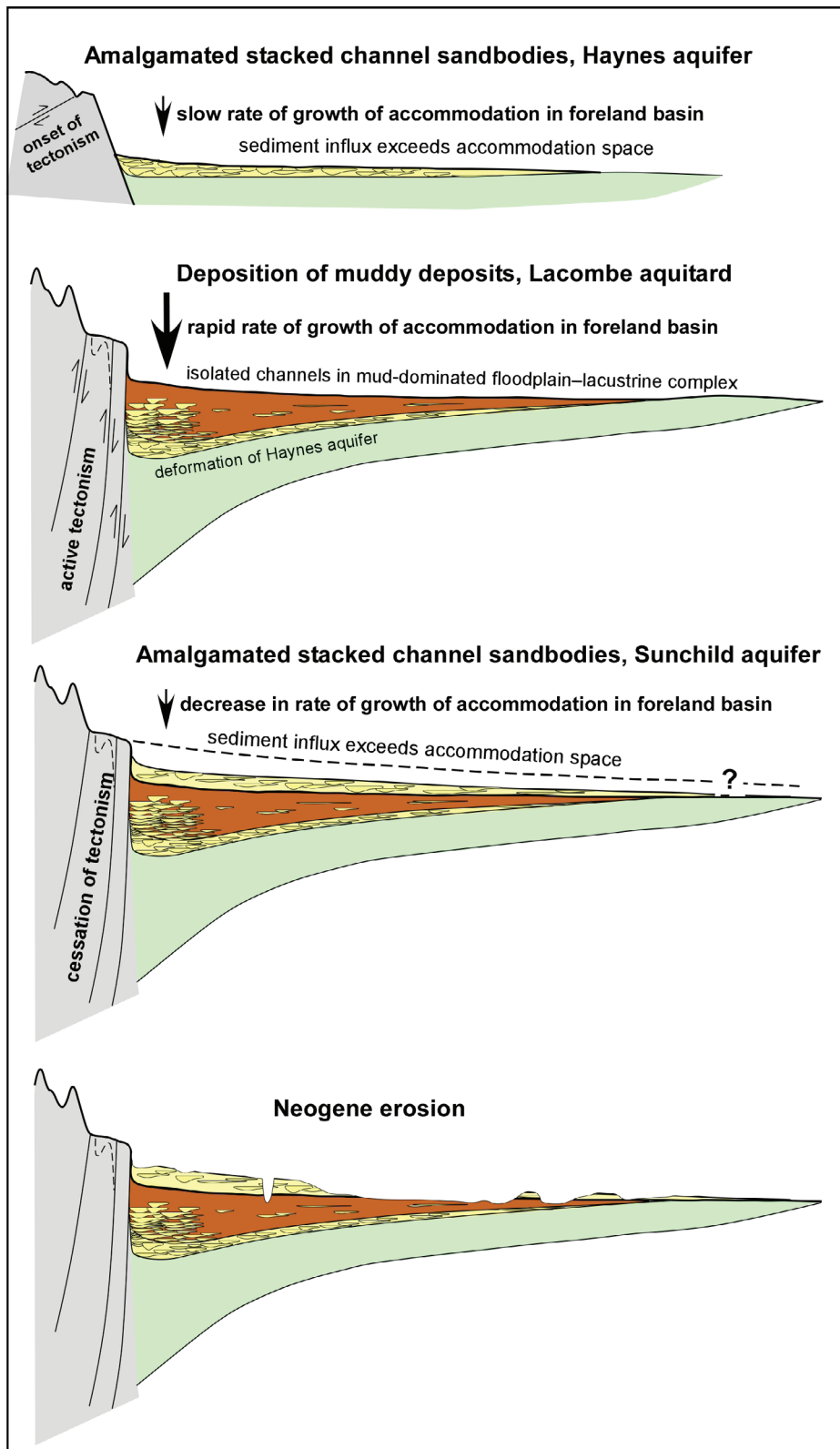
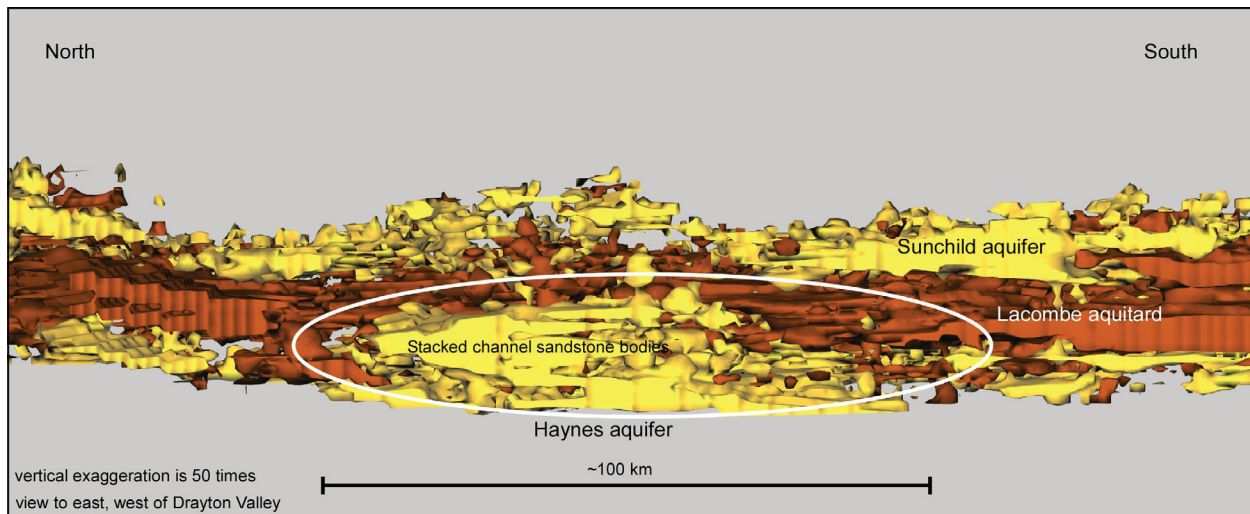


Figure 69. Structural and depositional history of hydrostratigraphic units as interpreted from the model of sandiness within the Paskapoo Formation.



**Figure 70. Stacked channel sandstone complex within the Haynes aquifer, west of Drayton Valley, illustrating possible loci of stream emergence into foreland basin.**

architecture possibly reveals multiple avulsion nodes in alluvial fan complexes, though poor preservation of the Sunchild sandstone-dominated complex due to ongoing fluvial erosion makes interpretation of genesis based on present-day geometry speculative. A shallow eastward slope of the contact between the Sunchild aquifer and the underlying Lacombe aquitard (Figures 51 and 58) indicates the deposition of coarse sediments during a period of relative tectonic quiescence, when foreland deformation and subsidence was at a minimum. Eastward thinning of the Lacombe aquitard results in sandstone bodies of the Sunchild aquifer resting nearly atop the Haynes aquifer (Figure 51b) as the latter rises to outcrop in the east. A future examination of the petrology and sedimentology may reveal differences in provenance and genesis, which may help differentiate the sandstone of the Sunchild aquifer from that of the Haynes aquifer. Based on petrographic analysis of a small number of samples, Carrigy (1971) reported that in west-central Alberta, sandstone in the upper Paskapoo Formation has a higher proportion of potassium feldspar and metamorphic rock fragments than that of sandstone in the lower part of the formation. This supports the premise that petrological analysis can differentiate between sandstone of the Haynes and Sunchild aquifers.

### Post-Depositional Erosion

The total thickness of the Paskapoo Formation deposited after the Sunchild sandstone-dominated complex is unknown. However, Nurkowski (1985) calculated that there must have been an additional 900 to 1500 m of sediment above the present-day topography based on the quality and rank of coal deposits in the central Alberta Plains. If so, then the present-day distribution and composition of the Paskapoo Formation likely represents the preserved lowermost part of what was once a much thicker and more extensive unit. The current landscape of the Paskapoo Formation is characterized by a fragmented cover of thick Sunchild sandstone bodies in the west, thin sandstone remnants of the Haynes Aquifer along the eastern edge, and the eroded surface of the underlying Lacombe mudstone-dominated complex elsewhere. Remnants of gravel and cobbles, preserved as lag deposits, provide a fragmentary record of the fluvial systems that eroded the Paskapoo Formation (and possibly overlying formations no longer preserved) during the Neogene. Subsequent glacial and postglacial processes during the late Quaternary have further modified the surface of the Paskapoo Formation.

## 8 Summary

The analytical processes developed and applied in this study enable us to map the major hydrostratigraphic units within the Paskapoo Formation. This, in turn, has enabled us to provide new insights into the lithostratigraphic architecture of this formation and to make inferences about its sedimentary history. The abundance of digital and descriptive borehole data, coupled with remotely collected airborne-geophysical data, permits a digital and geostatistical analytical approach to characterizing regional sandstone and mudstone distributions in an otherwise heterogeneous complex of fluvial and lacustrine deposits. From the perspective of defining regional aquifer systems, the incorporation of geostatistically designed mini-models, which assess probable geometries and 3-D connections of sandstone bodies, enables the definition of major hydrostratigraphic units having similar hydraulic properties. The construction of a digital, fully 3-D model of sandstone distribution within the Paskapoo Formation thus reveals the internal geometries and distribution of major regional hydrostratigraphic units.

Two of the three hydrostratigraphic units defined in this study are consistent with aspects of previously defined stratigraphic architectures, specifically the Haynes and Lacombe members (Demchuk and Hills, 1991). The third is a newly defined unit, herein informally named the Sunchild aquifer. Recognition of this unit may warrant a re-evaluation of the uppermost part of the Paskapoo Formation lithostratigraphic framework. The geostatistical differentiation of sandstone-dominated units in the Paskapoo Formation provides a basis for applying conventional geological methods, such as petrological analyses, to test the Haynes and Sunchild sandstones for differences in sediment provenance and paleoflow direction. The ability to define the geometries and subsurface distributions of these units from the modelled borehole data means that a hydrostratigraphic framework can now be incorporated into regional groundwater-flow models to better assess groundwater resources in the most heavily populated part of Alberta. The ability to apply different cutoff criteria when

mapping aquifers, based on the relationship between sandstone abundance and hydraulic connectivity, means that we can explore the volumetric consequences of applying conservative or liberal sandiness values to define aquifers. Furthermore, the quantitative aspect of our hydrostratigraphic model permits the testing of many possible, equally probable interpretations through the generation of simulations. We consider this a desirable, perhaps even necessary, method to characterize the internal structure of lithologically heterogeneous geological units.

Finally, the underpinnings of our model of the architecture of the Paskapoo Formation differ from those conventionally used to construct geological models. Except for the top and bottom of the Paskapoo Formation, we have not constructed structural surfaces using log picks, nor have we measured or described sedimentological features or stratigraphic boundaries, applied biostratigraphic classification methods, or mapped unconformable surfaces that might provide time-break markers. Furthermore, we have made assumptions about what constitutes sandiness within a rock; collapsed ranges of sediment type into a binary classification of sandstone or mudstone; assigned sandstone-abundance values to coarse, regional model cells; and made estimates about regional permeabilities and hydraulic connections based on theoretical models. Notwithstanding these unconventional approaches, our model incorporates geological information from tens of thousands of boreholes that span almost the entire depth and lateral extent of the Paskapoo Formation. The geostatistical analytical approach we have adopted to interpret hydrostratigraphic units from those data enables others to not only duplicate our methods, but also to test or alter each of our assumptions to assess different outcomes.

## 9 References

- Barker, A.A., Riddell, J.T.F., Slattery, S.R., Andriashek, L.D., Moktan, H., Wallace, S., Lyster, S., Jean, G., Huff, G.F., Stewart, S.A. and Lemay, T.G. (2011): Edmonton–Calgary Corridor groundwater atlas; Energy Resources Conservation Board, ERCB/AGS Information Series 140, 90 p.
- Boisvert, J.B. (2007): Mineral deposit modeling with pseudo-genetically constructed training images; M.Sc. thesis, University of Alberta, 72 p.
- Boisvert, J.B., Pyrcz, M.J. and Deutsch, C.V. (2007): Multiple-point statistics for training image selection; *Natural Resources Research*, v. 16, no. 4, p. 313–321.
- Bonomi, T. (2009): Database development and 3D modeling of textural variations in heterogeneous, unconsolidated aquifer media: application to the Milan plain; *Computers and Geosciences*, v. 35, issue 1, p. 134–145.
- Bridge, J.S. and Mackey, S.D. (1993): A theoretical study of fluvial sandstone body dimensions; *in* The geological modelling of hydrocarbon reservoirs and outcrop analogues, I.D. Bryant and S.S. Flint (ed.), International Association of Sedimentologists, Special Publication Number 15, p. 213–236.
- Burns, E.R., Bentley, L.R., Hayashi, M., Grasby, S.E., Hamblin, A.P., Smith, D.G. and Wozniak, P.R.J. (2010a): Hydrogeological implications of paleo-fluvial architecture for the Paskapoo Formation, SW Alberta, Canada: a stochastic analysis; *Hydrogeology Journal*, v. 18, no. 6, p. 1375–1390.
- Burns, E.R., Bentley, L.R., Therrien, R. and Deutsch, C.V. (2010b): Upscaling facies models to preserve connectivity of designated facies; *Hydrogeology Journal*, v. 18, no. 6, p. 1357–1373.
- Campbell, J.D. (1967): Ardley coal zone in the Alberta Plains: central Red Deer area; Research Council of Alberta, Earth Sciences Report 1967-01, 36 p., URL <[http://www.ags.gov.ab.ca/publications/abstracts/ESR\\_1967\\_01.html](http://www.ags.gov.ab.ca/publications/abstracts/ESR_1967_01.html)> [February 2012].
- Carrigy, M.A. (1971): Lithostratigraphy of the uppermost Cretaceous (Lance) and Paleocene strata of the Alberta Plains; Research Council of Alberta, Alberta Geological Survey Bulletin 27, 175 p., URL <[http://www.ags.gov.ab.ca/publications/abstracts/BUL\\_027.html](http://www.ags.gov.ab.ca/publications/abstracts/BUL_027.html)> [February 2012].
- Chen, Z., Grasby, S.E., Hamblin, T. and Xiu, S. (2007): Paskapoo groundwater study part II: sandstone thickness and porosity estimations using well log data for the aquifer system in the Tertiary Paskapoo Formation, Alberta; Geological Survey of Canada, Open File 5445, 14 p.
- Dawson, F.M., Evans, C.G., Marsh, R. and Richardson, R. (1994): Uppermost Cretaceous and Tertiary strata of the Western Canadian Sedimentary Basin; *in* Geological atlas of the Western Canadian Sedimentary Basin, G.D. Mossop and I. Shetsen (comp.), Canadian Society of Petroleum Geologists and Alberta Research Council, p. 387–406, URL <[www.ags.gov.ab.ca/publications/wcsb\\_atlas/a\\_ch24/ch\\_24.html](http://www.ags.gov.ab.ca/publications/wcsb_atlas/a_ch24/ch_24.html)> [February 2012].
- Demchuk, T.D. and Hills, L.V. (1991): A re-examination of the Paskapoo Formation in the central Alberta Plains: the designation of three new members; *Bulletin of Canadian Petroleum Geology*, v. 39, p. 270–282.
- Deutsch, C.V. (1999): Reservoir modeling with publicly available software; *Computers & Geosciences*, v. 25, issue 4, p. 355–363.
- Deutsch, C.V. (2002): Geostatistical reservoir modeling; Oxford University Press, New York, 376 p.
- Deutsch, C.V. and Journel, A.G. (1998): GSLIB: geostatistical software library and user's guide (2nd edition); Oxford University Press, New York, New York, 369 p.
- Deutsch, C.V. and Tran, T.T. (2002): FLUVSIM: a program for object-based stochastic modeling of fluvial depositional systems; *Computers & Geosciences*, v. 28, issue 4, p. 525–535.

- Domenico, P. and Stephenson, D. (1964): Application of quantitative mapping techniques to aid in hydrologic systems analysis of alluvial aquifers; *Journal of Hydrology*, v. 2, p. 164–181.
- Driess, S.J. and Johnson, N.M. (1989): Hydrostratigraphic interpretation using indicator geostatistics; *Water Resources Research*, v. 25, no. 12, p. 2501–2510.
- Fogg, G.E. (1986): Groundwater flow and sand body interconnectedness in a thick multiple aquifer system; *Water Resources Research*, v. 22, p. 679–694.
- Gibling, M.R. (2006): Width and thickness of fluvial channel bodies and valley fills in the geological record: a literature compilation and classification; *Journal of Sedimentary Research*, v. 76, p. 731–770.
- Gibson, D.W. (1977): Upper Cretaceous and Tertiary coal-bearing strata in the Drumheller-Ardley region, Red Deer Valley, Alberta; Geological Survey of Canada, Paper 76-35, 41 p.
- Grasby, S.E., Chen, Z., Hamblin, A.P., Wozniak, P.R.J. and Sweet, A.R. (2008): Regional characterization of the Paskapoo bedrock aquifer system, southern Alberta; *Canadian Journal of Earth Sciences*, v. 45, issue 12, p. 1501–1516.
- Guo, H. and Deutsch, C.V. (2010): Fluvial channel size determination with indicator variograms; *Petroleum Geoscience*, v. 16, p. 161–169.
- Hajek, E.A., Heller, P.L. and Sheets, B.A. (2010): Significance of channel-belt clustering in alluvial basins; *Geology*, v. 38, no. 6, p. 535–538.
- Hamblin, A.P. (2004): Paskapoo-Porcupine Hills formations in western Alberta: synthesis of regional geology and resource potential; Geological Survey of Canada, Open File 4679, 30 p.
- Hamilton, W.H., Langenberg, C.W., Price, M.C. and Chao, D.K., comp. (1999): Geological map of Alberta; Alberta Energy and Utilities Board, EUB/AGS Map 236, scale 1:1 000 000, URL <[http://www.ags.gov.ab.ca/publications/abstracts/MAP\\_236.html](http://www.ags.gov.ab.ca/publications/abstracts/MAP_236.html)> [February 2012].
- Hydrogeological Consultants Ltd. (1999): M.D. of Brazeau No. 77, part of the North Saskatchewan and Athabasca River basins, parts of Tp 045 to 050, R 03 to 11, W5M, revised regional groundwater assessment; Agriculture and Agri-Food Canada, Prairie Farm Rehabilitation Administration, 106 p., URL <<http://www.10714.com/pdf/rgwa/brazeau.pdf>> [February 2012].
- Jerzykiewicz, T. (1997): Stratigraphic framework of the uppermost Cretaceous to Paleocene strata of the Alberta Basin; Geological Survey of Canada, Bulletin 510, 121 p.
- Jones, L. (1977): Slice technique applied to uranium favorability in uppermost Tertiary of East Texas and West Louisiana; *Gulf Coast Association of Geological Societies Transactions*, v. 27, p. 61–68.
- Journel, A.G. (1994): Resampling from stochastic simulations; *Environmental and Ecological Statistics*, v. 1, no. 1, p. 63–91.
- Lerbekmo, J.F. and Sweet, A.R. (2000): Magnetostratigraphy and biostratigraphy of the continental Paleocene in the Calgary area, southwestern Alberta; *Bulletin of Canadian Petroleum Geology*, v. 48, no. 4, p. 285–306.
- Lerbekmo, J.F. and Sweet, A.R. (2008): Magnetobiostratigraphy of the continental Paleocene upper Coalspur and Paskapoo formations near Hinton, Alberta; *Bulletin of Canadian Petroleum Geology*, v. 56, no. 2, p. 118–146.
- Lerbekmo, J.F., Evans, M.E. and Hoyer, G.S. (1990): Magnetostratigraphic evidence bearing on the magnitude of the sub-Paskapoo disconformity in the Scollard Canyon-Ardley area of the Red Deer valley, Alberta; *Bulletin of Canadian Petroleum Geology*, v. 38, no. 2, p. 197–202.
- Lerbekmo, J.F., Demchuk, T.D., Evans, M.E. and Hoyer, G.S. (1992): Magnetostratigraphy and biostratigraphy of the continental Paleocene of the Red Deer valley, Alberta, Canada; *Bulletin of Canadian Petroleum Geology*, v. 40, no. 1, p. 24–35.

- Lerbekmo, J.F., Heaman, L.M., Baadsgaard, K., Muehlenbachs, K., Evans, M.E. and Sweet, A.R. (2008): Normal polarity magnetosubchrons in 24r and the age of the Paleocene-Eocene boundary; *Canadian Journal of Earth Sciences*, v. 45, no. 7, p. 781–793.
- Lyster, S. (2009): Simulation of geologic phenomena using multiple-point statistics in a Gibbs sampler algorithm; Ph.D. thesis, University of Alberta, 223 p.
- Mackey, S.D. and Bridge, J.S. (1995): Three-dimensional model of alluvial stratigraphy: theory and application; *Journal of Sedimentary Research*, v. 65, issue 1b, p. 7–31.
- Matthews, V.A. (2011): Stochastic modeling of the Paskapoo Formation; M.Sc. thesis, University of Calgary, 213 p.
- McLennan, J.A. (2007): The decision of stationarity; Ph.D. thesis, University of Alberta, 177 p.
- McLennan, J.A., Deutsch, C.V., Garner, D., Wheeler, T.J., Richey, J.F. and Mus, E. (2006): SAGD permeability modeling using geostatistics and minimodels; *Society of Petroleum Engineers*, SPE 103083, 14 p.
- Nurkowski, J.R. (1985): Coal quality and rank variation within Upper Cretaceous and Tertiary sediments, Alberta Plains region; Alberta Research Council, Alberta Geological Survey, Earth Sciences Report 1985-01, 39 p., URL <[http://www.ags.gov.ab.ca/publications/abstracts/ESR\\_1985\\_01.html](http://www.ags.gov.ab.ca/publications/abstracts/ESR_1985_01.html)> [February 2012].
- Parks, K. and Andriashek, L. (2009): Preliminary investigation of potential, natural hydraulic pathways between the Scollard and Paskapoo formations in Alberta: implications for coalbed methane production; Energy Resources Conservation Board, ERCB/AGS Open File Report 2009-16, 66 p., URL <[http://www.ags.gov.ab.ca/publications/abstracts/OFR\\_2009\\_16.html](http://www.ags.gov.ab.ca/publications/abstracts/OFR_2009_16.html)> [February 2012].
- Riddell, J.T.F., Andriashek, L.D., Jean, G. and Slattery, S.R. (2009): Preliminary results of sediment and bedrock coring in the Edmonton–Calgary Corridor, central Alberta; Energy Resources Conservation Board, ERCB/AGS Open File Report 2009-17, 81 p., URL <[http://www.ags.gov.ab.ca/publications/abstracts/OFR\\_2009\\_17.html](http://www.ags.gov.ab.ca/publications/abstracts/OFR_2009_17.html)> [February 2012].
- Shanley, K.W. and McCabe, P.J. (1994): Perspectives on the sequence stratigraphy of continental strata; *American Association of Petroleum Geologists, Bulletin*, v. 78, no. 4, p. 544–568.
- Shier, D.E. (2004): Well log normalization: methods and guidelines; *Petrophysics*, v. 45, no. 3, p. 268–280.
- Slattery, S.R. and Barker, A.A. (2010): Thickness of Quaternary and Neogene sediments in the Edmonton–Calgary Corridor (NTS 82O, 82P, 83A, 83B, 83G and 83H); Energy Resources Conservation Board, ERCB/AGS Map 548, scale 1:500 000, URL <[http://www.ags.gov.ab.ca/publications/abstracts/MAP\\_548.html](http://www.ags.gov.ab.ca/publications/abstracts/MAP_548.html)> [February 2012].
- Slattery, S.R., Barker, A.A., Andriashek, L.D., Jean, G., Stewart, S.A., Moktan, H. and Lemay, T.G. (2011): Bedrock topography and sediment-thickness mapping in the Edmonton–Calgary Corridor, central Alberta: an overview of protocols and methodologies; Energy Resources Conservation Board, ERCB/AGS Open File Report 2010-12, 16 p., URL <[http://www.ags.gov.ab.ca/publications/abstracts/OFR\\_2010\\_12.html](http://www.ags.gov.ab.ca/publications/abstracts/OFR_2010_12.html)> [February 2012].
- Srivastava, R.M. (1992): Reservoir characterization with probability field simulation; *Society of Petroleum Engineers*, SPE 24753, 12 p.
- Stauffer, D. and Aharony, A. (1994): Introduction to percolation theory (revised 2nd edition); Taylor & Francis, Ltd., New York, New York, 192 p.
- United States Geological Survey (2000): Shuttle radar topography mission digital elevation model data (3-arc second resolution); Earth Resources Observation and Science Center, URL <<http://seamless.usgs.gov>> [April 2004].

## Appendix 1 – Methodology Flowcharts

### Appendix 1a – Screening Digital Oil and Gas Gamma-Ray Logs to Calculate Net-Sand Thickness Using Slice-Mapping Methods

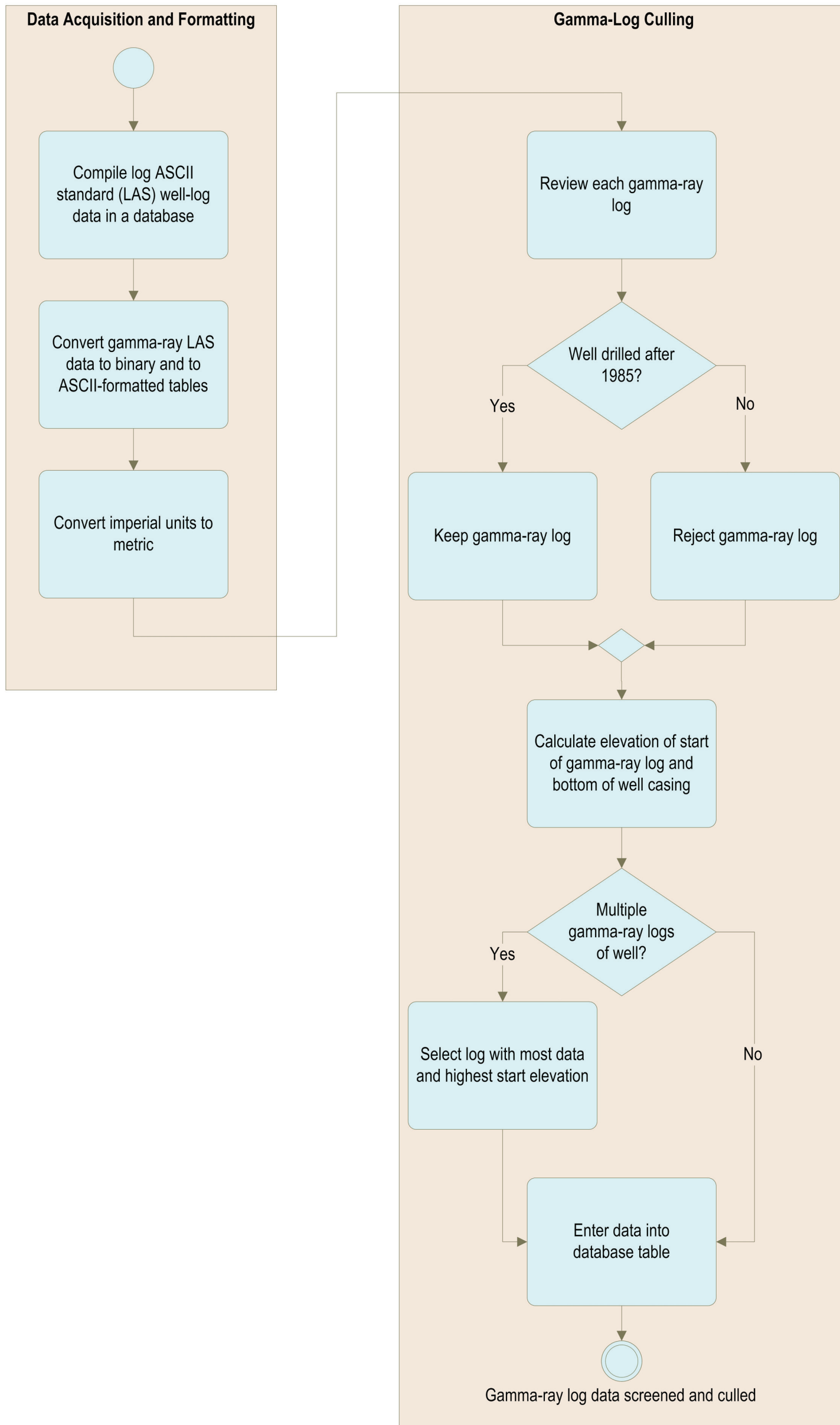


Figure 71. Screening digital oil and gas gamma-ray logs to calculate net-sand thickness using slice-mapping methods.

## Appendix 1b – Constructing Datums for Depth-Slice Analysis of Gamma-Ray Logs

To ensure geospatial integrity, adjust formation tops derived from unconstrained modelled surfaces for the top of the bedrock, the top of the Battle Formation, and the base of the Paskapoo Formation.

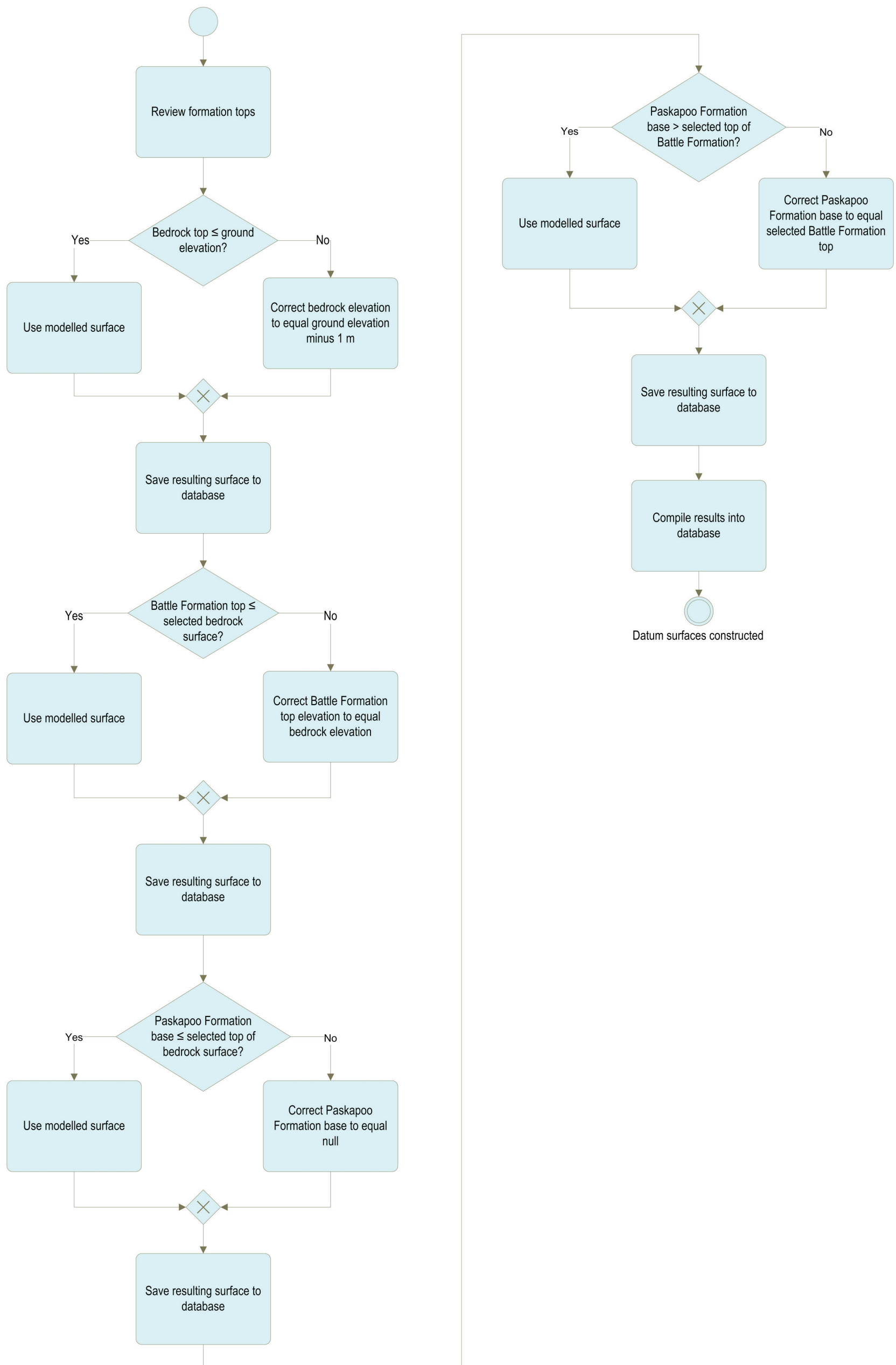


Figure 72. Constructing datums for depth-slice analysis of gamma-ray logs.

## Appendix 1c – Screening Water-Well Lithologs to Calculate Net-Sand Thickness Using Slice-Mapping Methods

In most cases, water wells do not penetrate through the Paskapoo Formation, or the base of the formation cannot be defined. As a result, the top of the Paskapoo Formation (the bedrock surface in this case) is selected as the datum from which depth-slice increments are constructed and propagated downward in 25 m thick intervals. This analysis was done to a depth of 150 m (six 25 m thick slices) below the bedrock surface, beyond which the lack of data made this analysis not meaningful.

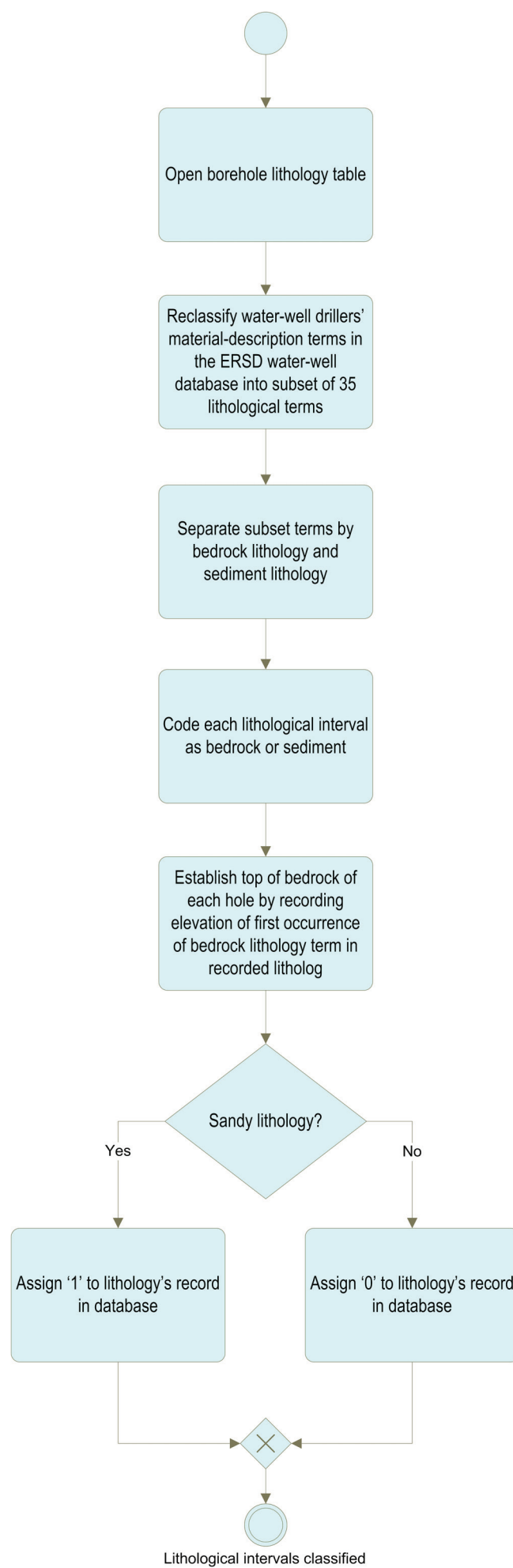


Figure 73. Screening water-well lithologs to calculate net-sand thickness using slice-mapping methods.

**Appendix 1d – Calculating Per Cent Sand in 25 m Thick Slices Within a Water-Well and Screening Results for 3-D Modelling**

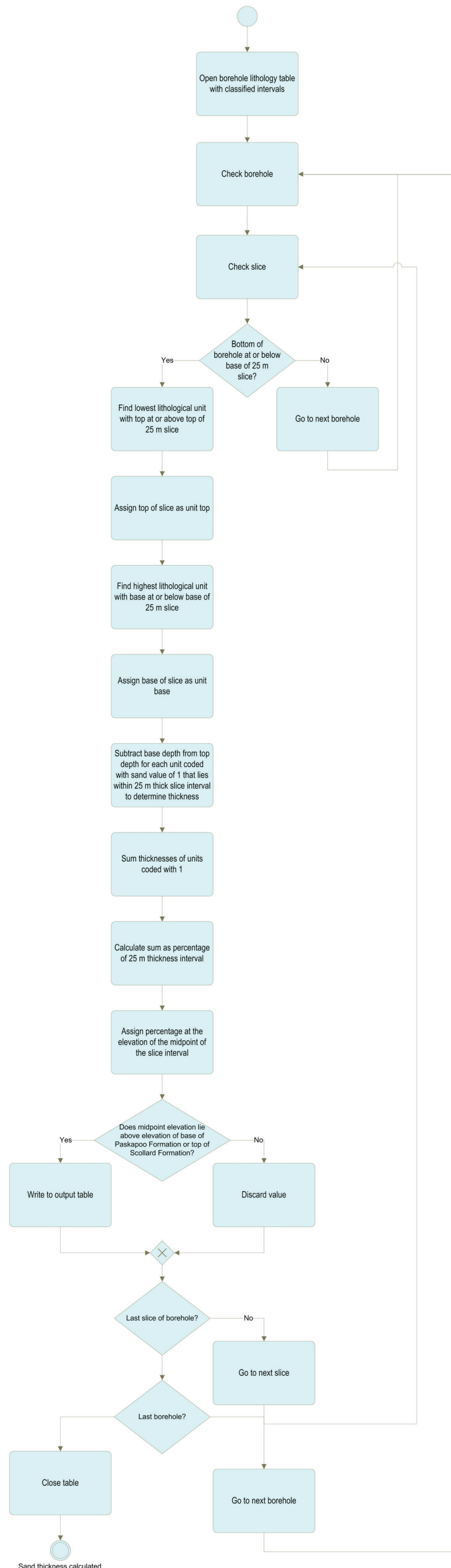


Figure 74. Calculating per cent sand in 25 m thick slices within a water-well and screening 3-D modelling.

Appendix 1e – Calculating Net-Sand Thickness in Oil and Gas Gamma-Ray Logs

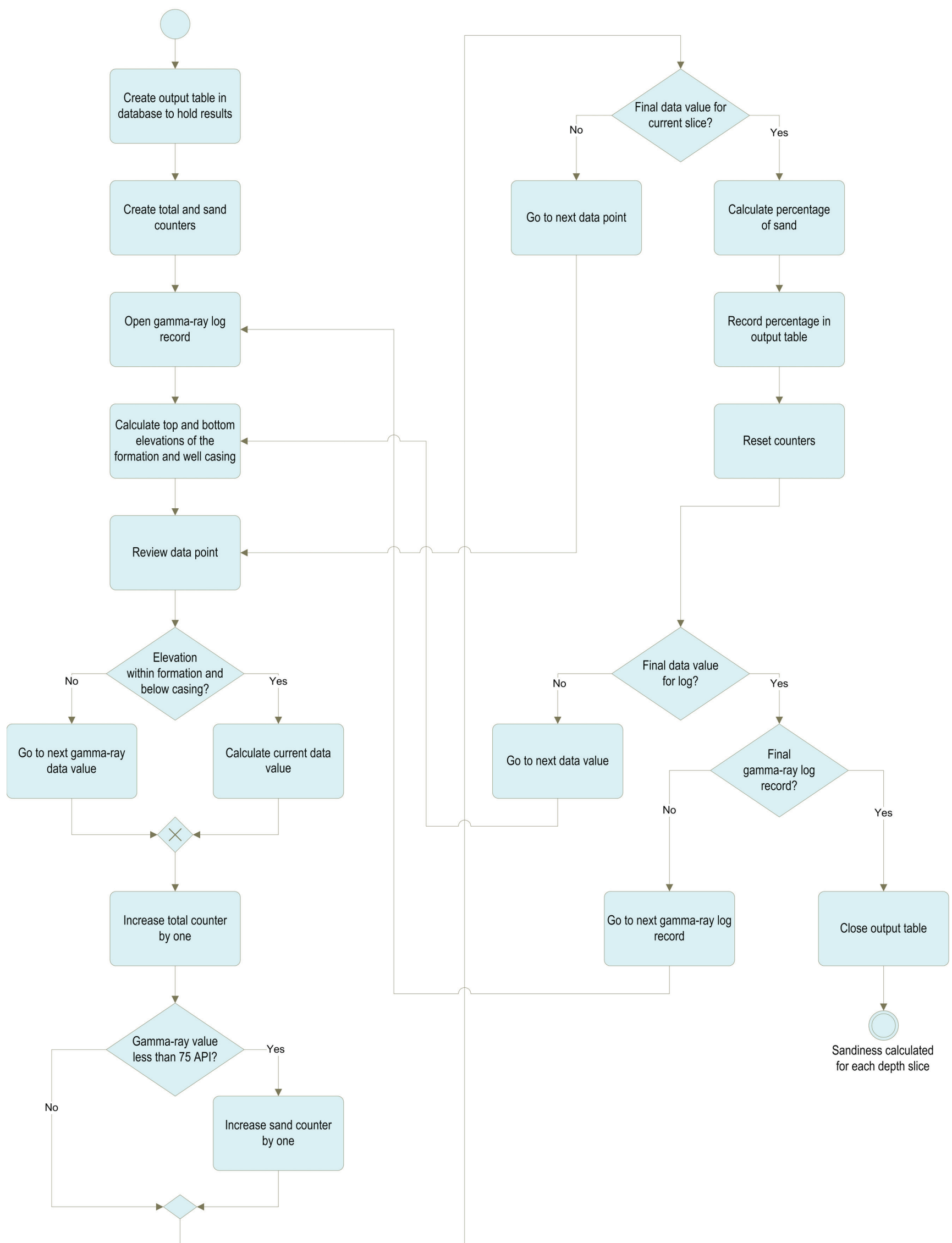
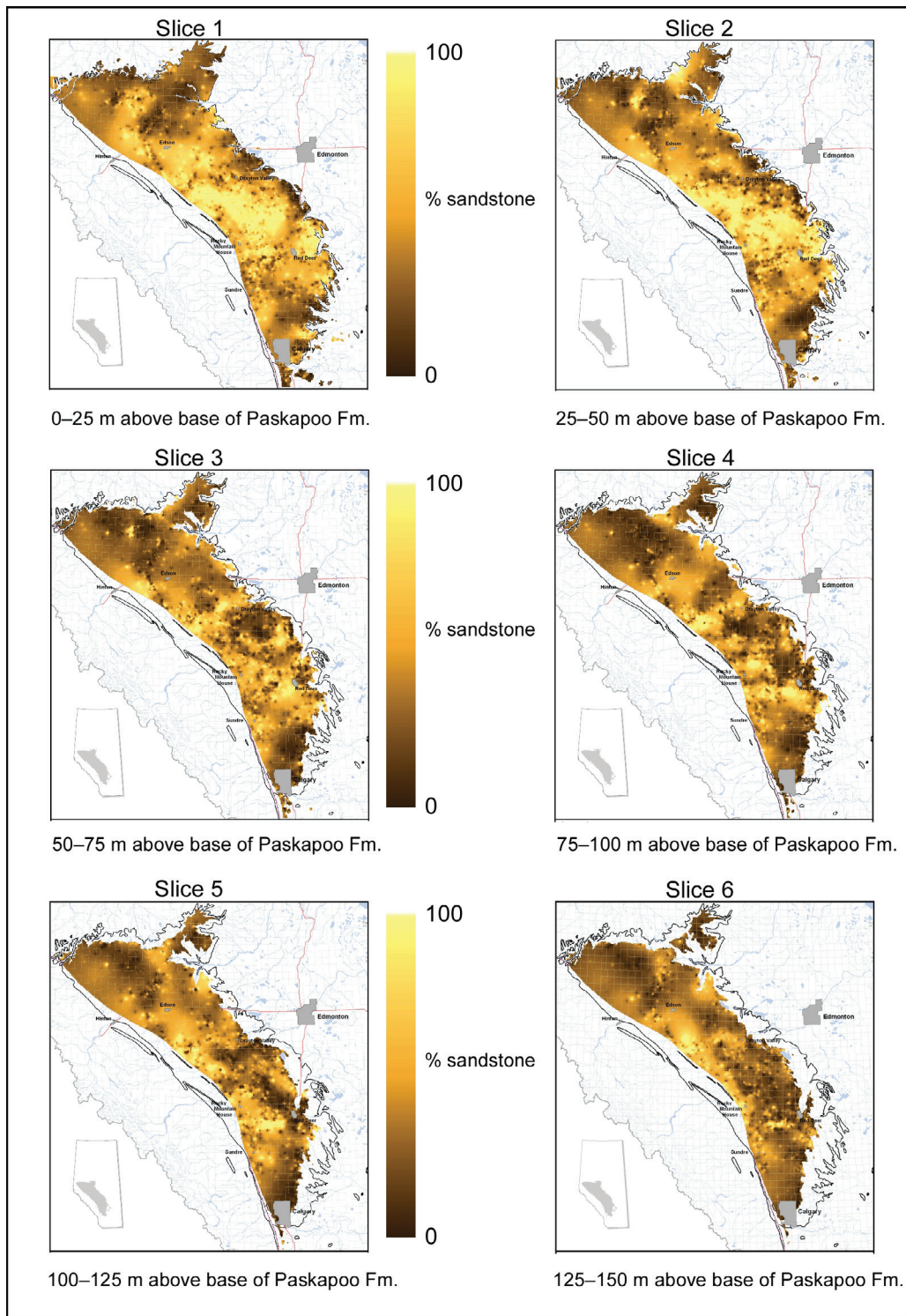


Figure 75. Calculating net-sand thickness in oil and gas gamma-ray logs.

## Appendix 2 – Depth-Slice Maps of Relative Sandstone Abundance in the Paskapoo Formation



**Figure 76. Distribution of sandstone in 25 m thick slices from 0 to 150 m above the base of Paskapoo Formation.**

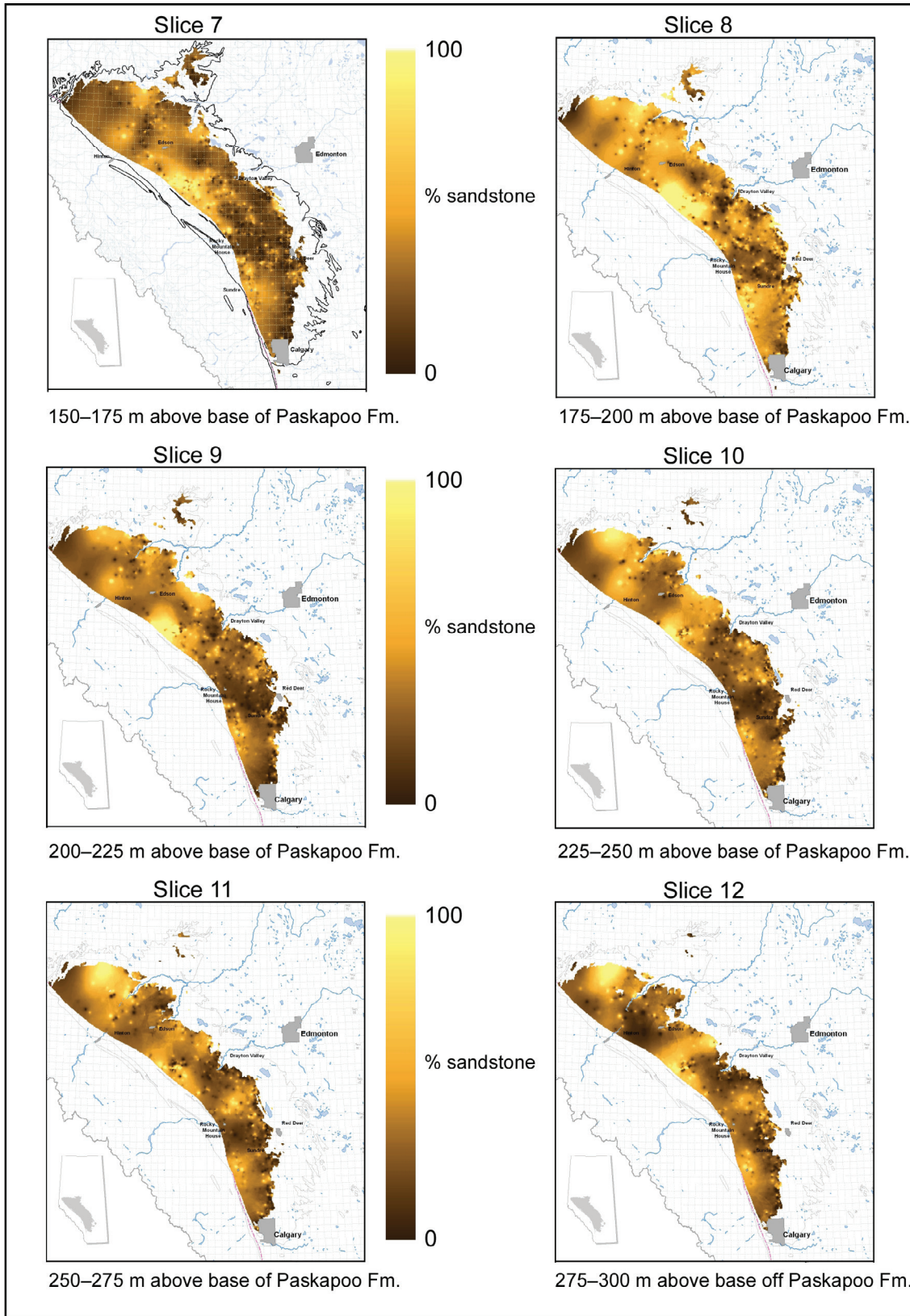


Figure 77. Distribution of sandstone in 25 m thick slices from 150 to 300 m above the base of Paskapoo Formation.

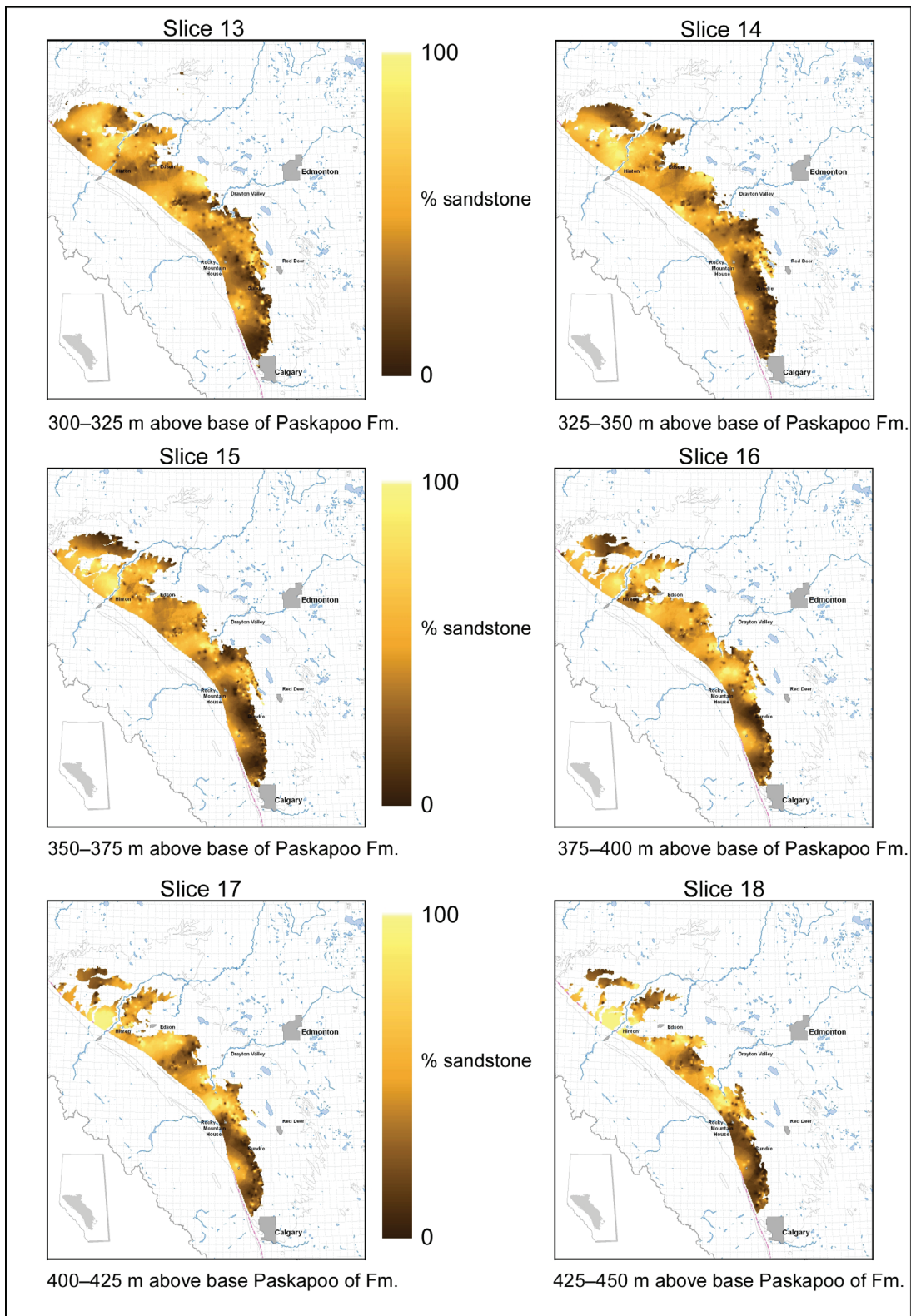


Figure 78. Distribution of sandstone in 25 m thick slices from 300 to 450 m above the base of Paskapoo Formation.

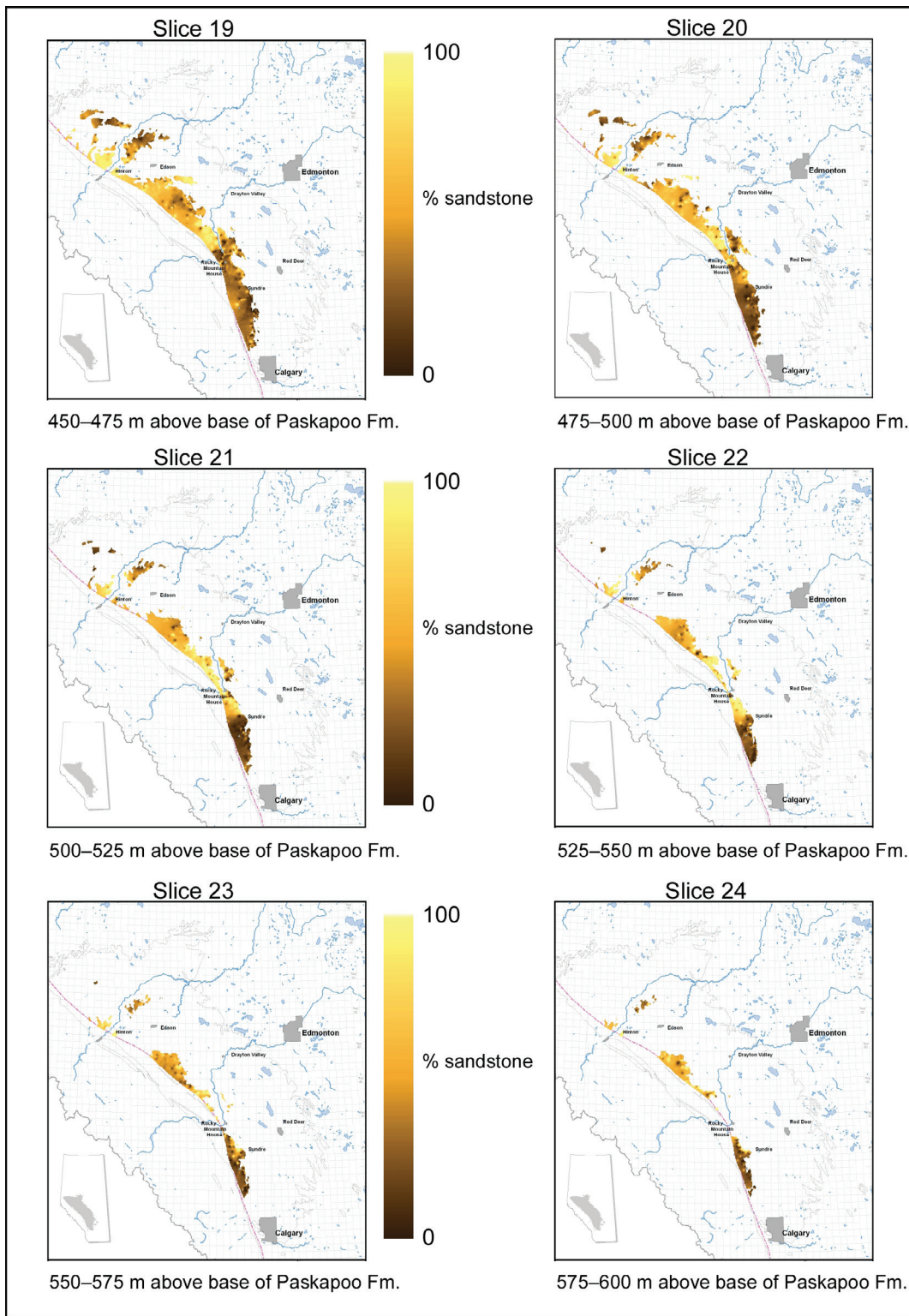


Figure 79. Distribution of sandstone in 25 m thick slices from 450 to 600 m above the base of Paskapoo Formation.

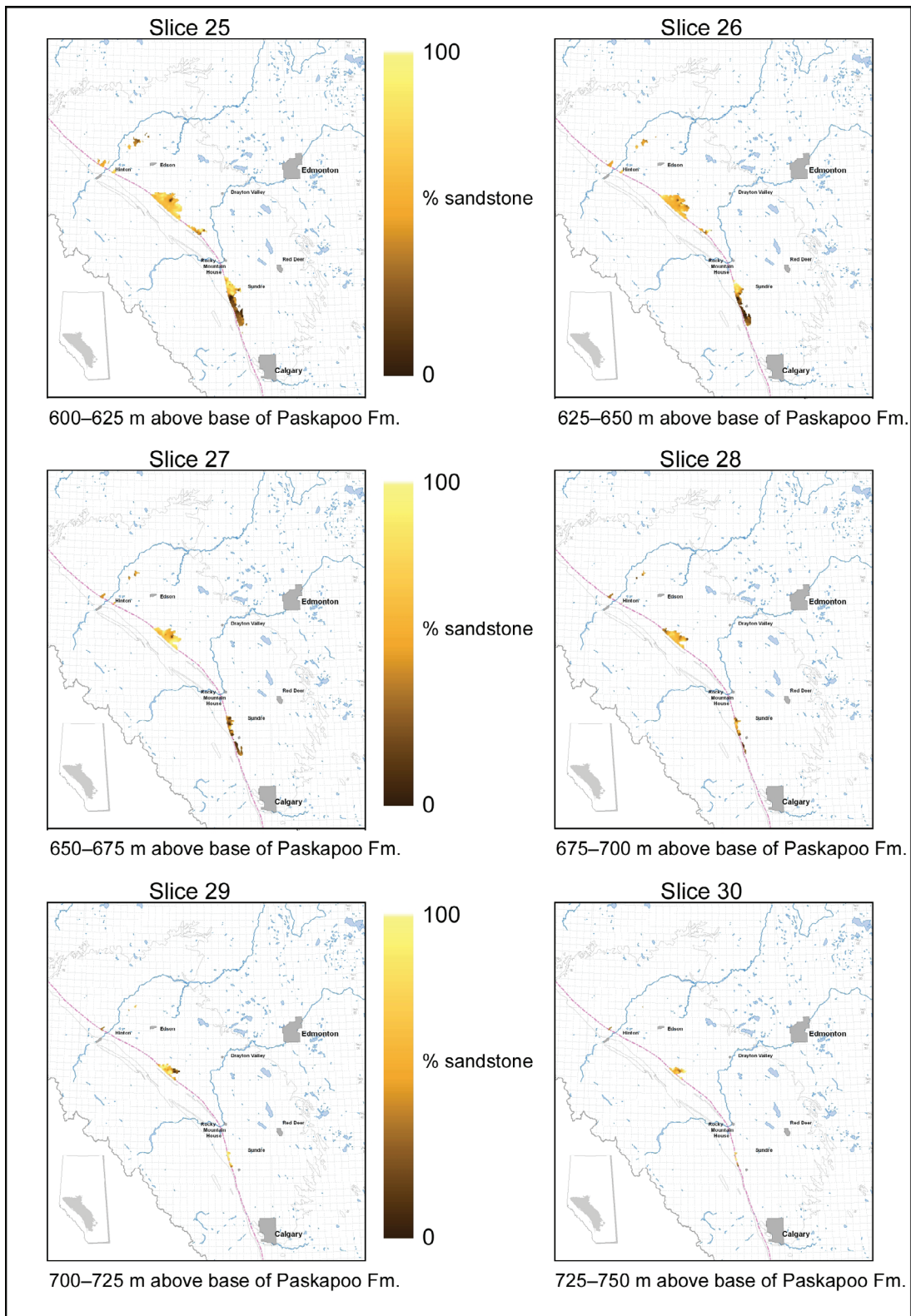


Figure 80. Distribution of sandstone in 25 m thick slices from 600 to 750 m above the base of Paskapoo Formation.

# Appendix 3 – Mini-Modelling

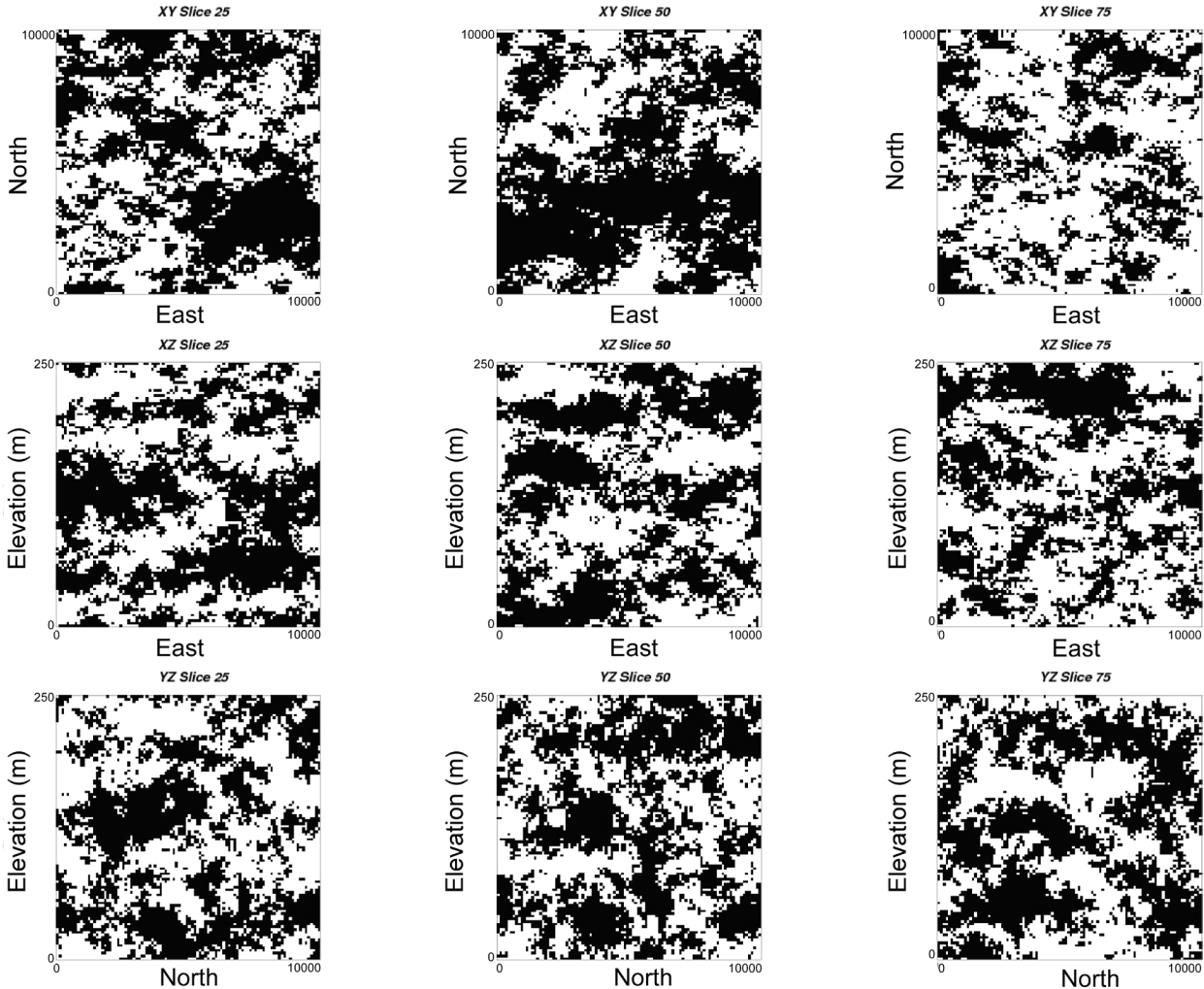


Figure 81. Slices of the mini-model created using the SISIM program. Vertical exaggeration is 40 times. Dark areas are sandy, light areas are muddy.

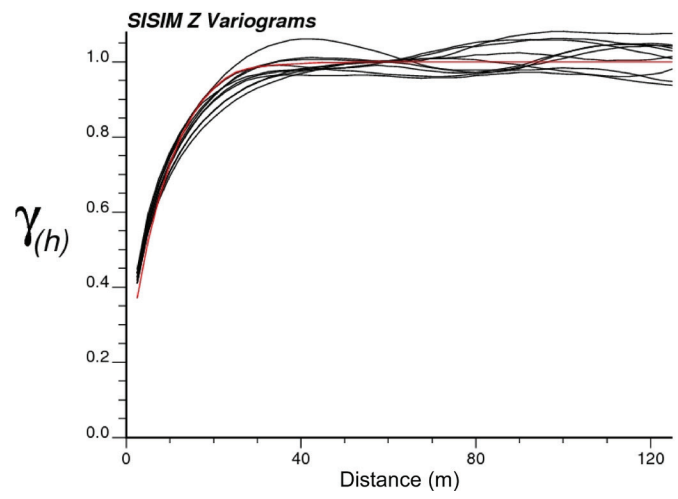
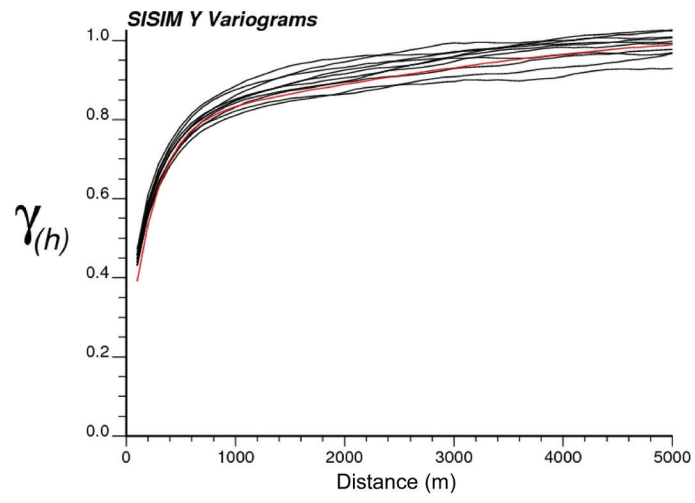
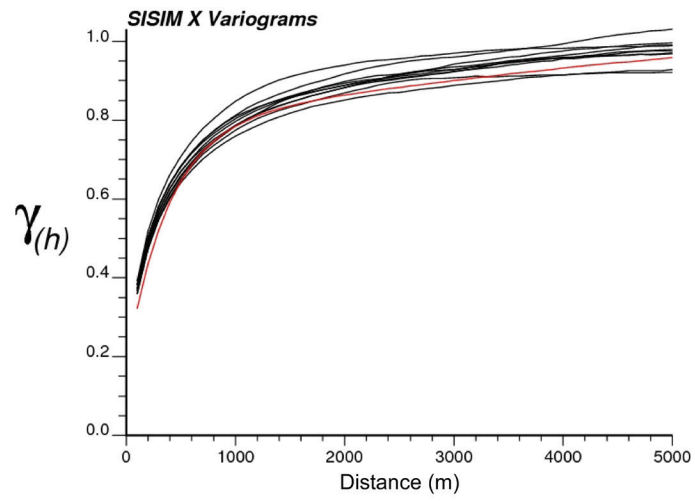


Figure 82. Mini-modelling variogram reproduction for SISIM.

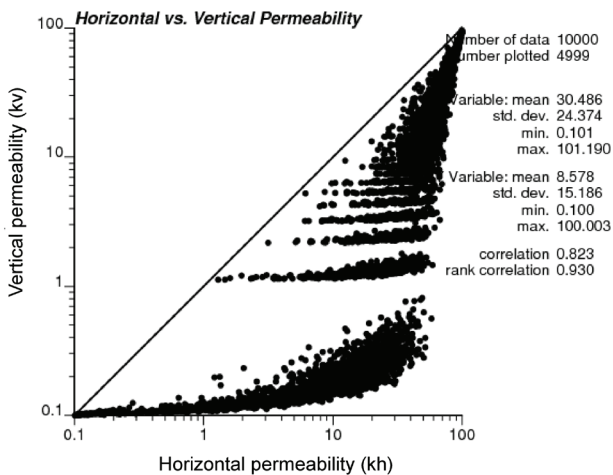
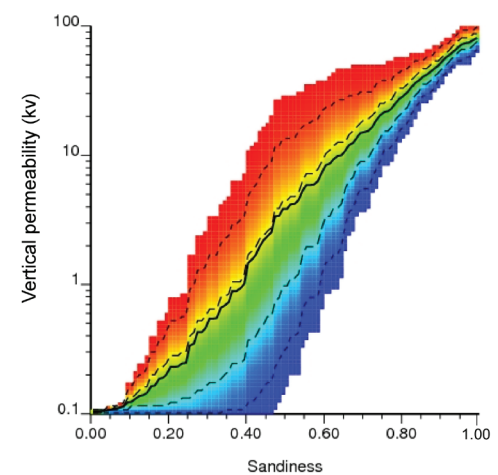
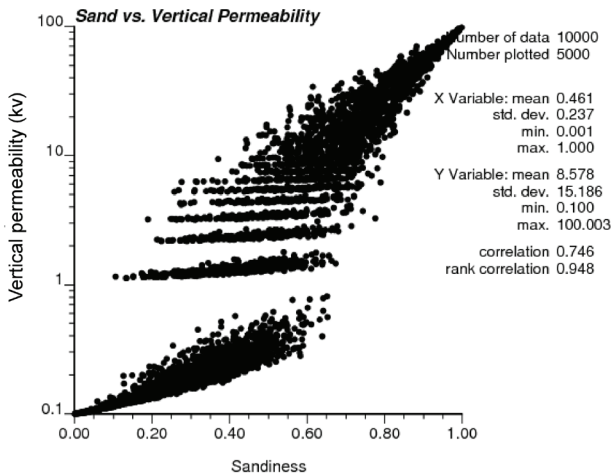
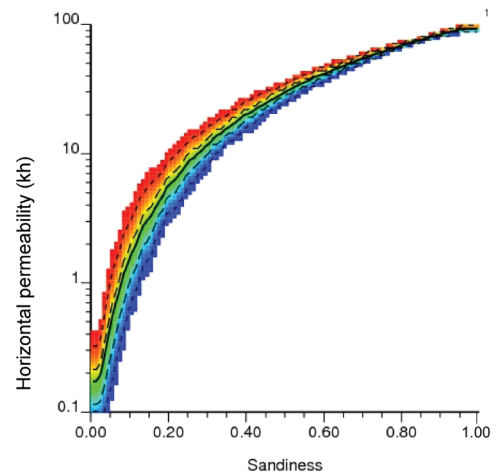
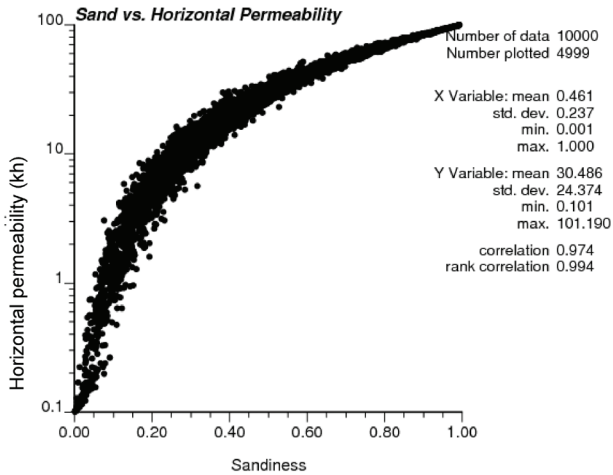


Figure 83. Sandiness–permeability relationships from the SISIM mini-models. Abbreviation: std. dev., standard deviation.

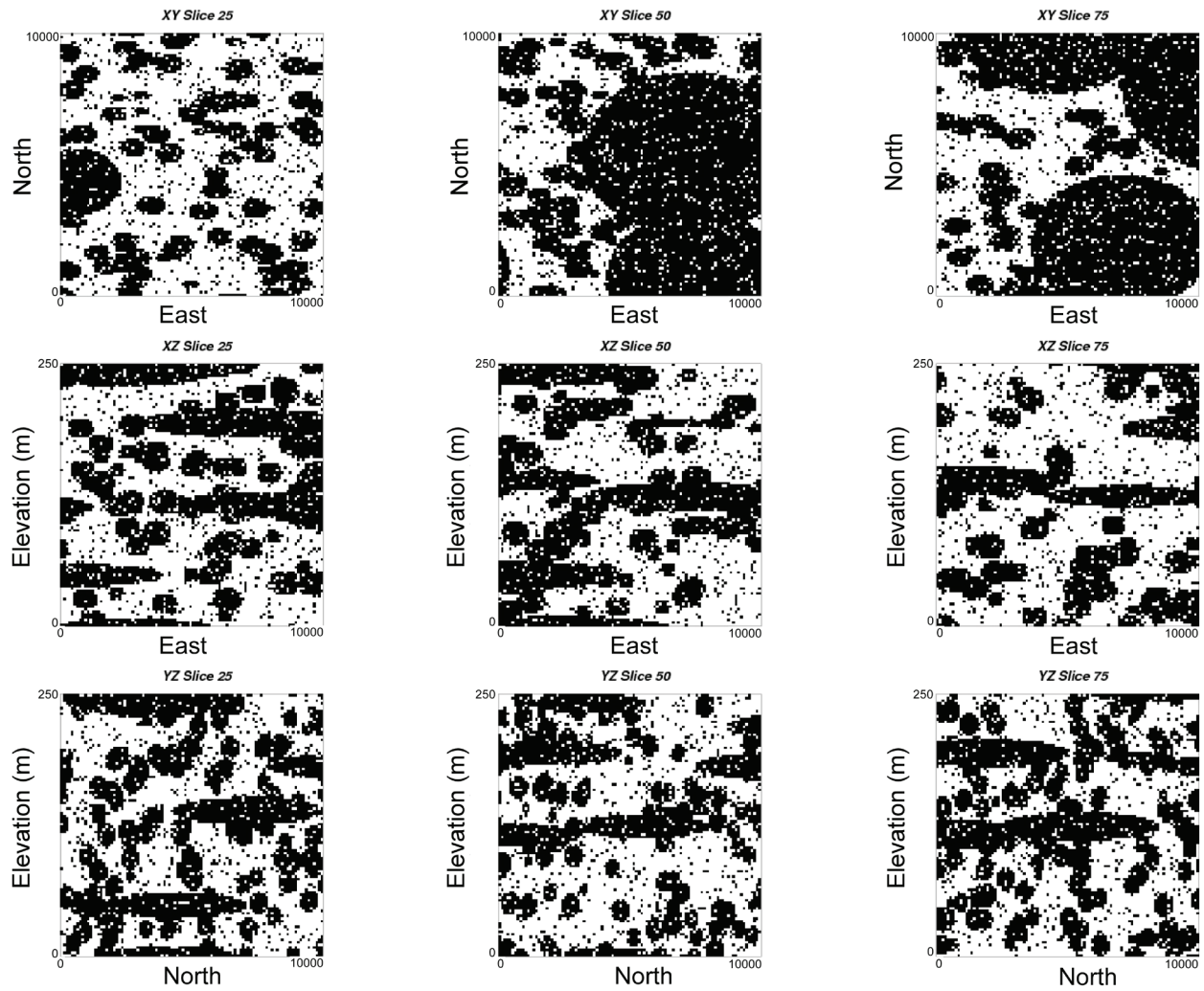


Figure 84. Slices of the mini-model created using the ELLIPSIM program. Vertical exaggeration is 40 times. Dark areas are sandy, light areas are muddy.

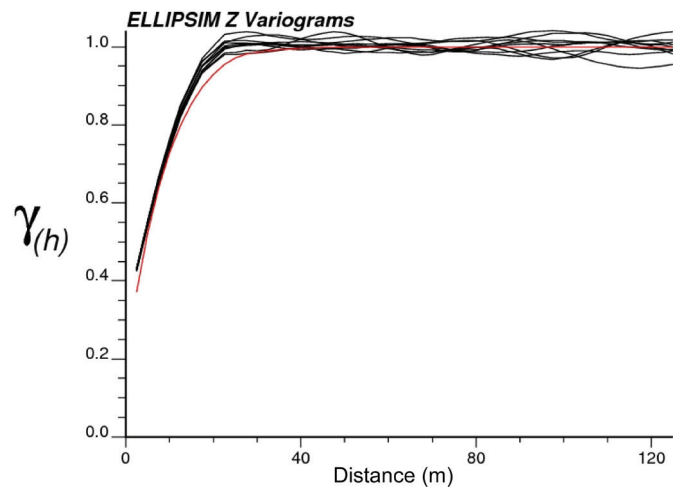
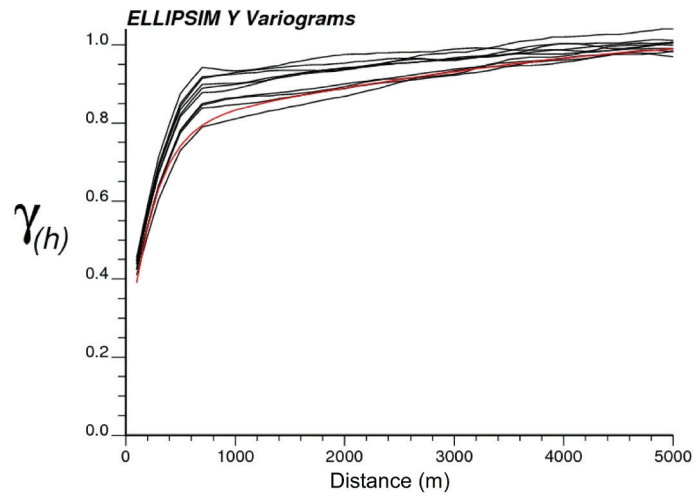
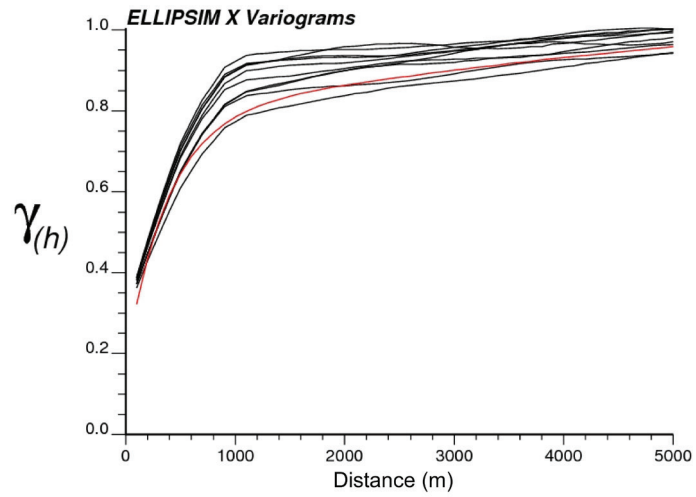


Figure 85. Mini-modelling variogram reproduction for ELLIPSIM.

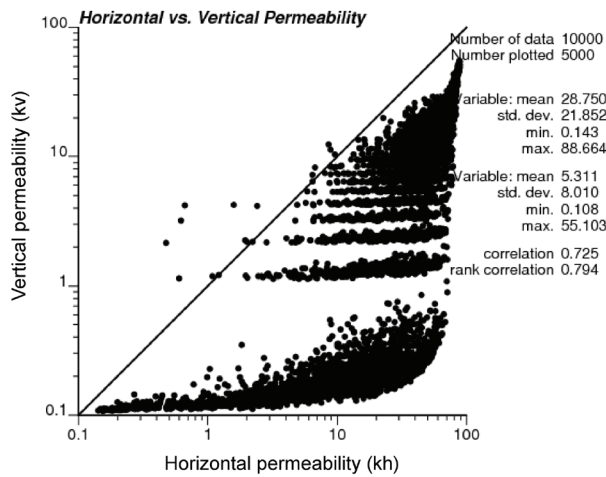
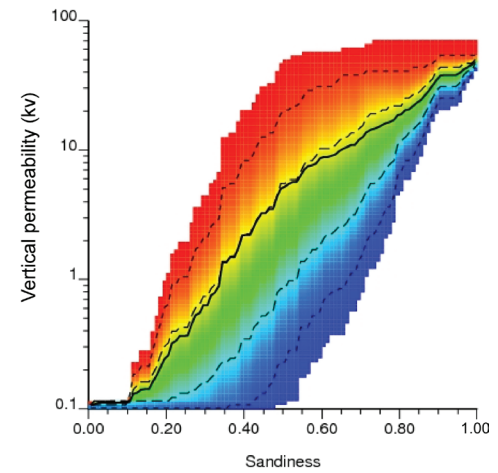
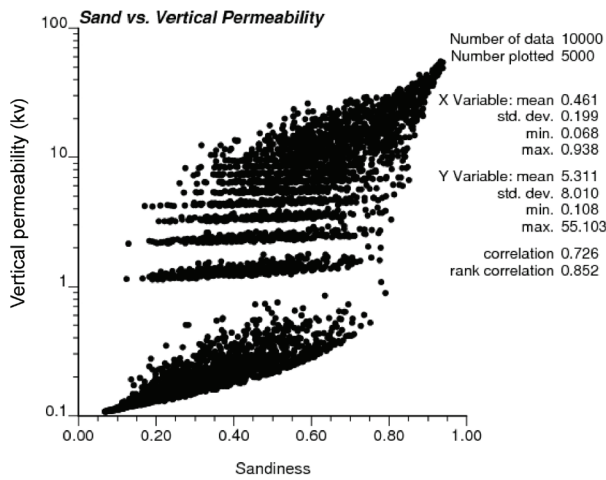
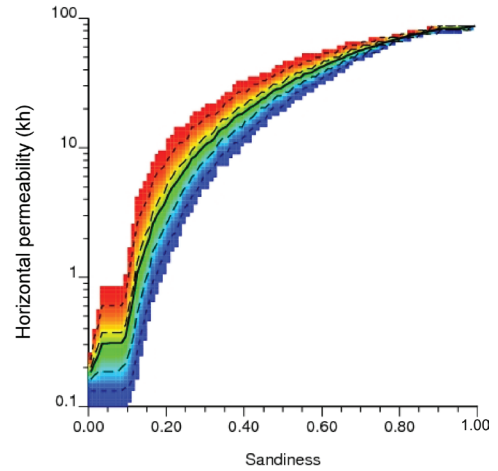
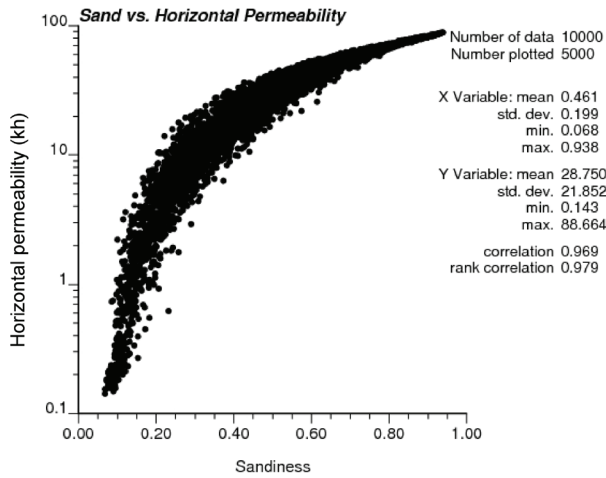


Figure 86. Sandiness–permeability relationships from the ELLIPSIM mini-models. Abbreviation: std. dev., standard deviation.

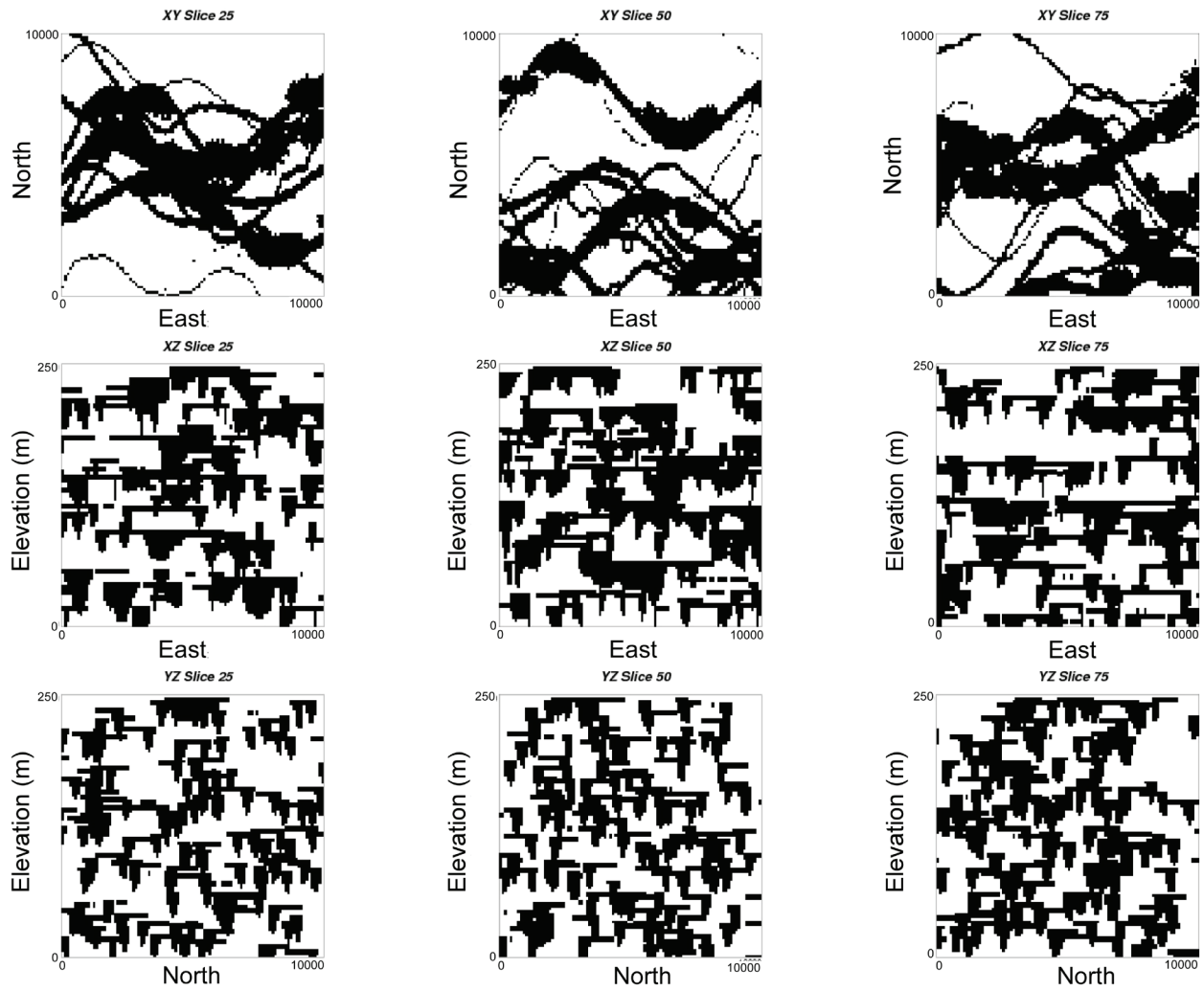


Figure 87. Slices of the mini-model created using the FLUVSIM program. Vertical exaggeration is 40 times. Dark areas are sandy, light areas are muddy.

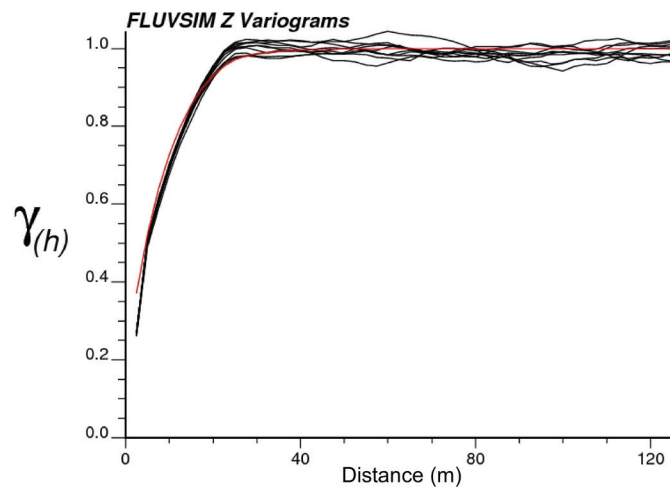
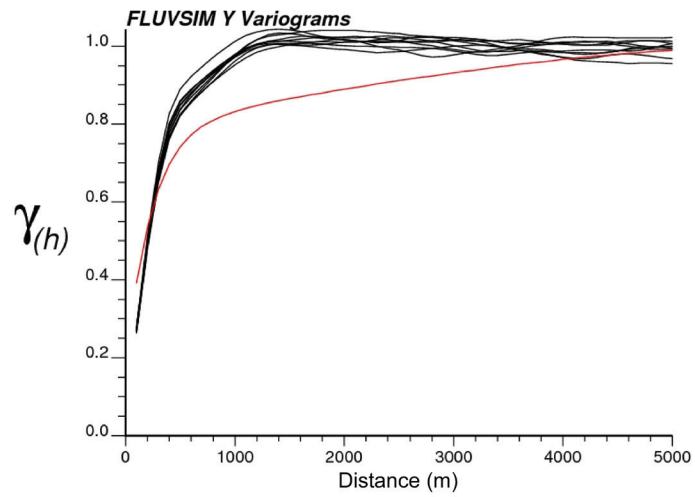
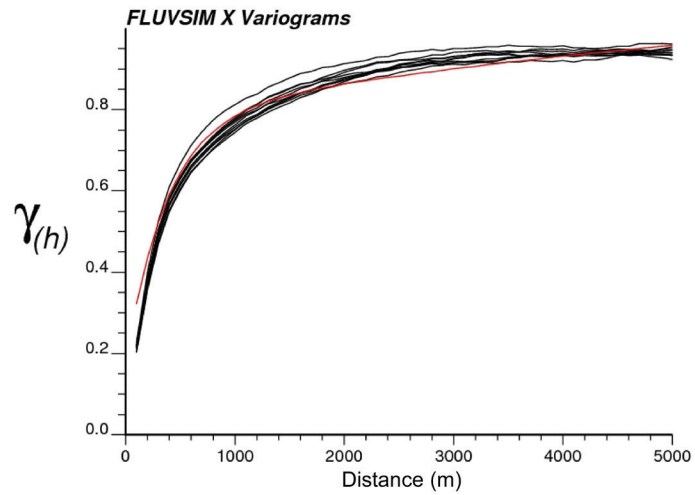


Figure 88. Mini-modelling variogram reproduction for FLUVSIM.

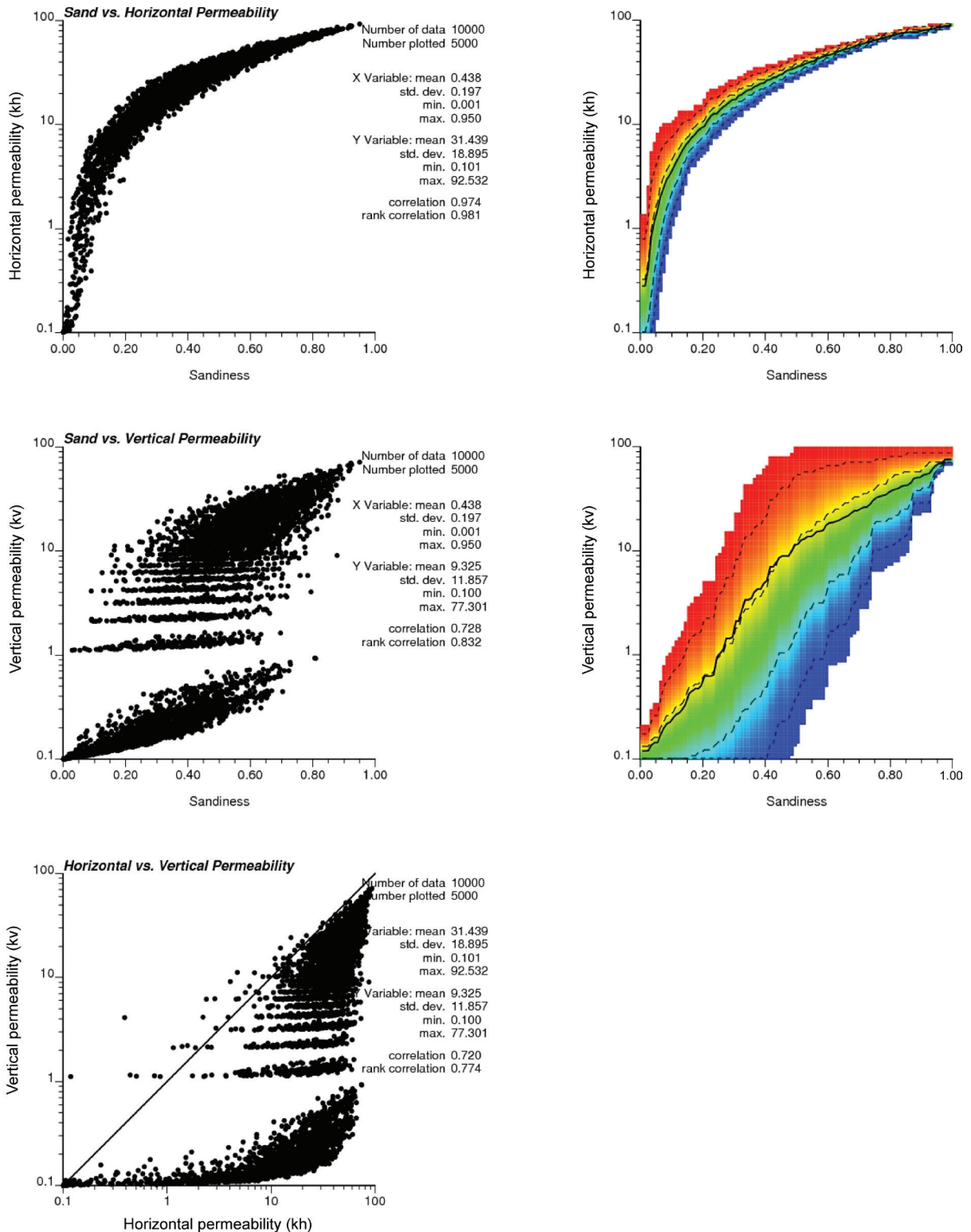


Figure 89. Sandiness–permeability relationships from the FLUVSIM mini-models. Abbreviation: std. dev., standard deviation.